Czech Technical University in Prague

Faculty of Electrical Engineering

Doctoral Thesis

August, 2017

Ladislava Černá

Czech Technical University in Prague

Faculty of Electrical Engineering

Department of Electrotechnology

METHODS OF FAULTS IDENTIFICATION IN PHOTOVOLTAIC SYSTEMS

Doctoral Thesis

Ladislava Černá

Prague, August, 2017

Ph.D. Programme: Electrical Engineering and Information Technology

Branch of study: (2602V009) Electrotechnology and Materials

Supervisor: prof. Ing. Vítězslav Benda, CSc.

Bibliography record

ČERNÁ, Ladislava. *Methods of faults identification in photovoltaic systems*. Prague, 2017. Doctoral thesis. Czech Technical University in Prague, Faculty of Electrotechnical Engineering. Supervisor Prof. Ing. Vítězslav Benda, CSc.

Anotace (abstrakt)

V současné době funguje v ČR i ve světě mnoho fotovoltaických (PV) elektráren, které se potýkají s různými známými i méně známými problémy. Např. PV moduly vyrobené z krystalického křemíku, které byly až donedávna považovány za relativně bezproblémové, jsou nyní předmětem zájmu z důvodu tzv. PID efektu (potenciálem indukovaná degradace), který způsobuje výrazné snížení výkonu celého systému. Pro ekonomicky i technicky efektivní provoz fotovoltaických systémů je proto nezbytné případné poruchy včas identifikovat. Za tímto účelem je vyvinuta řada diagnostických metod, které jsou úspěšně využívány provozovateli PV elektráren i servisními firmami. Tyto metody mají však také svá omezení, která nejsou vždy známa. Tato práce si tedy klade za cíl takové aspekty identifikovat a poskytnout vodítka k jejich eliminaci.

Kromě klasických metod existují také méně běžné metody, které mohou poskytnout řadu cenných údajů s menšími náklady. Možnosti použití některých diagnostických metod, jejich porovnání s konvenčními metodami a také vývoj nových je dalším cílem této práce.

V práci jsou shrnuty výsledky měření i simulací při použití jednotlivých metod a jejich vzájemné porovnání, s důrazem na metody, které lze použít přímo v místě instalace.

Klíčová slova

Fotovoltaika; Diagnostika; Měření Volt-Ampérových charakteristik; Měření temných proudů; Impedanční spektroskopie; Termografie

Abstract

Currently, there are many photovoltaic (PV) power plants in the Czech Republic and abroad, which face various known and also unknown problems. For example, PV modules produced from the crystalline silicon, which were considered to be relatively reliable and smooth, are now examined because of the so called PID (Potential Induced Degradation) effect, which causes a significant decrease in performance of the entire system. Therefore, for economical and technically effective PV systems operation, the early detection of possible defects is necessary. For this purpose, many diagnostic methods, which are successfully utilized by PV systems operators as well as by service companies, were developed. But these methods also have their limitations, which are not always known. Therefore, this work aims to identify such aspects and provide some guidance for their elimination.

Among the common diagnostic methods, there are also the less common ones, which can provide many valuable information with less cost demands. Possibilities of utilization of some of these methods, their comparison with the conventional ones and also development of some new are the next focus of this work.

Further, the results of measurements and simulations by the individual methods utilization, which can be used directly on site, are summarized.

Keywords

Photovoltaics; Diagnostics; *I-V* Curve Measurement; Dark Current Measurement; Impedance Spectroscopy; Thermography

Goals of the Thesis

The main objective of this thesis is to bring the overview of diagnostic methods which can be used directly at photovoltaic system and also describing their limits. The goals are especially the following:

- describing conventional diagnostic methods,
- determining limits of conventional diagnostic methods,
- finding correlations between conventional and less commonly used diagnostic methods,
- finding new approaches in evaluating the methods,
- development of methods for cost effective in-field diagnostics.

SOLEMN DECLARATION

I declare that I carried out this thesis independently, and only with the cited sources, literature and other professional sources.

I agree with making this work accessible for educational and research purposes.

In Prague 14. 8. 2017

Ladislava Černá

ACKNOWLEDGEMENT

At this place, I'd like to thank my supervisor prof. Ing. Vítězslav Benda, CSc. who taught me a lot in many aspects of photovoltaics as well as semiconductor physics and life and further all my colleagues, namely Pavel Hrzina, Tomáš Finsterle, Martin Horák, Tomáš Reichl and Jan Šutka for their help with measurements and general support during my whole study.

Contents

List of Used Symbols and Abbreviations

Symbol	Description	Unit
A	Irradiated area	m^2
BSF	Back Surface Field	
c	Speed of light	m/s
C_D	Diffusion capacitance	F
C_T	Transient/junction/barrier capacitance	F
C_P	Parallel capacitance	F
d	Depletion region thickness	m
D_n, D_p	Diffusion coefficient of electrons/holes	m^2/s
e	Elementary charge of electron	C
E	Energy	eV
E_g	Bandgap Energy	eV
E_i	Intrinsic Fermi level	eV
EL	Electroluminescence	
E_t	Energy level of the G-R centre (or trap)	eV
FF	Fill factor	-
FT	Flash Test	
G	Irradiance	W/m^2
G	Overall volume generation	$m^{-3}s^{-1}$
h	Planck's constant	Js
I	Current	A
IBC	Interdigitated Back Contact	
I_D	Current flowing through the PN junction	A
I_{DF}	Dark current flowing through the non-illuminated cell	A
I_{MP}	Current in MPP	A
I_{PV}	Photovoltaic current	A
I_{Rsh}	Shunt resistance current,	A
IS	Impedance Spectroscopy	
I_{01}	Diffusion component of the current	A
I_{02}	Generation-recombination component of the current	A

Symbol	Description	Unit
J_{PV}	Current density	A/m^2
J_{OPN}	Current density generated by the carriers within the depletion region	A/m^2
J_{PVN}	Current density generated by the carriers in N area	A/m^2
J_{PVP}	Current density generated by the carriers in P area	A/m^2
$L_{\mathrm{n}}, L_{\mathrm{p}}$	Diffuse length of electrons/holes	m
LS	Light Soaking	
mc-Si	Multicrystalline Silicon, *subst., adj.*	
mono-Si	Monocrystalline Silicon, *subst., adj.*	
MPP	Maximum Power Point	W
n_{i}	Intrinsic concentration	m^{-3}
n_{N0}	Equilibrium concentration of electrons in N area	m^{-3}
p_{P0}	Equilibrium concentration of holes in P area	m^{-3}
P_{MAX}	Maximum Power Point (MPP)	W
PECVD	Plasma Enhanced Chemical Vapour Deposition	
PERC	Passivated Emitter and Rear Cell	
PERL	Passivated Emitter Rear Locally Diffused	
PV	Photovoltaic(s), *adj., subst.*	
R	Overall volume recombination	m^{-3}s^{-1}
SA	Season Annealing	
S_{R}	Surface recombination at the top surface of the cell (0) and in vicinity of the back contact (H)	m^{-3}s^{-1}
SRV	Surface Recombination Velocity	m^{-3}s^{-1}
STC	Standard Test Conditions	
T	Thermodynamic temperature	K
TA	Thermal Annealing	
TCO	Transparent Conductive Oxide	
TDR	Time Domain Reflectometry	
TF	Thin-Film	
TT	Transition Time	s
V_{MP}	Voltage in MPP	V
Q	Injected positive charge	C

Symbol	Description	Unit
R_D	Diode resistance	Ω
R_S	Series resistance	Ω
R_{SH}	Shunt resistance	Ω
V	Voltage	V
V_B	Threshold Voltage	V
k	Boltzmann's constant	J/K
α	Absorption coefficient	m^{-1}
β	Number of carriers generated by the radiation of the given wavelength	-
η	Efficiency	-
η_1, η_2	Diode (ideality) factors	-
λ	Wavelength	m
τ_{p0}, τ_{n0}	Lifetime of the minority carriers in an N-type or P-type semiconductor	s
ε_S	Silicon permittivity	F/m
$\Phi(\lambda; x)$	Photon flux at the specific wavelength λ	s^{-1}
ψ_{bi}	Built-in potential	V
τ_{SC}	Recombination velocity in depletion region	s

List of Figures

List of Tables

1 Introduction

There is about 2 GW currently installed capacity of photovoltaic (PV) sources in the Czech Republic. Approximately 28 000 of individual installations was built mainly during the year 2010 which signifies demand overhanging the offer. This brings many problems connected with the quality of the systems, because there was installed everything that was possible to buy and also the experiences of PV systems designers were very poor. As a result, there are many installations that necessarily require the regular monitoring and in some cases also additional amendments which correct mistakes done during the installation.

The most crucial component is the photovoltaic module whose diagnostics can be sometimes relatively difficult. The main problem is that all the modules look very similar although their quality is totally different. Defects on the modules are usually not visible by the naked eye and also their causes should be found by the special methods. This work is aimed on using the current methods of such a diagnostics and using the new ones to provide new diagnostic tools suitable for PV systems operators.

To achieve it, it is necessary to understand the principles of function, defects creation mechanisms and known diagnostic methods first.

1.1 Photovoltaic Phenomenon

The base of every PV module creates PV cell. All of the PV cells, modules respectively, work on the principle of charge carriers generation. For the charge carriers generation, it is necessary to supply the energy which is in the case of photovoltaic phenomenon represented by the energy of absorbed light. This absorption is caused by the interaction between photons and matter particles. If the energy before photon incident is E_1, after absorption it is heightened by the photon energy $h\nu$ [1]:

$$E = E_1 + h\nu = E_1 + h\frac{c}{\lambda} \tag{1.1}$$

where h is Planck's constant [2],

ν frequency,

c speed of light in vacuum [2] and

λ wavelength.

After photon absorption, these interactions may occur:

- interaction with the grid,
- interaction with free electrons and
- interaction with bound electrons.

First two types of interactions lead to temperature rise. For the third interaction type, it is decisive whether the energy of incident photon is sufficient for freeing the electron from the bond or not. In the case of low energy, the temperature rise occurs again. If the energy is higher than the bonding energy of the electron, electron is freed from the bond – electron-hole pair generation. If we are able to separate the generated electrons and holes and get the potential difference, the current starts to flow through the material and we talk about the **photovoltaic phenomenon** (1839 Alexander Edmond Becquerel).

If the photon with energy higher than the band gap energy E_G is absorbed (minimal bounding energy), redundant energy is through the interaction with the grid transformed into the heat (thermalization process). For the photons with energy lower than E_G, the material is transparent (there is no photon absorption).

1.2 Photovoltaic Cell and Module – General Description

For electron-hole pair generation, the bounding energy value is essential. In the case of metals, this energy is equal to zero and the photon absorption thus doesn't cause the creation of the new charge carrier. Insulator has such a high bounding energy that the probability of electron freeing from the bond (valence band) is very low. The suitable material is the semiconductor which has valence and conduction band divided by the band of the energy within the range of units of eV. This energy is so called band gap energy E_G. But the solitary generation of electron-hole doesn't suffice. The charge carriers must be separated. To achieve it, the semiconductor structure with built-in electric field – PN junction is usually used. Common PV cell is basically the large-area semiconductor diode which contacts allow the light penetration inside its structure.

1.2.1 PV Cells and Modules Static Parameters

For PV cells description, it is possible to coming out the ideal equivalent circuit, where only current source and the diode exist; the parasitic resistances are thus neglected. This model has very low approximation level and is practically not used (**Fig. 1a**).

For better approximation, the series resistance is added to the basic scheme (**Fig. 1b**). This circuit is used very often, because its approximation abilities are sufficient, although one has to take into account the fact the calculated series resistance can take on negative values. For this reason, the new component, so called photovoltaic resistance, which can take on both negative and positive values, is loaded instead of series resistance which cannot take on negative values [3].

There is a standard model on the **Fig. 1c**, which is widely used for cells and modules characterization. The generation-recombination component is neglected and the diffuse component is then designated as saturation current I_0 (according to Shockley's theory).

The most precise model provides the circuit at **Fig. 1d**. This circuit provides the best results, but the large amount of parameters leads to relatively robust algorithms, thus it is used more for PV cells parameters determination.

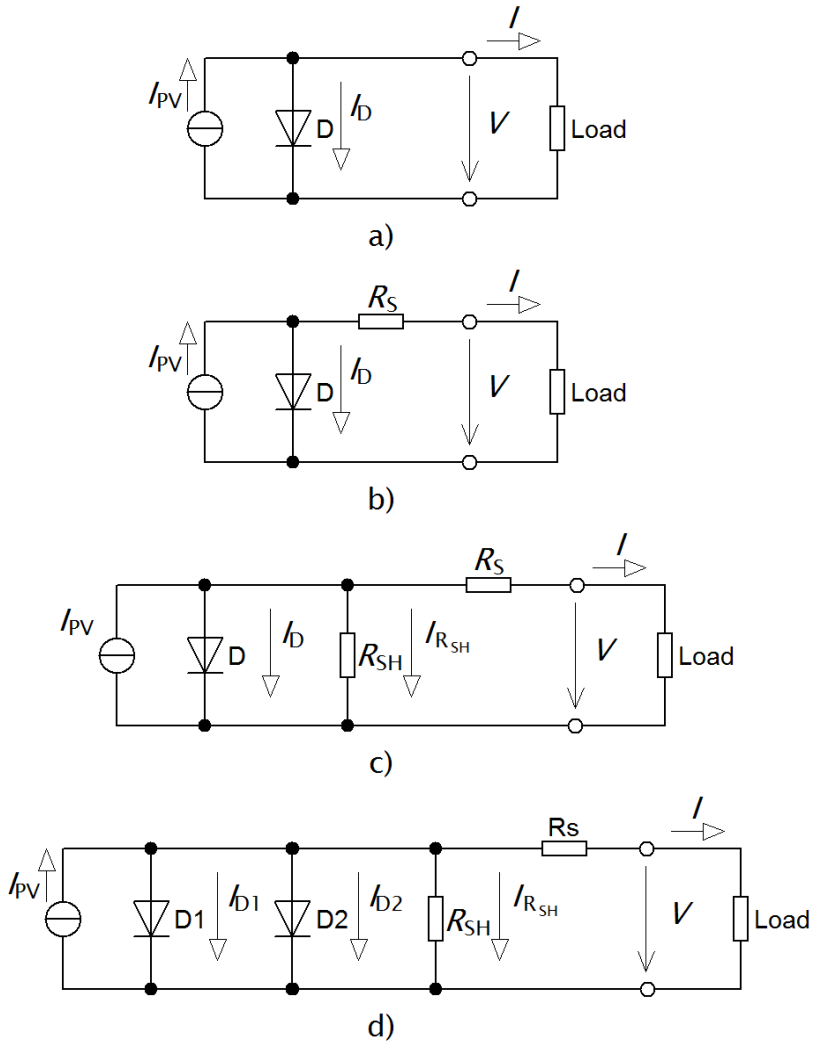

Fig. 1: Equivalent circuit of PV cells, modules respectively

From these models, also the other versions which use either simulated or measured data have been derived. All of the models are used for an evaluation of the real PV system operation. When the data from the inverters and PV power plant topology are known, then with the combination of the meteorological data, the prediction of the power plant electricity production can be calculated. This is very important, because the early detection of possible failures can save the system and consequently also money.

Mathematical description is than based on this equivalent circuit and is given by [1]:

$$I = I_{PV} - I_D - I_{R_{SH}} = I_{PV} - I_{01}\left[\exp\left(\frac{eV_j}{\eta_1 kT}\right) - 1\right] - I_{02}\left[\exp\left(\frac{eV_j}{\eta_2 kT}\right) - 1\right] - \frac{V + R_s I}{R_{SH}} \quad (1.2)$$

$$I = I_{PV} - I_{01}\left\{\exp\left[\frac{e(V+R_S I)}{\eta_1 kT}\right] - 1\right\} - I_{02}\left\{\exp\left[\frac{e(V+R_S I)}{\eta_2 kT}\right] - 1\right\} - \frac{V + R_s I}{R_{SH}} \quad (1.3)$$

where I_{PV} is the photovoltaic current,

I_D current flowing through the PN junction,

I_{Rsh} shunt resistance current,

I useful current that the PV cell can deliver to the external circuit,

I_{01} diffusion component of the current,

I_{02} generation-recombination component of the current,

η_1, η_2 diode (ideality) factors,

k Boltzmann's constant [2],

e electron elementary charge [2],

T thermodynamic temperature and

V voltage at the PV cell terminal.

Equation (1.3) describes the volt-ampere characteristics of the cell from which the basic PV cells parameters can be extracted [1], when the resistances can be in the first approximation calculated from the slope of the tangent in the point of open-circuit voltage V_{OC} and short-circuit current I_{SC} as marked on the **Fig. 2**.

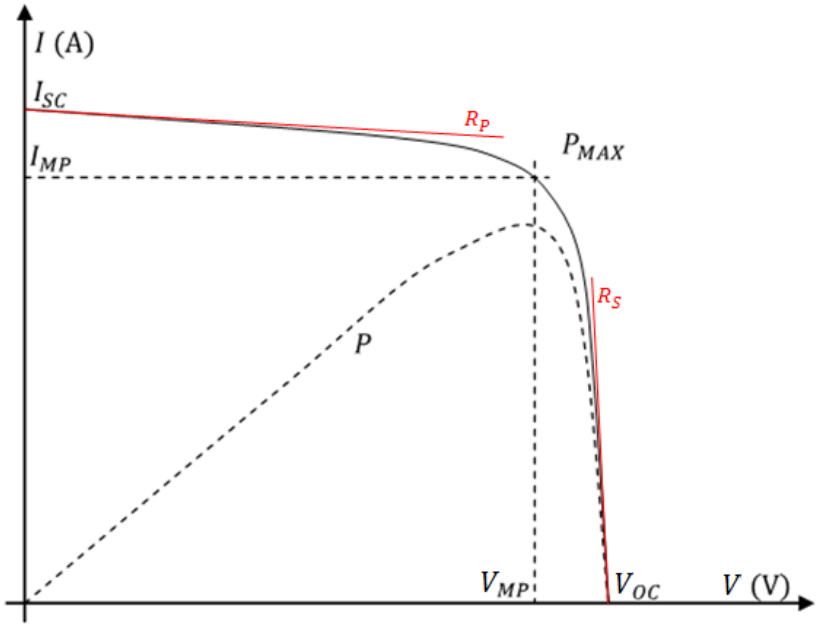

Fig. 2: PV cell *I-V* curve

where P_{MAX} represents maximum power point (MPP) and

V_{MP} and I_{MP} voltage and current in MPP.

Besides the parameters which can be established directly from the *I-V* curve of PV cell, there are also the other important parameters, namely cell efficiency η (%) a fill factor FF (%):

$$\eta = 100 \cdot \frac{P_{OUT}}{P_{IN}} = 100 \cdot \frac{P_{MAX}}{G \cdot A} \tag{1.4}$$

$$FF = \frac{U_{MP} \cdot I_{MP}}{V_{OC} \cdot I_{SC}} \cdot 100 \tag{1.5}$$

where G is irradiance and

A irradiated area (usually cell or module, surface area).

Individual PV cells have a working voltage lower than 1.5 V (in the case of crystalline silicon about 0.5 V) and a current density of a few mA/cm^2 (for crystalline silicon approx. 35 mA/cm^2). For this reason it is necessary to connect individual cells to series into function blocks – PV modules, as marked at **Fig. 3a)**. For serial connection, the cells should have ideally the same value of I_{MP}. In simplified approximation, marked at **Fig. 3b)**, the module can be represented by one value of series resistance R_S' and shunt resistance R_{SH}'. *I-V* curve of the module (*n* serially connected cells) than have analogical mathematical description to the equation (1.3):

$$I = I_{PV} - I_{01}\left\{\exp\left[\frac{e(V + R_S' I)}{n \cdot \eta_1 kT}\right] - 1\right\} - I_{02}\left\{\exp\left[\frac{e(V + R_S' I)}{n \cdot \eta_2 kT}\right] - 1\right\} - \frac{V + R_S' I}{R_{SH}} \quad (1.6)$$

The parameters as $V_{OC}, I_{SC}, I_{MP}, V_{MP}, P_{MAX}, FF$ and efficiency η is than possible to establish analogically to PV cells parameters.

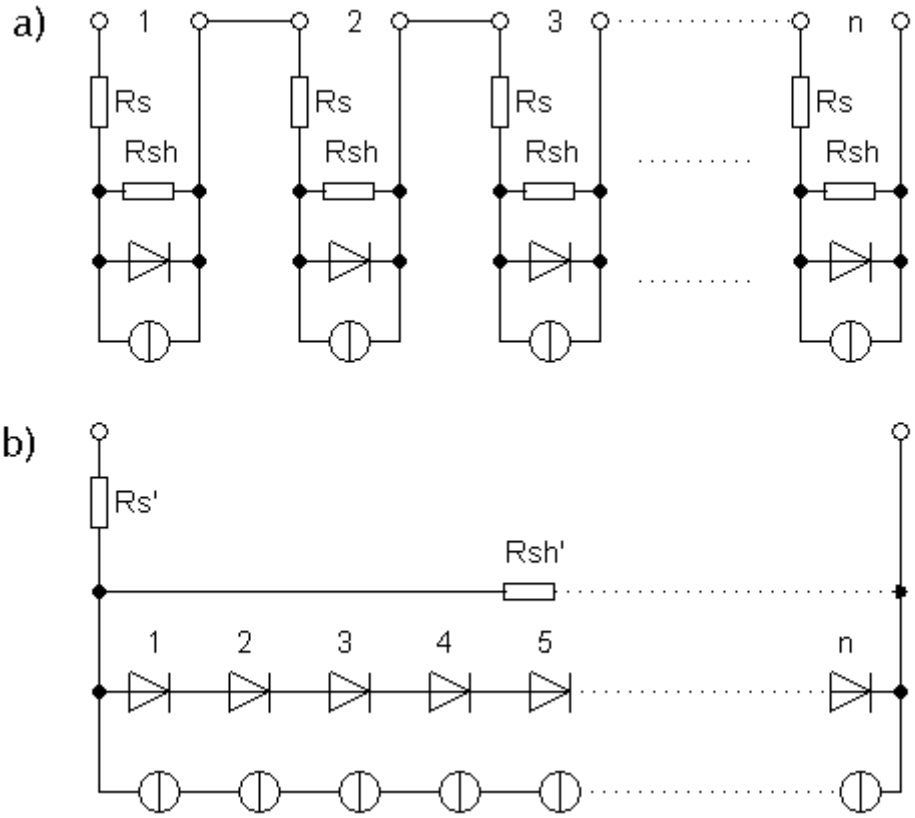

Fig. 3: a) Equivalent circuit of serially connected PV cells into the module
b) Simplified equivalent circuit of *n* serially connected PV cells

1.2.1.1 Series Resistance Determination and Dependence at Ambient Conditions

As mentioned above, determining the PV cells parameters comes from the measurement of *I-V* curves. The most often used equipment is flash tester, which is usually also a part of the production line. Firstly, when the cells are divided into the groups to be collected into the module, with as similar parameters as possible, secondly, at the end. From measured *I-V* curve, parameters like V_{OC}, I_{SC}, P_{MAX}, I_{MP}, V_{MP} and *FF* can be easily determined. The situation becomes more complicated when the shunt, or series, resistance should be extracted.

1.2.1.1.1 Determination from the Slope of a Line near the V_{OC} Point

For series resistance determination, it is possible to use a few methods. The basic method is determination of series resistance using the slope of a line within the vicinity of open circuit voltage point, which can be used particularly at higher irradiance values:

$$R_S \approx -\frac{dV}{dI}\Big|_{V \approx V_{OC}} \tag{1.7}$$

Series resistance obtained by this simple method provides good base for further analysis, but when compared with the real one, its value is used to be higher.

1.2.1.1.2 Method According to ČSN EN 60891

Another possibility, which is mostly used, is utilization of methodology given by the ČSN EN 60891 [4] standard, which for series resistance determination requires two *I*-*V* curves measurements under different irradiance with unchanged spectrum. The procedure is as follows:

- two characteristics at the ambient room temperature under different irradiance and same spectrum are measured,
- during measurement, the temperature shall be constant (permitted tolerance is ± 2%);
- two operating points are determined:
  - the current interval $\Delta I = 0.5 \cdot I_{SC2}$ (where index 2 is relevant for lower irradiance value) is determined,
  - based on this interval, voltages $V_1 = V\ (I_{SC1} - \Delta I)$ and $V_2 = V\ (I_{SC2} - \Delta I)$ are determined;
- and R_S is than calculated:

$$R_S = \frac{V_2 - V_1}{I_{SC1} - I_{SC2}} \tag{1.8}$$

1.2.1.1.3 Approximation Method

This method uses the measured data and fits them by the function based on some of the model described above, optionally with some other simplifying presumptions like one-diode model, constant shunt resistance and so on. The method is based on the fitting of the measured data in such a way that will lead to as small deviations between the measured and simulated data as

possible (e.g. [5]). By using the various numerical methods (like Newton iteration) and various algorithms, all the parameters, which best correspond to measured data, can be found. The problem can be either the complexity of the algorithms or sometimes also the unreality of the obtained parameters, which is done namely by using polynomial functions, evaluation of the function only within the measured interval and wrong initial parameters values.

1.2.1.1.4 Derivative Method

Very favourite method for series resistance determination is the derivative method which uses determination from only one *I-V* characteristic [5], [6] (the shunt resistance is expected to be infinite):

$$\frac{\mathrm{dV}}{\mathrm{dI}} = -R_{\mathrm{S}} - \eta_1 \left(\frac{kT}{e}\right) / (I_{\mathrm{SC}} - I) \tag{1.9}$$

Series resistance is the limiting factor for the PV cell as well as module performance. When its value rises five times, the FF and PMAX value is decreased by the quarter [7]. With regard to which components series resistance comprises of, within the whole volume, it is not constant. This inhomogeneity is especially apparent when the series resistance of the cell is determined. Therefore, for its evaluation, the suitability of the equipment for measurement of such a cell should be also taken into account. For example, in the case of measurement of cell with three busbars using the equipment intended for two-busbars cells measurement, the unsuitability of the contacting system can cause higher measured resistance value than the real one. Inhomogeneity of R_{S} distribution can be also advantageously displayed using photoluminescence. This method is further described e.g. in [8].

1.2.1.1.5 Temperature Dependence of *I-V* curve and Static PV Cells/Modules Parameters

The density of the current flowing through the diodes represented by the components I_{01} and I_{02} can be expressed by [9]:

$$I_D = I_{01} + I_{02}$$
$$I_{\mathrm{D}} = An_{\mathrm{i}}^2 e \left(\frac{D_{\mathrm{n}}}{L_{\mathrm{n}}}\frac{1}{p_{\mathrm{P0}}} + \frac{D_{\mathrm{p}}}{L_{\mathrm{p}}}\frac{1}{n_{\mathrm{N0}}}\right)\left[\exp\left(\frac{e(V + R_{\mathrm{S}}I)}{\eta_1 kT}\right) - 1\right] + A\frac{en_{\mathrm{i}}d}{\tau_{\mathrm{SC}}}\left[\exp\left(\frac{e(V + R_{\mathrm{S}}I)}{\eta_2 kT}\right) - 1\right] \tag{1.10}$$

where n_{i} is intrinsic concentration,

$D_{\mathrm{n}}, D_{\mathrm{p}}$ diffusion coefficient of electrons/holes,

$L_{\mathrm{n}}, L_{\mathrm{p}}$ diffusion length of electrons/holes

p_{P0} equilibrium concentration of holes in P area,

n_{N0} equilibrium concentration of electrons in N area,

d depletion region thickness and

τ_{SC} characterizes the recombination velocity in depletion region.

If the R_{SH} would be considered as high, the V_{OC} can be rewritten as [1]:

$$V_{\mathrm{OC}} = \frac{2kT}{e} \ln\left(\frac{-I_{02} + \sqrt{I_{02}^2 + 4I_{01}(I_{02} + I_{01} + I_{\mathrm{PV}})}}{2I_{01}}\right). \tag{1.11}$$

Also if $I_{\mathrm{PV}} \gg I_{01} + I_{02}$, the whole equation is simplified and for the V_{OC} value it is possible to write:

$$V_{\mathrm{OC}} \approx \frac{kT}{e} \ln \frac{I_{\mathrm{PV}}}{I_{01}}. \tag{1.12}$$

According to (1.10), it is obvious that $I_{01} \sim n_i^2$ and $I_{02} \sim n_i$. Than it is possible to write:

$$n_i^2 = BT^3 \exp\left(-\frac{E_g}{kT}\right) \Rightarrow \frac{\partial V_{\mathrm{OC}}}{\partial T} < 0 \tag{1.13}$$

where B is the constant independent on temperature.

From the expressions written above, it is obvious that with the rising temperature, the V_{OC} value will decrease. It can be also proved that with rising temperature, series resistance R_{S} and short circuit current I_{SC} slightly increase and contrariwise the R_{SH} significantly decreases. In practical applications, especially the voltage decrease is observed, which is higher than the current increase. Voltage and power decrease with the temperature rises about approx. 0.4 % per 1 K. The quality of the cell can be, among others, evaluated just from the point of view of temperature coefficient, when the more quality cell should have lower temperature coefficient (although the fact that the coefficient decreases with rising band gap value should be also taken into account).

1.2.1.1.6 Irradiance Dependence of *I-V* Curve and Static PV Cells/Modules Parameters

Energy of incident radiation is in the PV cell PN junction area transformed into the electric energy. The amount of this energy corresponds to the amount of incident radiation, as proved by the following equations [1]:

$$J_{\mathrm{PV}} = J_{\mathrm{PVN}} + J_{\mathrm{PVP}} + J_{\mathrm{OPN}} \tag{1.14}$$

where J_{PVN} is the current density generated by the carriers in N area,

J_{PVP} is the current density generated by the carriers in P area and

J_{OPN} is the current density generated by the carriers within the depletion region.

$$J_{\mathrm{PVN}} = \int_0^{x_i} G dx - \int_0^{x_i} R dx - S_{\mathrm{R}}(0) \tag{1.15}$$

$$J_{\mathrm{PVP}} = \int_{x_i+d}^{H} G dx - \int_{x_i+d}^{H} R dx - S_{\mathrm{R}}(H) \tag{1.16}$$

where G represents the overall volume generation,

R states for overall volume recombination and

S_{R} the surface recombination at the top surface of the cell (0) and in vicinity of the back contact (H).

Equations (1.15) and (1.16) imply dependence of the generated current, current density respectively on the irradiance, namely through dependence on number of generated carriers, which can be quantified as follows:

$$G_{tot}(x) = \int_0^{\infty} G(\lambda; x) d\lambda = \int_0^{\infty} \alpha(\lambda)\beta(\lambda)\Phi(\lambda; x) d\lambda \tag{1.17}$$

where Φ is the photon flux at the specific wavelength λ (in the depth x),

α absorption coefficient for the specific wavelength and

β number of carriers generated by the radiation of the given wavelength.

Therefore, with rising irradiance, I_{SC} significantly increases and also the V_{OC} value slightly increases.

1.2.1.2 Series Resistance and its Dependence on Temperature and Irradiance

As apparent from the temperature influence on PV cells and modules parameters, temperature doesn't play a very significant role. Above that, when series resistance is estimated, its

independency on irradiance is also presumed. But as proved by the measurement done during working at this thesis, there is strong dependence of R_S on irradiance. The results were also presented at a conference [10].

An influence of series resistance on the dependence of cell efficiency on irradiance have been discussed mainly in connection with concentrator photovoltaic [11], [12], sometimes the effect of series resistance is even practically neglected [13] and more attention is paid to effects connected with the cell temperature increase. But the dependence of the cell efficiency on irradiance at lower irradiance level exists.

The current density J_{PV} generated by incident light depends on the cell material and structure. The generation rate is proportional to irradiance. Therefore, the current density J_{PV} can be in a good approximation considered to be directly proportional to the irradiance, even the charge carriers lifetime may depend on excess carriers concentration Δn [14], [15].

Using the two-diode model of PV cell, the influence of series resistance R_S on the cell characteristics and consequently, on the cell (or module) efficiency may be evaluated. For these simulations, the current density J_{PV} has been considered as linearly increasing with irradiance reaching the value 35 mA/cm^2 at irradiance 1000 W/m^2. The calculations have been done for a cell of area of 100 cm^2 and the shunt resistance R_{SH} = 50 Ω. To obtain parameters of the parasitic diode, I_{01} and I_{02}, acceptor concentration 10^{18} cm^{-3} and carriers lifetime 100 μs in P-type region and donor concentration $5 \cdot 10^{19}$ cm^{-3} and carriers lifetime 5 μs in N type have been used for simulations [16].

I-V curves of cells have been calculated using equation (1.2) for different values of series resistance R_S. These simulations ensue, that in general, the cell efficiency increases with irradiance at low irradiance level, at some irradiance reaches its maximum and then with increasing irradiance efficiency decreases. The point of maximum efficiency strongly depends on the series resistance R_S, as demonstrated in **Fig. 4**.

A set of measurements was conducted for authentication of the influence of temperature and irradiance on the PV cell parameters using cell tester Pasan IIb. The irradiance was regulated by the device and by changing the distance between the flash lamp and the measured photovoltaic cell. Lower irradiance was achieved using a grey filter that was put in front of the lamp. This way, irradiance ranging from 200 W/m^2 to 1000 W/m^2 was obtained. The temperature has been ranged from 25°C to 110°C. It was found, that series resistance of PV

cells slightly increases with temperature, but more significantly decreases with irradiance, as demonstrated in **Fig. 5**.

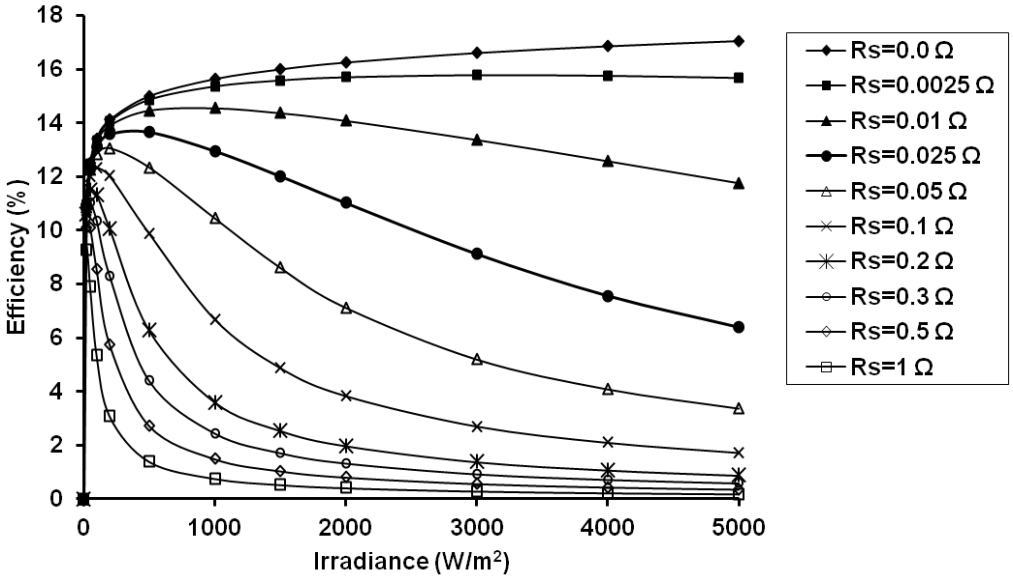

Fig. 4: Simulation of c-Si cell efficiency dependence on irradiance by different R_S

Presuming that R_S must have a positive value, the dependence of series resistance R_S on irradiance G can be described as:

$$R_S(G) = R_{S\infty} + AG^{-B} \tag{1.18}$$

Parameters $R_{S\infty}$ (Ω), A and B can be extracted from experimental data. For crystalline silicon solar cells measured in our experiments, this function well fits to experimental data, as shown in **Fig. 6a)**, and found constants are as followed:

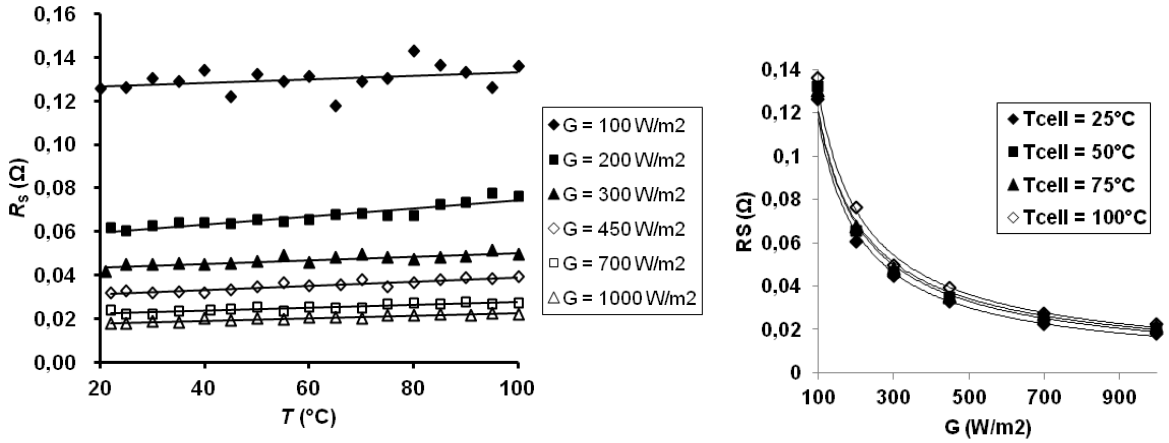

Fig. 5: Temperature and irradiance dependence of c-Si cell R_S [10]

$$R_S = 0.0103 + 22.32 \cdot G^{-1.14} \tag{1.19}$$

The dependence of series resistance on irradiance slightly changes courses of the efficiency dependence on irradiance. The decrease of series resistance with irradiance makes efficiency maximum more flat and the cell efficiency decreases slower than in a case of constant values of R_S. In the **Fig. 6b)**, the results of simulations for cells for different fix values of R_S with simulation using values R_S (G) from Eq. (1.19) and measured data are compared. The experimental data is in a good agreement with simulation using R_S (G) for G > 200 Wm-2. Differences for low irradiance levels may be caused by a decrease of carriers lifetime in P-type cell region with injection level [14]. The result can be projected in module simulation to explain influence of technological parameters on the irradiance dependence of module efficiency. In a simple approximation, modelling a silicon PV module by n in series connected PV cells, the module I-V curve equation can be written in a form of (1.6). Therefore, the same procedure of R_S dependency on irradiance determination has been done with the following result:

$$R_S = 0.579 + 567 \cdot G^{-1.18} \tag{1.20}$$

This knowledge of this dependency can be advantageously used when the most appropriate technology is chosen for some specific installation, as was also discussed at NZEE conference [17]. When the PV module performance and suitability for the specific application is evaluated, then the similar procedure like in the case of inverters can be applied. Therefore,

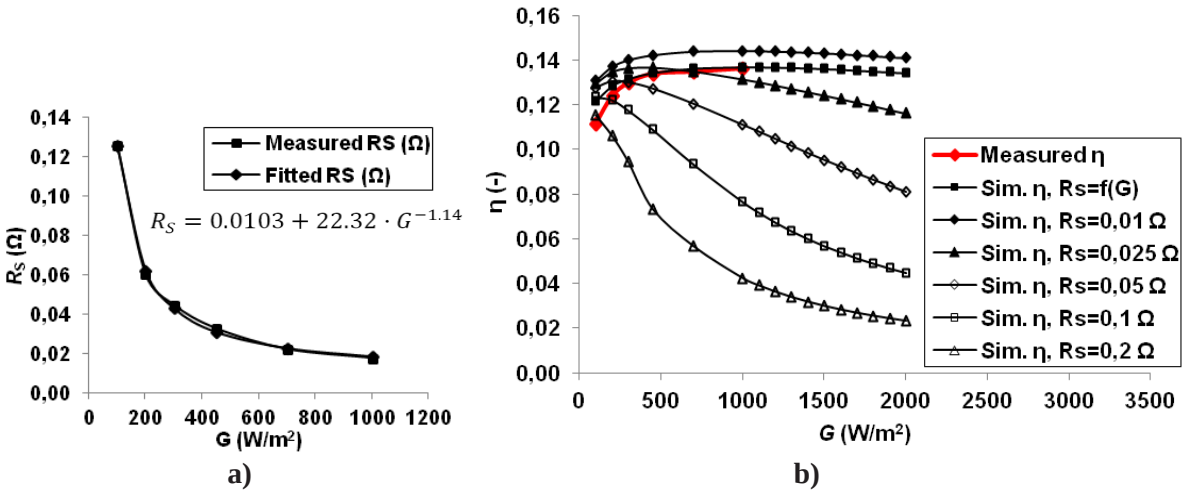

Fig. 6: a) Measured and fitted dependence of c-Si cell R_S on irradiance,
b) Comparison of simulated and measured dependencies of c-Si cell efficiency on irradiance, R_{SH} = 50 Ω [10]

for this purpose, the EURO efficiency of the modules was calculated. It comes from the fact, that every module will show different behaviour under different climatic conditions. For example, in the tropical climate, the temperature of the module will be entirely different when the same irradiance like in the middle European climate is achieved [18].

The dependence of inverters efficiency on ambient conditions is given by the European inverters efficiency (loaded by the research institute Joint Research Centre – JRC), which is a common parameter in inverters datasheets. It is interesting that no similar parameter is listed for the key PV system component – PV module (although there are the efforts from the TÜV SÜD to evaluate it using Energy labels for marking the suitability of the given module to the specific climate area). The European inverter efficiency is defined as weighted average efficiency at different powers [19]:

$$\eta_{EURO} = 0.03 \cdot \eta_{5\%} + 0.06 \cdot \eta_{10\%} + 0.13 \cdot \eta_{20\%} + 0.1 \cdot \eta_{30\%} + 0.48 \cdot \eta_{50\%} + 0.20 \cdot \eta_{100\%} \quad (1.21)$$

Once the similar algorithm is applied on PV modules, the STC efficiency can be compared with such a fictitious efficiency which takes into account the concrete PV modules technologies under the local climatic conditions. Individual weights then will come from the histogram of irradiance levels distribution in concrete locality with concrete orientation and tilt angle. For the Czech Republic, when the histogram given in [20] and measured data (see **Fig. 7**) are used, the following equations can be calculated and results in **Tab. 1** obtained:

$$\eta_{35^\circ} = 0.05 \cdot \eta_{100} + 0.12 \cdot \eta_{200} + 0.23 \cdot \eta_{400} + 0.35 \cdot \eta_{700} + 0.25 \cdot \eta_{1000} \quad (1.22)$$

$$\eta_{90^\circ} = 0.09 \cdot \eta_{100} + 0.16 \cdot \eta_{200} + 0.34 \cdot \eta_{400} + 0.37 \cdot \eta_{700} + 0.04 \cdot \eta_{1000} \quad (1.23)$$

Tab. 1: Weights extracted from the irradiance histogram, efficiency for individual technologies under ideal tilt angle and angle corresponding to façade utilization (both at optimal orientation) [17]

Wages for CR			**Technology**	η_{STC} **(%)**	η_{35° **(%)**	η_{90° **(%)**
G (W/m^2)	**wage 35 °**	**wage 90 °**	**CdTe**	10.13	10.15	10.13
100	0.05	0.09	**CIGS**	9.60	9.15	8.89
200	0.12	0.16	**Sanyo HIT**	18.30	18.25	18.21
400	0.23	0.34	**mono c-Si**	12.80	12.59	12.47
700	0.35	0.37	**multi c-Si**	14.29	14.21	14.14
1000	0.25	0.04	**a-Si**	7.97	7.50	7.29

As apparent from the previous sections, the subject of series resistance and its correct value and dependences is a relatively complicated matter. However, this dependence of series resistance can also be caused by the faulty methodology, as assumed in [21]. The problems

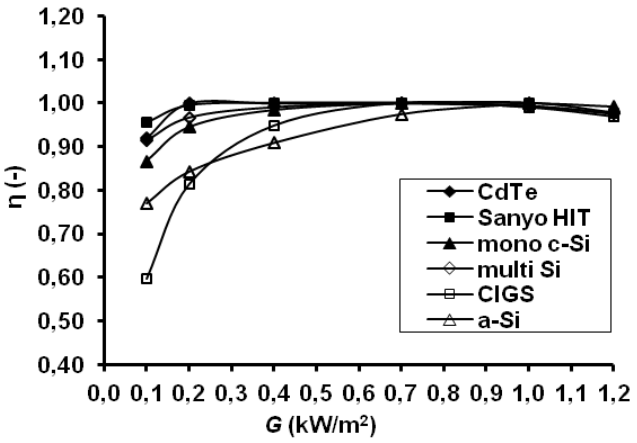

Fig. 7: Dependence of different technologies of PV modules efficiency on irradiance – normalized values [17]

with the R_S determination methodology are shown also in [22], where the problems with methodology are described in ČSN EN 60891 for lower irradiances discussed. One way or another the fact is that this parameter should be more examined and defined.

1.2.2 PV Cells and Modules Dynamic Parameters

Every cell is characterized by its basic static parameters, which were described above. Moreover, there are also other parameters based on the AC equivalent circuit like transient (called also junction or barrier) capacitance (C_T), diffusion capacitance (C_D) and also diode resistance (R_D) which represents the non-ideality of the diode characteristics. A solar cell (module) can be modelled using the equivalent circuit shown at **Fig. 8** [23]:

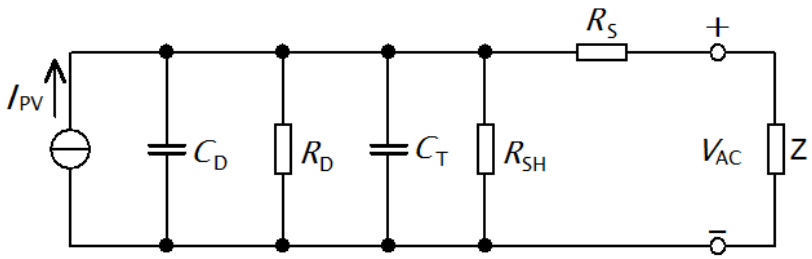

Fig. 8: Dynamic equivalent circuit of PV cell (module) [23]

When combining C_D with C_T and R_D with R_{SH} the simplified dynamic model of PV cell, module respectively, can be obtained as shown on **Fig. 9** [23].

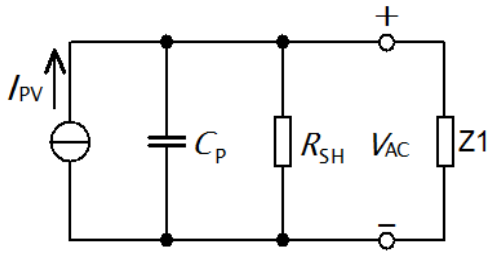

Fig. 9: Simplified dynamic equivalent circuit of PV cell (module) [23]

PV module consists of cells which are serially connected in order to reach a sufficiently high voltage output, so the module can be modelled using the same circuit and parameters whose values represent the serial connection of the parameters of individual cells.

2 Photovoltaic Cells and Modules Types

Construction of individual PV cells depends on properties of the original material. If the material has the so called direct band gap structure (e.g. GaAs or amorphous Silicon), the absorption coefficient, representing the ability of the material to absorb different wavelength, for photons with $h\nu \geq E_G$ rises very quickly with their energy, thus the sun radiation is fully absorbed in the layer within the thickness range of units of μm. In the case of the materials with indirect band gap structure (eg. crystalline Silicon), the absorption coefficient increases with the photon energy slowly and for the absorption of long wavelength part of sun spectrum, the material with the thickness in the range of hundreds of μm is required.

According to the long tradition and availability, most of the current PV cells is produced from crystalline silicon, also designated as the I. generation of PV. Even though, other concepts, mainly thin-film, based on other materials and technologies which will allow cost reduction, efficiency increase or technological flexibility, were and still are apparent. To understand the possible modules failures which may occur during the PV modules operation, it is necessary to know their construction, especially the PV cells material content and individual layers configuration. In the following paragraphs, the basic types with emphasis on silicon PV cells (both crystalline and amorphous) will be described.

2.1 Crystalline Silicon Cells

The base material for this cell type is the crystalline silicon wafer. According to the production technology, the following sorting can be applied:

- monocrystalline (mono-Si),
- multicrystalline (mc-Si, also called polycrystalline),
- ribbon.

During the last few decades, the production technology of crystalline silicon cells has undergone many changes. All the efforts to humble efficiency limits at this technology are made on mono-Si. Basically, there are three generations of basic mono-Si crystalline PV cells – the standard back surface field (BSF) cells, cells with selective emitter and back contacted cells.

2.2 Standard Monocrystalline PV Cells

Most of current mono-Si PV cells are still produced from silicon ingot doped by Boron (P type) made by Czochralski method [24]. After ingot creation, the wafer has to be cut into thin slices – wafers (usually by multi-wire cutting saw), and other procedures take place. The oldest group, which represents 80 % of the current market [25], is made by the procedure marked at **Fig. 10**. First, the saw damage removal by etching is done and then the creation of pyramid-like structure is formed by etching so the wafer is prepared for diffusion process. After diffusion of phosphorus, it is necessary to remove created glassy layer (phosphosilicate glass – PSG) at the surface area of the cell and edge shunt (usually done by HF). Another tool for reducing optical losses is to deposit special layer (usually SiN_x:H) which uses interferential effects. When the thickness is suitable[1], the radiation reflected by the layer interferes with the radiation reflected by semiconductor structure so the resulting reflected light is a zero and entire incident light comes into the cell structure. This layer also serves like passivation of surface recombination, because the free dangling bonds which create local recombination centres are filled.

Next step is forming the contact system. First, on the front side, the Ag paste with an addition of lead borosilicate glass frit (PbO-B_2O_3-SiO_2) is deposited using screen-printing and co-fired by low-temperature (approx. 200 °C) drying oven. Second, the back contact realized in the form of Al paste and Ag/Al paste busbars is screen-printed. The entire cell is than co-fired at

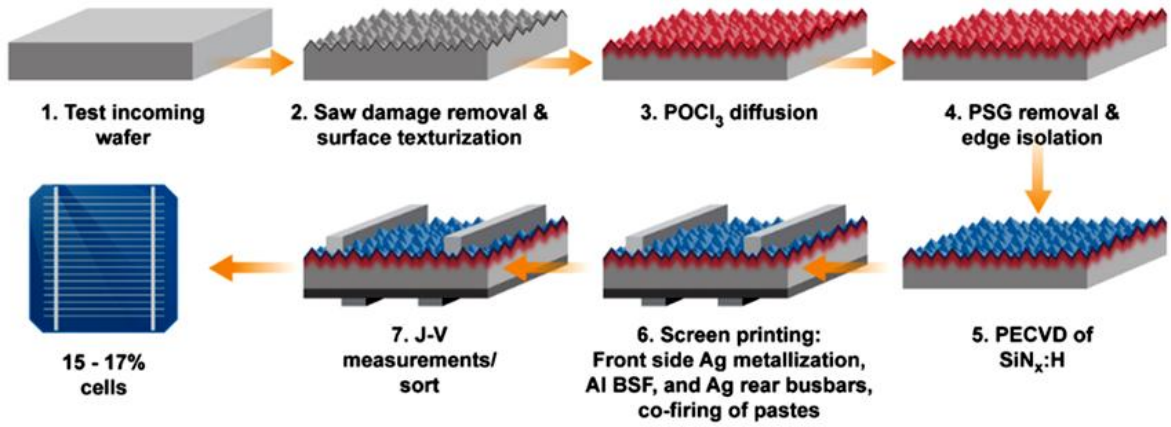

Fig. 10: Manufacturing process of basic monocrystalline PV cells [25]

[1] The thickness of this layer sets the resulting colour of the cell (usually blue). If the thickness of this layer is different than the optimal one, also different colour of the final cell can be achieved.

around 810 °C where the lead borosilicate glass frit etches the SiN_x:H layer in the area under the front gridlines, thus good contact of structure and gridlines is achieved [26]. Similarly, good contact is simultaneously created by Al paste on the back site of the cell: first, the aluminium-silicon melt is created, then, during the cooling, silicon doped by aluminium is excreted at the interface (the P^+ layer is created), and finally, eutectic AlSi, which has good contact with P^+ layer, solidifies. This layer must be created on the whole back surface because among the good contact assurance, it also prevents the recombination at the back side of the cell by creating so-called back surface field (BSF). These cells are often marked as BSF cells.

The parameters that can be achieved are summarized in the **Tab. 2** together with the comparison of the following Si monocrystalline technologies.

Tab. 2: Comparison of basic parameters of individual crystalline Si PV cells (modules) [26], [27], [28]

Parameter	BSF cell (module)	Cells with selective emitter	PERL	N-type IBC	N-type HIT	N-type HIT+IBC
J_{SC} (mA/cm^2)	35	38	42.7	42.54	41.8	42.65
V_{OC} (V/cell)	0.62	0.70	0.706	0.725	0.740	0.738
FF (-)	78	80	82.8	83.3	82.7	84.9
η (%)	17 (14.5)	20-22 (18.7)	25 (-)	25.7 (-)	25.6 (23.8)	26.7 (24.4)

2.3 Improved BSF Cells – Cells with Selective Emitter

For bettering the parameters of basic cells, there are many ways, some of which are also sufficiently cost-effective. One of the most important ones is the creation of special emitter layer which is heavily doped than the rested area of the emitter thus to allow channel the generated electrons-holes to their appropriate electrodes. The principle of function of this layer is based on creation of high built-in potential profile that will separate the holes and electrons quickly. It is located under the busbars, so the generated charge carriers flow quickly out from the cell and the possibility of their recombination is than lowered. The vicinity of surface also leads to higher utilization of charge carriers generated in this area, which consequently influence the quantum efficiency of blue photons.

This layer, designated as "selective emitter", is usually created by screen-printing and consecutive fire process of special dopant paste placed directly at the area of the future busbar position, or can be deposited at the whole surface and then etched at the places where the metal contacts will be located. The differences from the previous manufacturing process are apparent from the **Fig. 11**.

"Selective emitter" concept and its construction were inspired by the well-known PERL – "Passivated Emitter Rear Locally Diffused" structure, which kept the efficiency record of single-junction crystalline silicon cell (year 1999 – 25.0% efficiency under STC) until 2017. The PERL cell structure is shown at the **Fig. 12**. The base of the cell is created by mono-Si made by Float zone technology [30] which ensures lower oxygen contamination, but it is very expensive. Next production process is similar to the one used for cell described above (term passivated emitter corresponds with selective emitter in this case) but there are significant differences which allow performance increase (see **Tab. 3**).

Similar principle as selective emitter at front side is used also for bettering the parameters of rear side of the cell, where the special layer for surface recombination is used. In standard

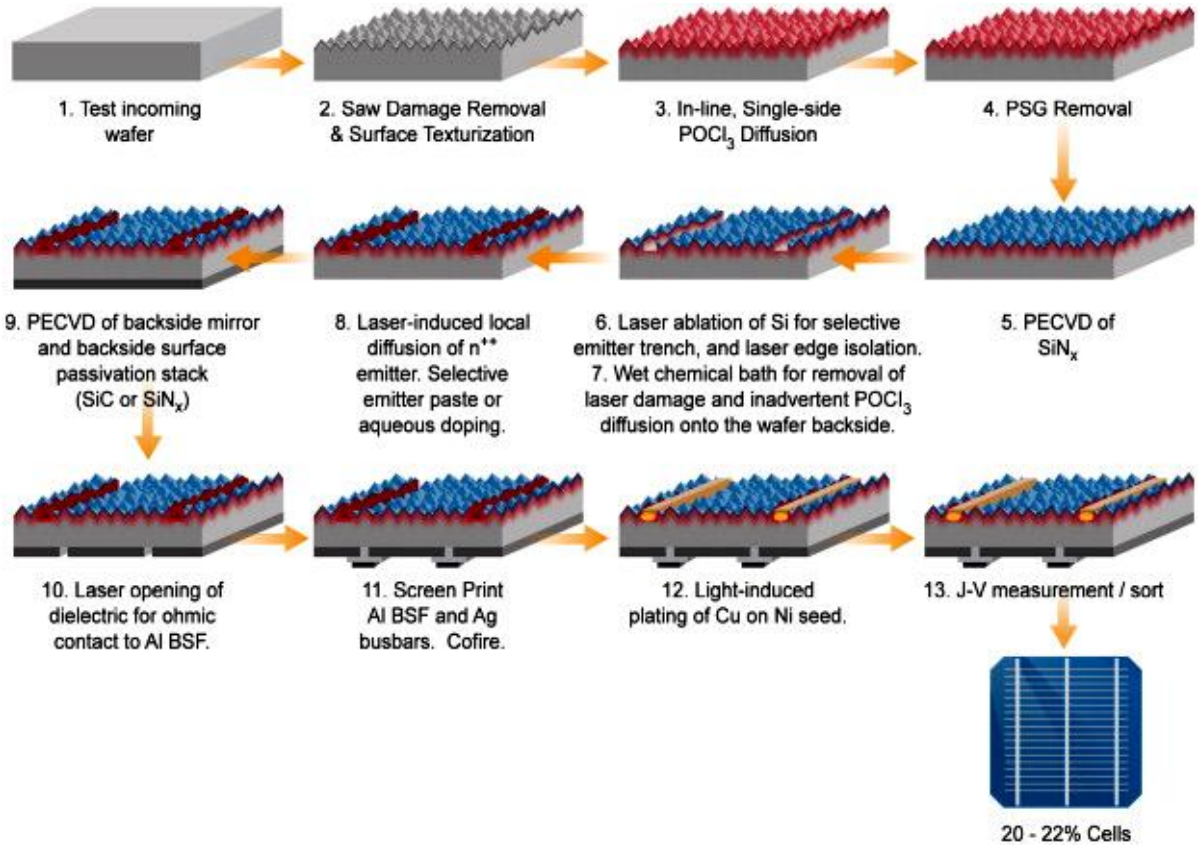

Fig. 11: Manufacturing process of cells with selective emitter [26]

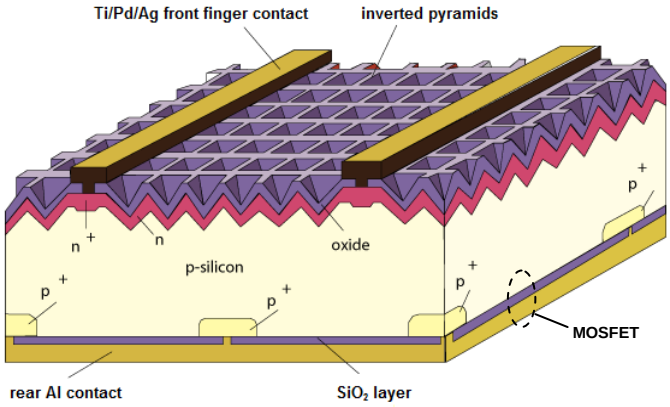

Fig. 12: PERL PV cell structure [32]

Tab. 3: Technological differences between PERL and common cell [25], [27], [31]

Technological aspect	Common cell	PERL cell
Thickness of the cell	120 µm – 150 µm	370 µm – 400 µm
Silicon quality	High purity	"solar grade" 6N
Monocrystalline ingot	Czochralski method	Float zone method
Antireflection coating	SiO_2 single layer	Double layer (ZnS and MgF_2)
Texturation	Pyramids like structure (by etching)	Inverted pyramids structure (by photolithography)
Front metallization	Screen-printing/LGBG	Ti/Pd/Ag – photolithography and evaporation
Rear side passivation	SiN_x:H, a-Si:H, SiC or Al_2O_3 in combination with Al metal	$Si0_2$ in combination with local Boron diffusion and Al metal

cells, only back surface field created by Al dopant was used. This allows lowering the surface recombination velocity (SRV) to relatively satisfactory level – about 200 cm/s when optimized, but in comparison with PERL structure, it is approximately one hundred times higher. SRV reduction was achieved using dielectric layer insertion between the Al back contact and substrate, which behaves then like MOSFET and therefore creates extra field to repel the charge carriers from recombination traps. PERL structure has moreover the locally highly doped (by boron) areas around the Al contact layer which further reduces the recombination around the contact [33]. The Al layer can be realized in the form of screen printed grooves (localized at holes made for this purpose in the dielectric layer) – standard cells with selective emitter, or at the whole rear surface. If the whole rear surface is used, the structure "passivated emitter and rear cell (PERC)" is created.

Another difference between standard BSF cells and cells with selective emitter lies in metallization techniques used for contacting the front cell side. While standard cells use thick-film technology (screen-printing of Ag paste), newer BSF cells use laser-grooved buried-grid (LGBG) technology where thinner layers are deposited using light-induced plating. This technology allows lower shading and also less consumption of silver.

2.4 Interdigitated Back Contact (IBC) c-Si Cells

The recent development of future mass-produced PV cells is based on back contacted cells. These cells have no gridline metallization on the front side, so there must be a different construction approach. The standard construction counts with relatively quick utilization of carriers generated near to the front surface, but when back contacted, these carriers must traverse through the entire cell to achieve the rear side contact. If the standard layers configuration is used, then carriers will quickly recombine instead of contributing in current flow. Because of this, the N-type silicon with bottom location of PN junction is used instead of P-type with P-doped layer for the base, which allows sufficient charge carriers lifetime. The relatively long trip from point of generation to contacts also causes high probability of interaction with surface and thus high SRV. For this reason, there is no passivation of the front or rear surface only, but additionally at the cell sides. This can be efficiently assured by using SiO_2 layer which is created under high temperature directly from Si cell base material. SiO_2 can also be used to separate N^{++} and P^{+} areas which are located very close to each other at the rear side of the cell (positive and negative terminals are interdigitated there). Other technological aspects are very similar to BSF cells. Resulting structure and technological process is apparent from the **Fig. 13** and **Fig. 14**.

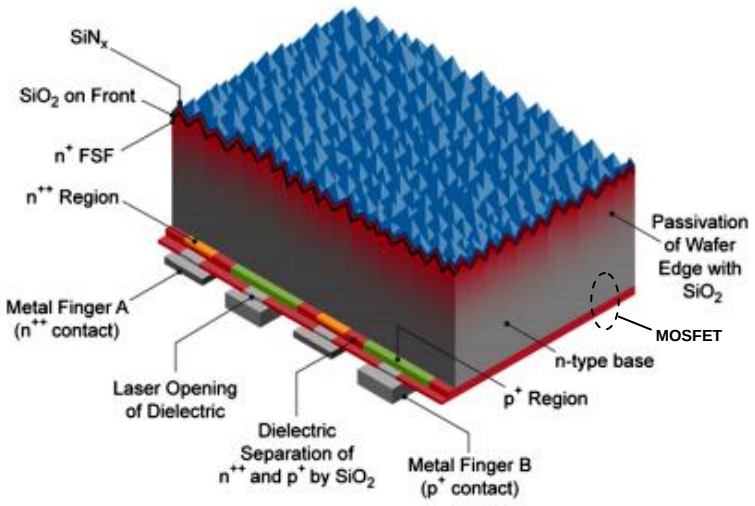

Fig. 13: IBC c-Si cell structure [25]

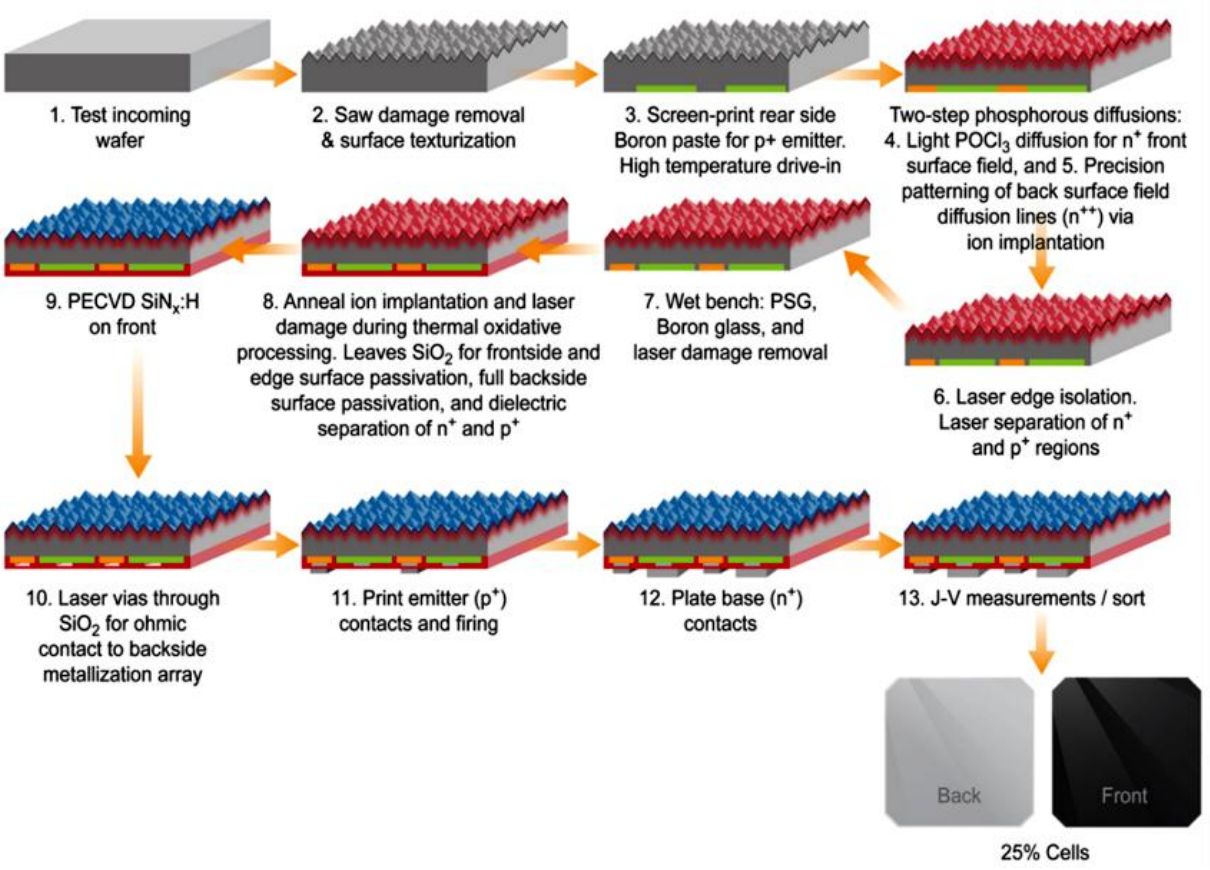

Fig. 14: Manufacturing process of IBC c-Si cells [25]

Very interesting modification of IBC structure is the utilization of tunnel oxide passivated contacts which leads to higher V_{OC} and thus to higher efficiency [30]. Currently (from 3/2017), this technology keeps the efficiency record (25.7 %) of single-junction crystalline silicon cell [28].

Other PV cells technology improvements by addition of a next layer to c-Si base to create multijunction cells have been achieved. As the first representative of this group, the heterojunction with intrinsic thin layer cell (HIT) can be considered. First, they were produced only by company Sanyo, later Panasonic (protected by patent), but now they are produced by other companies as well. Its weakest link is the contacting system, which was recently improved by IBC technology adoption. The result is the new efficiency record of 26.7 % (from 3/2017) [28].

2.5 Multicrystalline Si PV Cells

Multicrystalline PV cells are produced from multicrystalline silicon wafer using similar procedure to the one used for mono-Si cells production. The biggest difference comes in the

beginning of the production process, where the ingot is created. Although monocrystalline PV cells are made mostly by Czochralski method which is relatively complicated, mc-Si ingot is produced by slow cooling of molten Si in large crucible. The slower cooling of the ingot is the larger grains creation can be achieved. The final ingot is then a composition of individual crystals – grains. The grain boundaries then cause a recombination which significantly influences the final efficiency of the whole cell, so the passivation process of these recombination centres as well as surface recombination is crucial. Similarly to mono-Si cells, SiN_x:H antireflection layer produced by PECVD is used. During this deposition, SH_4 and NH_3 react and create the required SiN_x layer at the surface of the cell, but a massive hydrogen production also occurs [1]. Hydrogen can serve like a passivation of both surface and bulk defects, including grain boundaries, so the final recombination caused by these defects is minimized to sufficient level. Multicrystalline PV cells, with 65 % of market share [25], represent currently the leading PV technology.

2.6 Ribbon Silicon Cells

This special type of multicrystalline PV cells the ribbon cells are. These cells were predominantly produced in the past because of the high price of crystalline silicon in previous years. Nowadays, there is only a small amount of PV modules in the operation that use this technology (namely producer Evergreensolar).

Among the silicon cells, there are also cells made from other materials, which are for a high price used only for special purposes e.g. in aerospace applications (InP, GaAs) or concentrator systems.

2.7 Module Production

For the basic single-junction crystalline PV cells the voltage of one cell in operating point is about 0.5 V. This voltage is too low for the practical utilization and the serial connection of more cells is necessary. The serial or serial-parallel connection is then called photovoltaic module. During the operation, the cells must also bear the environmental conditions as well as other mechanical stress, so the cells encapsulation should be done. This is ensured by the lamination process when the cells are hermetically encapsulated by highly transparent folia (mostly Ethyl-Vinyl-Acetate – EVA) together with a front cover glass and back sheet foil (mostly based on tedlar). The created sandwich structure is mounted into the Aluminium

frame and gird with junction box. The final efficiency for serially produced common PV modules is about max. 18 %.

The procedure of individual PV cells connection and encapsulation is essential for the future PV module reliability. The first step is PV cells connection. There are more procedures which are used for doing this. The most common one is soldering. Every cell is equipped with busbars which serve both for current collection and cells interconnection. For connection, the cuprum ribbons are used. These ribbons are soldered to the PV cells busbars using lead-free Sn solder. Another process which is currently used for cells connection is based only on pressure application. There are only gridlines at the cell (no thick busbars) and the contacts are provided by the thin metal wires which are forced down to the cells surface. In both connection procedures, the applied force must be precisely controlled because possibly dangerous (from the point of view of reliability) cracks can appear.

The second step is moving the substrings to the encapsulation folia and finishing the connection process. The substrings are connected into one module by thicker busbars using soldering. Than the encapsulation process follows. During this process, the whole sandwich structure (backsheet foil-encapsulation folia-PV cells-encapsulation folia-glass) is put into the laminator (pressing machine) and heated to 110 °C – 120 °C (lamination) for 4 to 10 minutes and then to 140 °C – 150 °C (curing) for 6 to 30 minutes (temperature and time depends on the encapsulation foil type). The temperature and time adjustment is very important, because the wrong setup of these factors can lead to yellowing, and consequently to transmittance losses, of encapsulation folia in the future. During heating, the encapsulation folium polymerizes and becomes transparent. The crucial parameter is a good vacuum during this step (before the encapsulation folia is melted) and also the proper pressing of the cells substring. There are many problems which can occur during lamination process, like inhomogeneous pressure, temperature distribution or unclean environment. All of these mistakes can lead to delamination of the module during the operation which may worsen the isolation state of the module. Another important step is the isolation against the moisture and water ingress in the edges of the module. This is usually done by the polybutyl or silicone sealing around the whole module edges. Wrong sealing can also lead to PV module delamination and thus to the module failure.

The last step is the connection of junction box with bypass diode (Schottky diodes) and finally, the inspection of the final product.

3 Thin Film Cells and Modules

In order to save materials (and thus costs), thin-film PV modules have been developed. These modules, against conventional crystalline modules, have the lower conversion efficiency. But this is offsets by lower prices (production is less materially and usually less technologically demanding) and improved properties at low irradiance levels. Currently, their low price is considerably questionable, because thanks to rapid development of photovoltaics worldwide, there has been so significant reduction in the production costs of conventional Si crystalline modules, thus thin film modules will very difficult to compete them.

Thanks to their properties, thin film (TF) modules are achieving higher annual revenues against crystalline modules, especially in diffuse irradiation, so their use for example in the Czech Republic is suitable for all applications, where there is no limitation of the installation surface. Another advantage is the possibility of deposition on multiple kinds of substrates, enabling production of e.g. flexible PV modules. On the other hand, their space severity also causes the higher demands on BOS (balance of system components), so thanks to the current low price of c-Si cells the price of the entire TF photovoltaic system may be higher.

During the production, the layers are deposited on the substrate and the cells are formed by scratching (usually using the laser). By suitable scratching procedure the cells are directly serially connected without the need of a consecutive soldering process. Contacting of the cells is realized by specialized large band gap semiconductor structure - transparent conductive oxide (TCO), deposition. Thanks to the cells shape and configuration, usually long narrow strips, the modules are less sensitive to shading than conventional crystalline modules (if the entire strip is not eclipsed). From the viewpoint of the material, it is possible to divide modules into:

- $CuInSe_2$ (CIS), Cu(In, Ga)Se_2 (CIGS) a $CuGaSe_2$ (CGS) modules,
- CdTe modules,
- amorphous and micromorphous silicon modules,
- other thin-film cells.
    - multi-junction cells,
    - cells using nanostructures,
    - organic cells.

The description of individual technologies is relatively complicated task due to the variations of individual producers. Furthermore, there is a description of three main technologies, which are used for electricity production (technologies used at PV power plants).

3.1 CIGS Modules

The modules based on this technology were first introduced in 1970s. Since then it went through a rapid development. The most impressive change was achieved by using soda-lime glass instead of ceramic or borosilicate glass. This step was initially done due to a cost reduction, but the indiffusion of sodium ions inside the structure led to higher modules performance. The structure of current type of CIGS modules is usually divided into two groups – with CdS buffer layer and Cd free technology. The structure of the cell is apparent from the **Fig. 15**.

The production process of the module is the following:

1) Substrate, usually glass, is covered by the Mo layer using DC sputtering.
2) Laser pattering to create individual cells.
3) Cu(In, Ga)Se_2 absorber co-evaporation
4) Buffer layer creation – CdS + i-ZnO or Al:ZnO + i-ZnO
5) Pattering (often mechanical)
6) Deposition of front contact – ZnO:Al, by DC sputtering
7) Pattering
8) Bonding of metal tapes – contacts
9) Encapsulation and sealing – polymer + glass + desiccant-type tapes

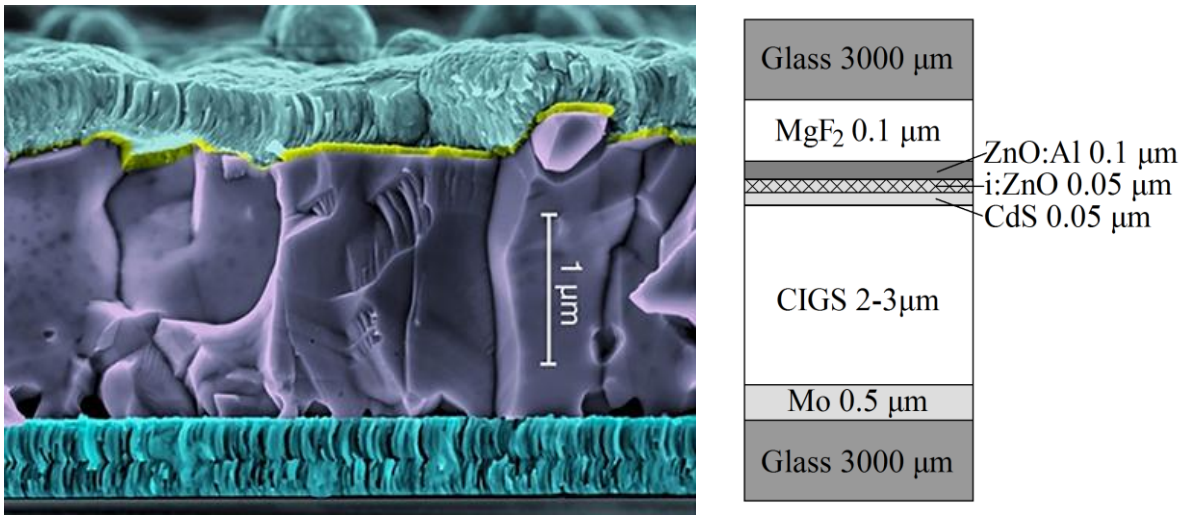

Fig. 15: Currently used CIGS structures [34]

At the beginning of 2000s, there was a strong initiative to use CIGS material. There were many prognoses which promised bright future to this material, especially in the USA, but then the year 2008 came and the drastic decrease of the price of crystalline silicon started the suppression of development in this area. However, there are still some producers with relatively significant contribution to PV modules production.

3.2 Micromorphous Silicon Modules

Micromorphous silicon modules are tandem modules based on amorphous silicon technology. The structure of every thin-film silicon module is not simple PN junction, but P-i-N structure. This is caused by the fact that the carriers generated by the absorbed light in the doped region would recombine very quickly (large amount of recombination centres), so there is an effort to generate as many carriers as possible in intrinsic layer where the concentration of recombination centres is far lower. The built-in potential then causes the drift of generated carriers to the appropriate region where it becomes the majority carrier. The carriers generated inside the doped layer can be considered as wasted, so this layer must be far thinner than the intrinsic layer. The efficiency of the simple single-junction device is very low, so the use of tandem cells is usual in this case. The first one were tandem of a-Si:H (amorphous silicon layer must be hydrogenated, otherwise large amount of dangling bonds serving like recombination centres would remain in the structure) with a-SiGe, but a-SiGe requires germane (GeH_4) gas which is expensive and toxic. So this material was replaced by the nanocrystalline, usually designated like microcrystalline layer and the resulting structure is called micromorphous. The structure of the common micromorphous silicon tandem cell is shown in **Fig. 16**.

3.3 CdTe Modules

The last technology which is used in industrial scale (meaning for the electricity production) is CdTe. Practically, there are two significant producers – Calyxo and especially, First Solar. The production is very like the other thin films. Although it consists of toxic Cadmium, there are a few advantages which still predominate this fact. First, its efficiency is currently about 16 %, so it is very close to the crystalline silicon technologies. Second, its annual yield, especially in middle Europe's cloudy climate, can be even higher by 10 % than the crystalline silicon PV modules. The basic structure of common CdTe module is given on the **Fig. 17**.

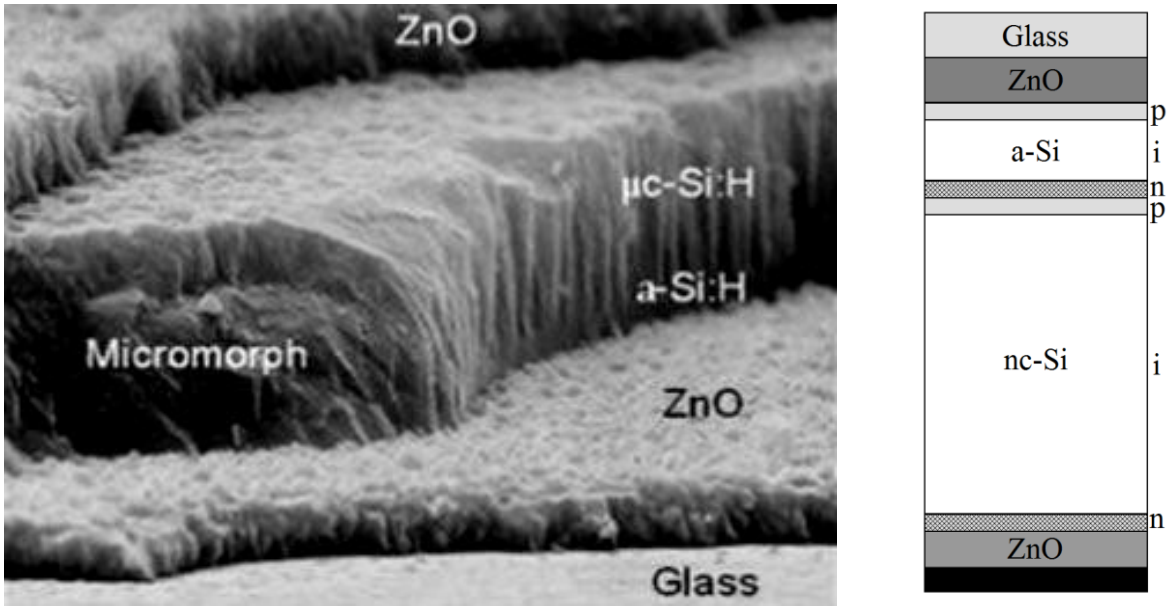

Fig. 16: Typical structure of micromorphous silicon tandem cell [35], [1]

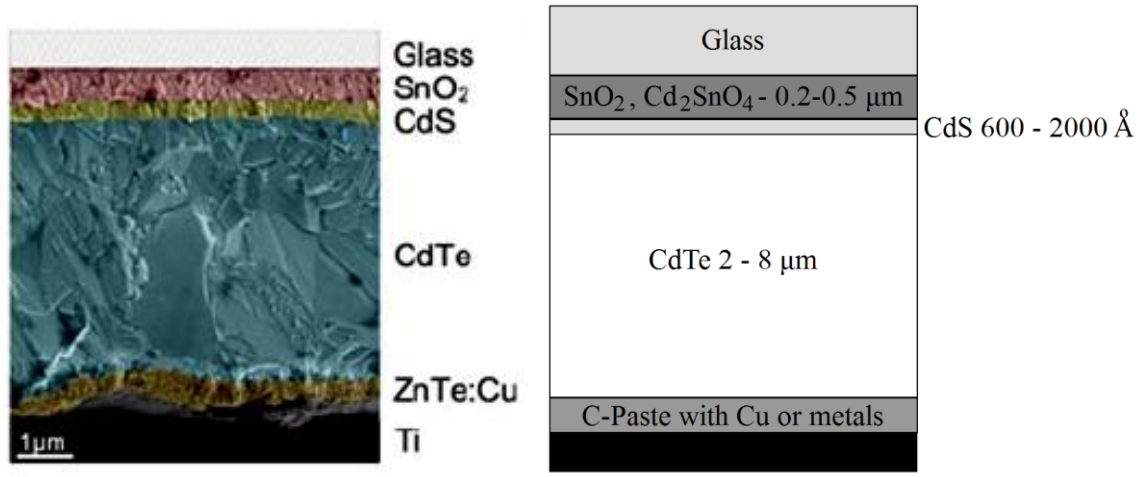

Fig. 17: Typical structure of CdTe PV module [36]

4 PV modules defects and degradation

There are many defects that can appear during the PV modules lifetime. Some of them have origin in the manufacturing process and others can be caused by wrong maintenance or even installation. The key parameter for defects evaluation is the performance, which is also the most important parameter for systems operators (performance represents money in the end). PV modules manufacturers usually declare the performance decrease to not exceed 0.8 % for one year. Some of them guarantee this decrease to be linear, the other ones have the performance limits typically after 10 (12) and 25 years of operation (rarely after 30 years). This warranty counts with the performance decrease caused by the common operation which also includes some types of defects like microcracks inside the cells which cannot be avoided. Contrarily, there are some other defects which can cause significant decrease in performance and should be recognized and diagnosed in time to avoid larger losses of system as well as money.

There are many approaches to PV modules defects classification. In the following paragraphs, the distribution according to the defect position based on the document [37] is presented.

4.1 Defects of the Frame

Most of the PV modules are, apart from the glass, protected also by the aluminium frame. Its advantage is a relatively easy montage at the system; disadvantage is its price, which is relatively high.

The frame can be damaged by the mechanical stress caused e.g. by the wrong maintenance or wrong design of supporting constructions. The consequence is the loss of PV module integrity which leads to the risk of the occurrence of problems connected with the isolation state of the module. A damaged frame always leads to replacing the module.

4.2 Glass Defects

The glass which is usually used for covering the modules can be divided into two groups from two points of view:

- according to the location – front glass and back glass,
- according to the texturation – smooth glass and patterned glass.

The modules produced from crystalline silicon usually use only one cover glass – front patterned glass (as mentioned before) or they can use also the back glass, if they are bifacial. The thin-film modules are often frameless, so they use front and back glass as well. In this case, they are smooth (there is no reason for texturing the glass, because thin-film module works with both the direct and diffuse irradiation). Defects of glass are explicitly caused by the damage because the degradation rate of used glass is too high to be important during the usual PV modules lifetime (special soda-lime low iron glass is used).

4.2.1 Front Patterned Glass Defects

The usual damage of the front textured glass is the breakage of the glass caused usually by the local mechanical stress – hail impact, stones flying while mowing grass. In case the damage has been caused by the long lasting mechanical stress, the breakage looks very similar, but there are no apparent impact zones. In this case, the wrong construction is usually the initial cause of such a defect. The front cover glass is tempered, so both local stress and surface stress will lead to the breakage of the whole glass. Luckily, the encapsulant serves like glue in this case, so the mechanical integrity of the module still allows easy replacement of the damaged module, which is unavoidable because of safety risk and isolation state. The example of the damaged front glass caused by the stone is shown in the **Fig. 18**.

Fig. 18: Front glass damage caused by a stone

4.2.2 Defects of Glass at Glass-Glass modules

The situation is different when the glass-glass module is damaged. These modules are usually frameless which results in a relatively high risk of damage by the punch at the edge of the module, especially at the corner. Whereas in the previous case, the whole glass is broken, the glass at glass-glass structure behaves differently. It is due to the fact that the front glass can be tempered thermally or chemically and the back glass is not tempered, so the damage at the back side of the module creates only long lines. The usual cause of defects of glass-glass

modules is the mechanical stress caused by mounting clamps and by the wrong maintenance. The consequence is the same as the previous case, a replacement of the defective module. An example of broken front and back glass is given in the **Fig. 19**

Fig. 19: Front glass damage caused by the stone and back glass damage caused by edge punch

4.2.3 Cables and Connectors

Cables at PV modules should be able to hold relatively heavy loads; they are even tested on the endurance against the mechanical stress. The most critical moment when operating is the instant when the PV module is being disassembled from the system. When the sun shines, the voltage at the string is about 500 V or higher and the current flowing through is in the order of units of Amperes. When the module is getting disconnected from the string, then the electric arc can emerge. Another cause of damage is the low contact inside the PV module (**Fig. 20**) which can be caused by both the maintenance and manufacturing, and can even lead to fire. Installation in the areas with the air pollution can also be problematic, because the plastic materials degrade quickly.

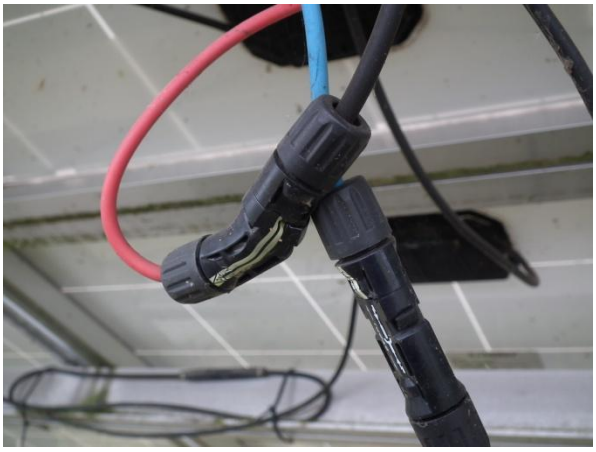

Fig. 20: Thermally damaged connector

4.2.4 Junction Box Defects

Junction box is located at the rear side of the module and serves as an interface between the internal module circuit and the connectors. That is also where bypass diodes are located. Usually, there are no problems with the junction box itself, but its damage can be caused by the following causes:

- destroyed bypass diode (produces heat),
- wrong connection between the modules busbars and the cavity for cable connection,
- wrong sealing of the box causing the water ingress.

a)

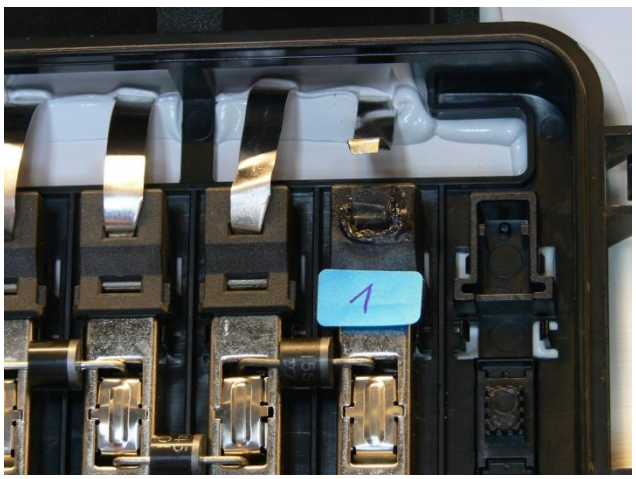

b) **c)**

Fig. 21: Junction box destroyed due to: a) bypass defect b) wrong connection, c) the water ingress

4.3 Encapsulant Defects

There are two basic defects apparent at the encapsulant foil – delamination and yellowing.

4.3.1 Delamination

The delamination process is usually connected with the manufacturing defects, or rather with the technological indiscipline. Delamination itself, when in low level occurs, doesn't represent any serious endangering of the future reliability of the system, but if it occurs between the PV cells and the edge of the module, the problems with isolation state of the module will arise. Such a case is also interpreted as the major visual defect and is a reason for replacing the module at the system.

Delamination can take place between the encapsulant and the cell or, rarely, between the glass (front glass or backsheet foil) and encapsulant (**Fig. 22**). In both cases, there is a risk of the water ingress. The most critical part of the module from the point of view of delamination is the edge of the module. In case of frameless modules, only a layer of the sealant is present and it can be wrongly deposited.

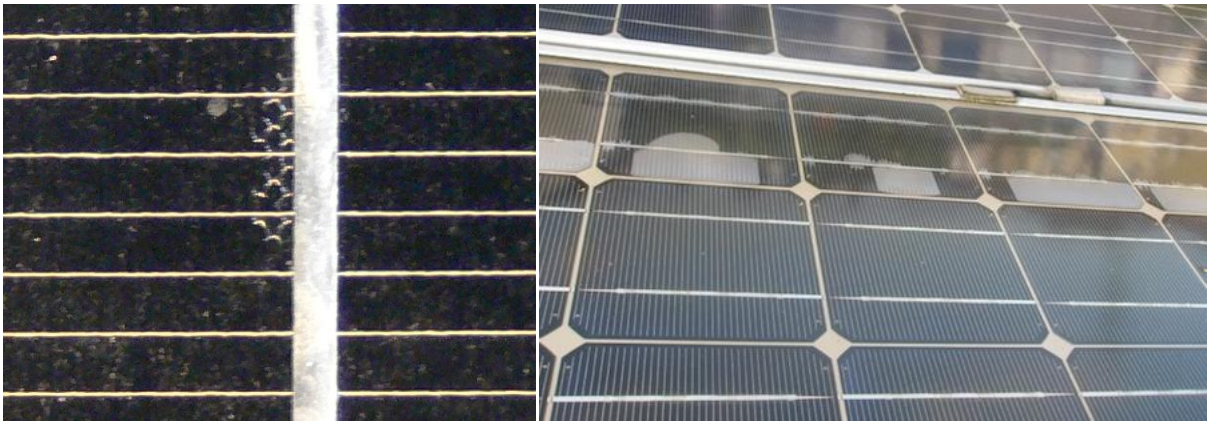

a) **b)**

Fig. 22: Delamination between the: a) encapsulant and cell (early state), b) glass and encapsulant

The special case, where different shape of encapsulated parts is visible, thin-film modules represent. While delamination occurs first in the form of bubbles and later bands in crystalline modules, the worm-like traces (**Fig. 23**), which can gradually affect the whole area, can be seen at thin-film modules.

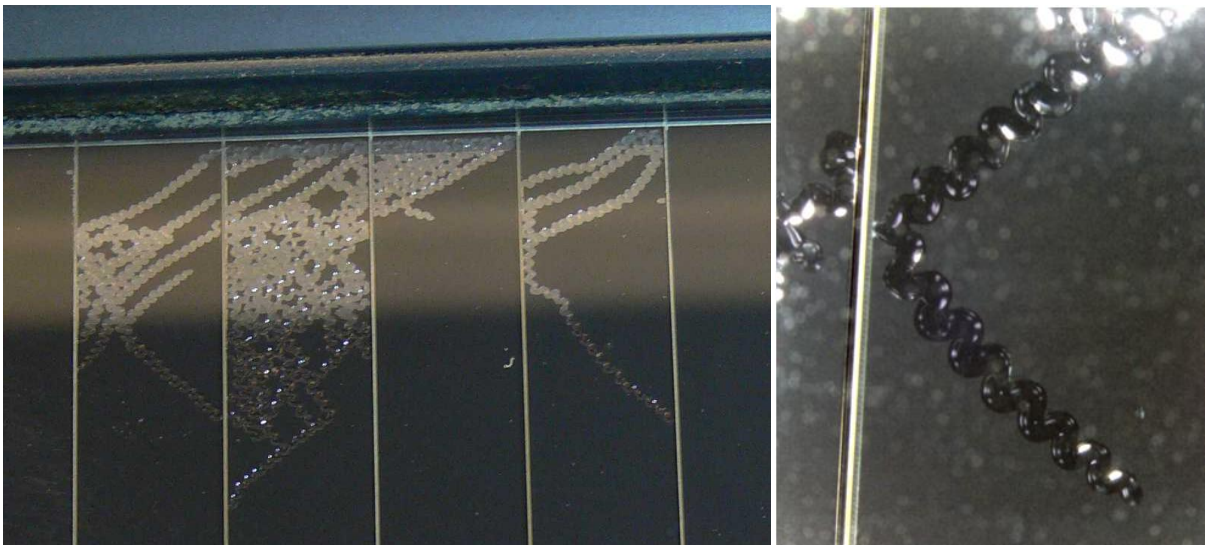

a) **b)**

Fig. 23: Delamination of thin film module: a) global look at affected area, b) microscopic picture

Delamination process, in the case of thin-film modules, can be caused either by the wrong encapsulation or by the damaging of the layer edge (it spreads over cracks) or by the TCO corrosion. The TCO corrosion also causes the series resistance increase and therefore can be diagnosed by electric methods.

4.3.2 Yellowing

Yellowing is a very common defect which occurs mostly at crystalline PV modules. Although it doesn't contribute to the degradation rate significantly, it is very often discussed between PV system operators. Its occurrence is connected with higher temperature and the acetic acid presence (created thanks to substances inside the encapsulator, namely EVA).

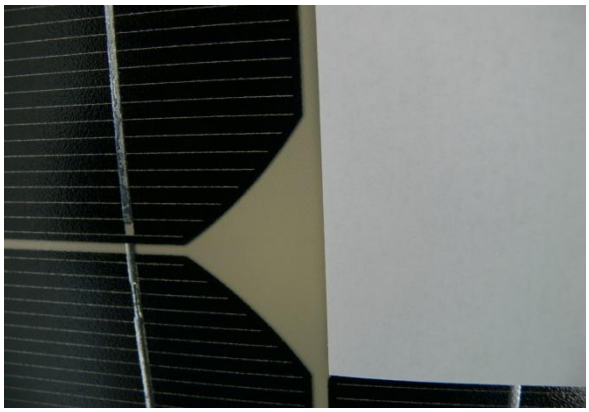

Fig. 24: Example of EVA yellowing – comparison with white paper

4.4 Backsheet defects

A very important part of every module is the back covering foil – backsheet, usually tedlar. Tedlar is the brand name of the company DuPont and refers to polyvinyl fluoride (PVF). Usually the backsheet consists of more than one layer, typically three: Tedlar/Polyester/Tedlar, but the designation "Tedlar" usually covers the whole group of Tedlar based backsheets. This layer serves as a very reliable protection of the PV module rear side. Its defects are usually connected practically exclusively with the mechanical damage (see **Fig. 25**). If such damage is caused by high temperature occurrence, then also other parts should be damaged. Therefore it can be easily recognized by basic diagnostic methods. The problem lies with the mechanical damage caused by some mechanical stress like stone impact. In this case, the whole module works properly and only a negligible hole is apparent at the module. The problem is that this defect can cause water ingress, so it is a serious problem after all.

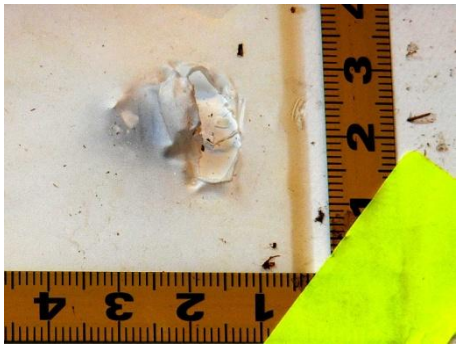

Fig. 25: Example of mechanical damage of Tedlar backsheet

4.5 PV Cells Defects

The major group of defects present at PV modules creates defects of PV cells. There are plenty of them, some of them more serious and some of them not. There are also publications which deal with the sorting, e.g. [37] or [38].

4.5.1 Hot-spot

Hot-spot is the small part of PV cell which is overheated. In the first instance, it doesn't influence the PV module parameters, thus it is problematic to diagnose by electrical measurement. In the second phase, it is so serious it can cause the destruction of the whole module (melting of tedlar or EVA, explosion, fire) – see **Fig. 26**. Hot-spot can be caused by faulty interconnections (soldering or adhesives faults) or by the long lasting shading.

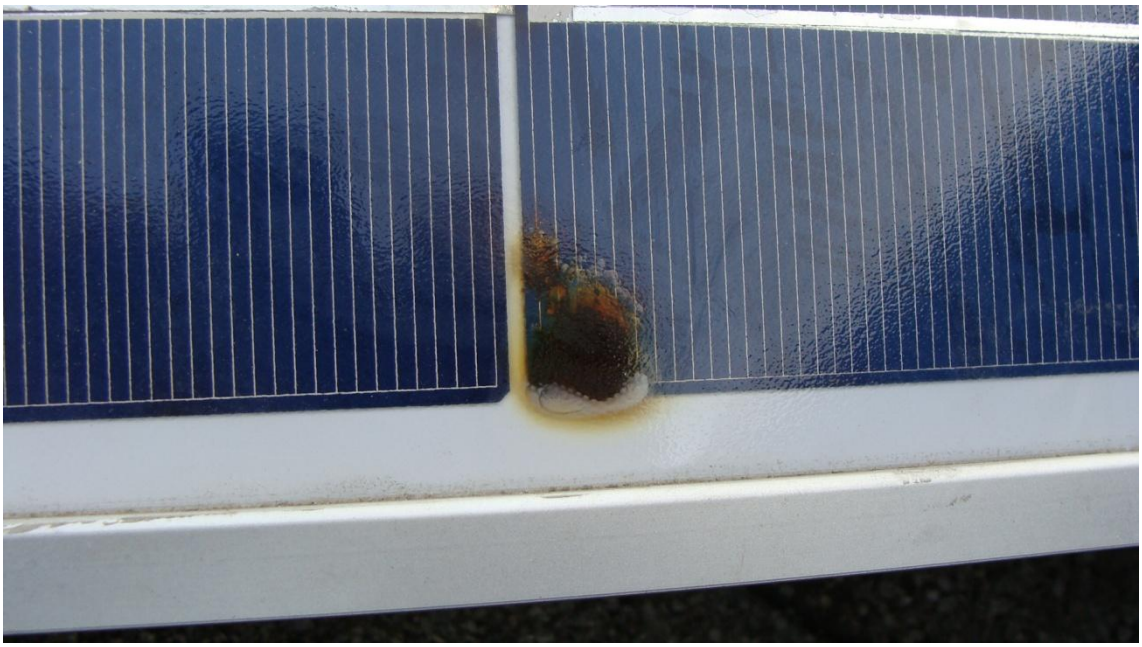

Fig. 26: Example of hot-spot

4.5.2 Cracked Cell

A very common defect is the crack inside the cell. Usually, they are not visible by the naked eye (microcracks), so other methods, like electroluminescence have to be used to reveal them. Actually, in case of the older modules – produced during the years 2008 – 2012, the cracks were visible sometimes due to the so called "snail trails", but this defect is currently well known and usually doesn't represent any reliability lowering. Although there are also the cases, where the damage is so extensive that they will occur (**Fig. 27**).

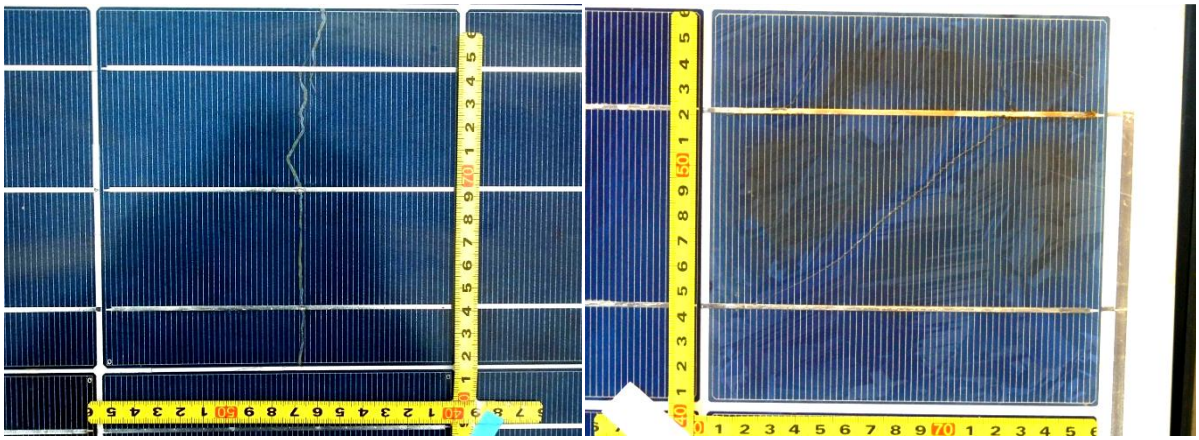

Fig. 27: Example of visible cell crack (on the right, also the hot-spot is apparent)

Microcracks are usually less serious and they are covered in the product warranty (PV module manufacturer bears in mind the fact that the cracks will appear during the operation). Some of them don't represent any future performance decrease, but some of them can cause the

separation of the part of the cell and logically will lead to performance decrease (then it will also influence the electrical parameters and therefore can be diagnosed by measurement of electric quantities). This sorting is given e.g. in [38].

4.5.3 Broken Cell

This defect is visible by the naked eye (**Fig. 28**) and suggests that the module is of a very poor quality. This type of cells shouldn't be present in the A class module, because it is the B class cell. Unfortunately, it can still be found. Form the point of view of a possible influence on performance, usually less than 10 % of missing cell is tolerated by the standards.

Fig. 28: Broken cell

4.5.4 Faulty Interconnections and Joints

Very important parts of the internal structure of the modules are the conductive paths – soldered or bonded joints. If these joints are damaged due to thermal or mechanical stress, or if they were produced improperly, the series resistance increases. The result of this defect is the emergence of hot spots and excessive degradation due to rising temperatures. The examples of defective interconnections are in **Fig. 29**.

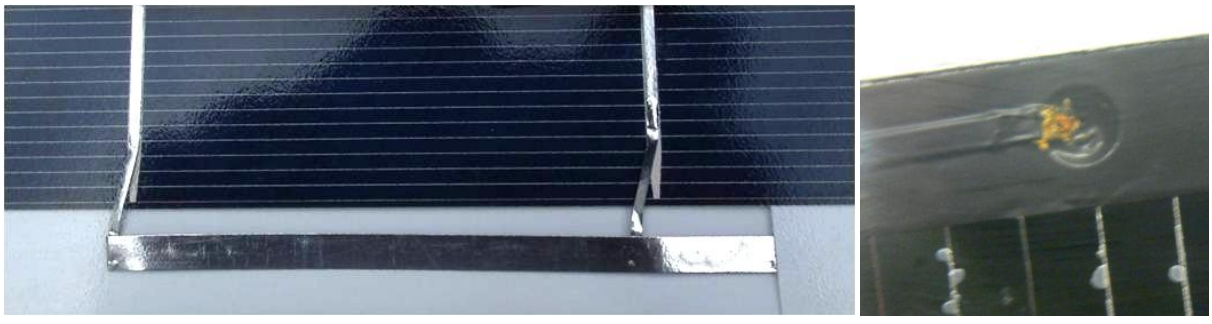

a) **b)**

Fig. 29: Defective interconnections: a) mechanical stress, b) thermally damaged

5 Common Diagnostic Methods of Photovoltaic Cells and Modules

During the whole life cycle of photovoltaic cells, or more precisely modules, it is needed to evaluate whether or not the PV devices have the declared parameters. During the time of use, i.e. the time of operation, it is necessary to perform not only diagnostics of visible defects but also preventive diagnostics which helps to detect possible defects in time and thus eliminate economical losses, e.g. possibly dangerous microcracks. There are many methods for evaluation of parameters in operation phase of a PV device, some of which have support in international standards.

5.1 Diagnostic Methods Using a Detection of Radiation

5.1.1 Thermography

When assessing parameters gained through electric measuring, it is necessary to disconnect the cells and especially the modules from the rest of the device and to measure them separately, usually in a laboratory. In case of PV modules, this method can be quite expensive as well as rather time consuming with less accessible installations. If only for this reason, the use of any method, enabling defect detection without the need of disassembly, is necessary. One such method is thermography which is frequently used in diagnostics of faults of PV installations.

The method works at a principle of detection of thermal irradiation using an appropriate detector. The cells in the module are connected serially. Therefore if we consider an ideal state where all the cells are identical, the same current flows through them while having the same voltage, i.e. they have the same short circuit current I_{SC}. When the short circuit current flows through all the cells, the voltage is zero. In case of one faulty cell, the current and voltage proportions in the circuit change. The cells don't deliver short circuit current and as is apparent from *I*-*V* curve (see **Fig. 2**), the voltage on their terminals increases. Given that the overall voltage in short circuit state has to stay zero, the damaged cell is reverse polarized towards other cells and the voltage in it is the total sum of voltage of other cells in forward direction. According to the equation $P = V \cdot I$ it is evident that, to damaged cells, incoming current causes a considerably higher performance loss converting into heat then in case of undamaged cells. In case of the real operation, the cells function on a level of the highest output, but the mechanism of heating of the damaged spots is identical. The whole process is apparent from the **Fig. 30**.

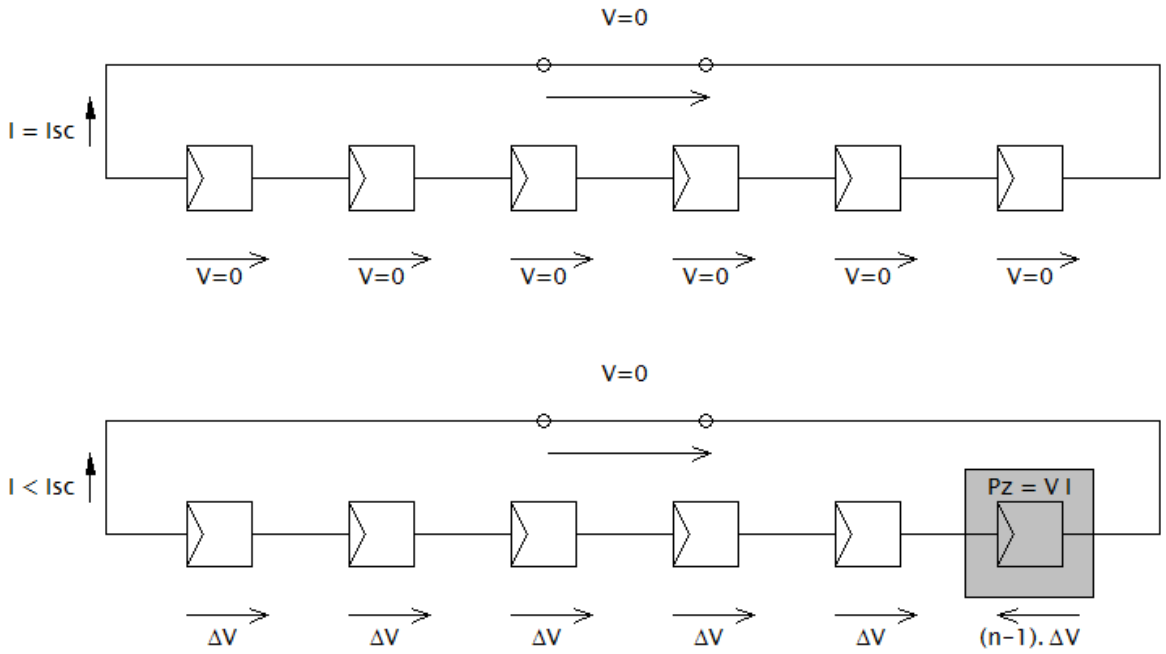

Fig. 30: The principle of defective cells heating

This effect can be caused either by the defect in the cell or by shading. For a reduction of this influence so called bypass diodes are used. These diodes open in case the voltage drop in a reverse direction exceeds their threshold voltage V_B (**Fig. 31**).

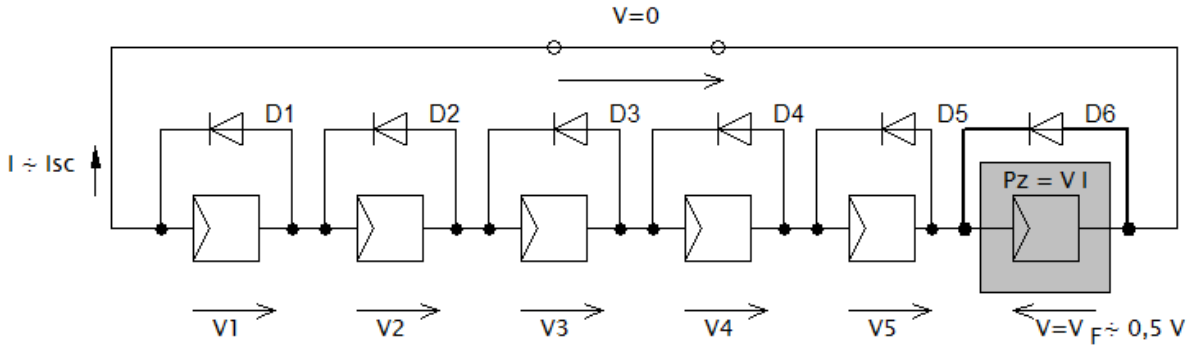

Fig. 31: Influence of bypass diodes at the function of PV modules

The bypass diode is not used for every single cell in the actual modules but it has an antiparallel connection to a group of serially connected cells (usually 20 to 24 cells). Bypass diodes are located in the junction box. The usual amount of such segments in one module and also the amount of diodes is three. By-passing the defective/shaded part, the losses rapidly decrease and the affected part of the module is partially protected against the overheating and consequently destruction. Important fact is that when the modules are connected into the strings, there is no current limitation in the whole string, but only the decrease of voltage in one module. This voltage decrease can affect also the voltage of all connected parallel strings,

but in the real situation, such decrease can be almost neglected (when single). The functionality of the bypass diode is also apparent from the *I-V* curve, where the "stairs" will occur, which can complicate the detection of MPP, because more than one local extreme is then present at the curve (**Fig. 32**).

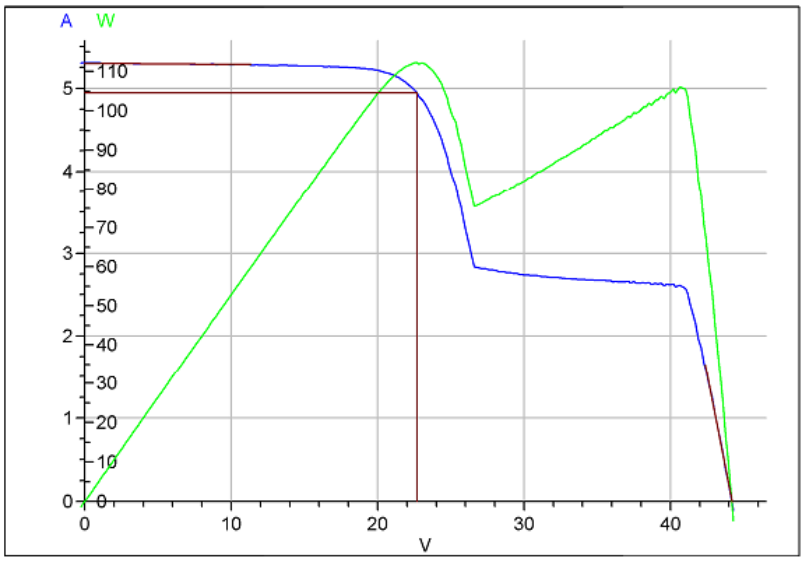

Fig. 32: *I-V* curve of PV module with one partially shaded cell (measured under STC)

The distribution of temperatures can be detected by the use of appropriate equipment. Reading of thermal field used to be done by thermometer (whether they were contact or contactless). These days, thermocameras are broadly used thanks to the drop in their price.

Detection with the thermocamera allows uncovering a wide range of defects. However, the disadvantage is that the thermogram does not provide a quantitative assessment of the examined module.

5.1.2 Electroluminescence

Another very useful diagnostic tool is electroluminescence (EL). This method is utilized for cells and modules defects like cracks (the usual short is than ELCD - Electroluminescence Crack Detection Test), technological defects and other inhomogeneities evaluation. Thus it can also serve as the visual evaluation of the modules. It works at the principle of electroluminescence radiation detection which is emitted by recombined charge carriers during the radiative recombination process. The equipment should be located in a place with sufficiently low irradiance (the dark room is the best) and the sensor must be a special sensor which allows detection in near IR area (the radiation of PV modules has the wavelength of about 1 μm). The usually used sensors are cooled CCD (Charge-Coupled Device), CMOS or

InGaAs sensor (these cameras are often designated like SWIR – Short Wave Infra-Red cameras). The third one has the advantage of a much higher sensitivity in the useful wavelength area, so lower exposition time can be used – in the case of CCD camera, the good EL image takes about 5 minutes, in the case of InGaAs camera, only a few milliseconds.

The PV module is connected to the current source and the current which should not exceed I_{SC} value flows through it (when higher current is used, the heat production should exceed the permitted value and the module can be damaged). The intensity of emitted radiation is dependent on this current and on lower current level, different defects will occur (very important especially in the case of thin-film modules). Places, which are affected by some damage, places with higher defects density respectively, are seen as dark places at the EL images. Such places don't contribute to electricity production. The radiation intensity is then the scale of PV module functionality.

5.1.3 Photoluminescence

This method is used for PV cells diagnostics. Unlike the EL it doesn't need the sample with the contact system, because the radiative recombination excitation is stimulated by the strong light impulse, so the method can be used like the control procedure during the manufacturing process, which can be very useful, for example, during layers deposition. The method disadvantage is the need of special sensor (like the EL case) and also much more complicated equipment for radiation excitation.

5.1.4 Microplasma Luminescence

This method provides the information about shorts inside the structure. Unlike the EL measurement, the module in this case is connected in reverse direction, but the reverse polarization mustn't exceed the breakdown voltage of the cell (similar to the case of simple semiconductor diodes). The reverse polarization in the areas affected by some defect (cracks, shorts) causes the microplasma occurrence. Microplasma manifests either like the noise (which can be electrically measured) or like the light emission. The light emission causes light places in obtained pictures, which means that these pictures are as a matter of fact inverse to the electroluminescent ones [39].

5.2 Static Characteristics Measurement – Volt-Ampere Characteristics

Volt-Ampere characteristics (*I-V* curves) measurement method, sometimes also called JV analysis or Voltammetry, is the most widespread method for PV cells and modules diagnostics. It allows determination of basic PV components parameters which were described in paragraph 1.2.1. The measurement can be performed either in a lab or directly at the installation, but it is used mostly for the precise measurement under Standard Test Conditions which are specified in international standards (e.g. [4] or [40]) like irradiance G = 1000 W/m^2, cell temperature 25°C and spectrum AM1.5. This can be achieved by using continual solar simulator or by flash solar simulator. Usually, the measurement is performed under flash solar simulator – flash tester, because it is much less complicated and cheaper solar simulator than the continual one and the pulse duration (typically within the range of 2 ms to 100 ms) is sufficient for most technologies (for some of them, this simulator is used in the regime of multi-flash or equivalent procedure). During PV component irradiation, the whole *I-V* curve through the electronic load control is measured.

The continual solar simulator is necessary only in the special cases like concentrator modules or solar thermal collectors.

For outside measurement, the solar analysers, which usually allow also connection of external sensors for ambient conditions measurement (irradiance, temperature, humidity, wind speed), are used.

During the work on this thesis, many measurements of static characteristics have been performed. Most of them were done using equipment PASAN Sun Simulator 3c with the specification of double class A tester (AA-AA-AA according to ČSN EN 60904-9) in the case of modules and Sun Sim 2b with the specification of B tester in the case of the cells. In the area of both cells and modules measurements, number of papers has been presented (e.g. [41] or [10]).

5.2.1 Specific Issues for Thin-Film and High Capacitance Modules *I-V* Curve Measurements

The most problematic part is testing thin films due to season annealing effect and high capacitance.

5.2.1.1 Season Annealing Effect

During measurement of thin-film modules, it was relatively early observed, that the performance and efficiency is very dependent on the history of operation. It means that during the operation, the module has for example MPP of 100 W (under STC). After putting it into the dark storage and measuring it again, only 90 W is measured. It was found, that the temperature and irradiance cause metastable states of PV modules which must be either eliminated or calculated when measured.

Season annealing effect covers two phenomena: light-soaking (LS) effect and temperature annealing (TA) effect. The first one is very well known especially from amorphous silicon based PV modules, where so called Staebler-Wronski effect occurs [42]. Within this effect, optically excited carriers are breaking weak Si-Si bonds leaving them free, so it means that the recombination centres are then created and the carriers lifetime is lowered. This drop occurs during the first several hundreds of hours of operation and can reach up to 30% efficiency decrease. For suppression, the hydrogen is used and also tandem cells show lower level of LS effect. The other thin-film technologies also display similar behaviour.

In many experiments it has been detected, that CdTe PV modules often have a significant increase in device performance in the range from a few percent up to 10 % within the first hours of light soaking [43]. This performance decrease can be also achieved by applying a forward biased current in the dark conditions. The CdTe modules biggest producer has its own methodology for measuring their modules, which is based on the presumption that when the module is measured between April and September, its performance should be stable if measured before the third day of storage. Positive influence of light soaking can be observed also in the CIGS modules. Unlike the CdTe modules, there is still no satisfactory theory explaining this effect in CIGS modules.

Temperature annealing always has a good influence on the thin-film modules performance. When higher temperature is applied, even Staebler-Wronski effect can be recovered.

The example of LS effect is given in **Fig. 33**, where the values before and after storing the CIGS module are compared. The other aspects of meta-stable effects will be further examined in the future.

5.2.1.2 Capacitance Effects

The modules with higher capacitance, e.g. thin-film modules, can be easily wrongly evaluated when measured by the flash tester. This is caused by charging or discharging the capacity. When the module is measured from the short circuit state (designated as forward direction), the measured performance value can be lower than the real one – the capacity is charged. During the reverse measurement – from open circuit state to short circuit state, this capacity is discharged and it can cause the virtual increase of the measured performance. If there are no visible differences between forward and reverse regime, the pulse duration can be considered as sufficiently long. The general recommendations are given in the following table [44]:

Tab. 4: Capacitive effects and recommended pulse duration – different technologies

Capacitive effect	Recommended pulse duration	Technology
NO / Low	2 ms	c-Si, CI(G)S, CdTe
Middle	> 10 ms	Technologies based on a-Si
High	> 100 ms	High efficiency c-Si

The pulse duration influence can be eliminated either by a sufficiently long pulse duration or using multi-flash measurement or also by the so called "dragon back pulse" tester of company PASAN (now part of Mayer Burger Group) who developed the special measurement method of high-capacitance modules using one single controlled 10ms pulse [45].

It's surprising how many publications were written on the topic of *I-V* curves measurements and in all cases there is only the statement about "this is due to the capacitance" without any other explanation. The problem with this behaviour is that if it is modelled like the common capacitor, it doesn't work. With larger amount of PV cells, the resulting capacitance should be

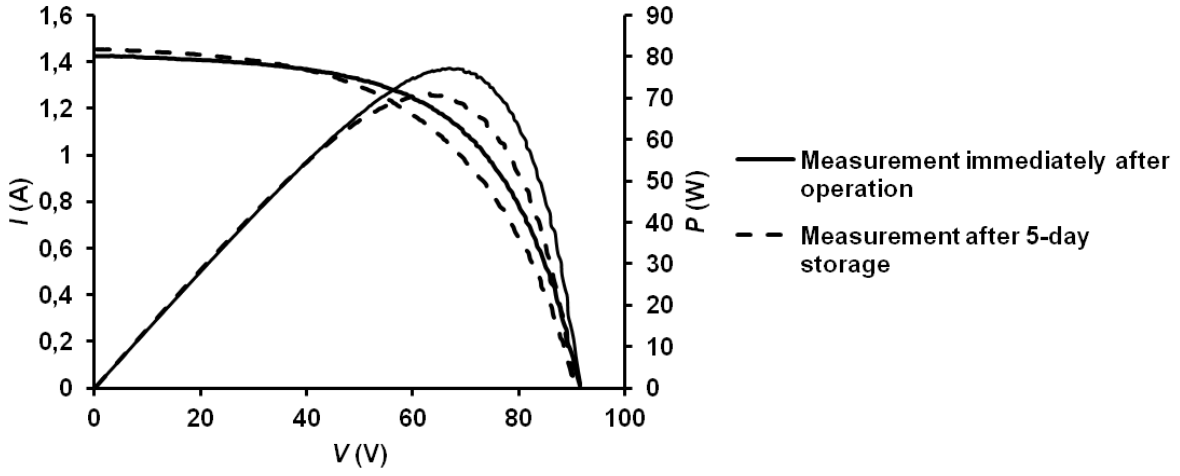

Fig. 33: Comparison of CIGS module measurement before and after storage

lower (because of the serial connection of capacitors), but the opposite situation happens. These effects can be relatively easily simulated using SPICE (parameters of the diode can be edited to achieve PV cell behaviour). Unlike the classical diode model, SPICE diode model covers these effects by "borrowing" the Transition Time (*TT*) parameter from the transistors theory. It is very useful, because this explains a lot in the connection with the "strange" behaviour of the capacitance inside the structure. During irradiation, the capacitance is in ideal case infinite - the electrodes of the virtual capacitor, it means grounds of P and N type area are infinitely close to each other. Whole area is then full of nonequilibrium carriers. These carriers need some time to leave and create the depletion region again to recover the previous equilibrium state, if the module is put into the dark again. This time, it can be characterized just by the transition time parameter, so the resulting value of serial connection of capacitors inside the module can be imagined more as the connection of batteries and some kind of transition charge. The similar effect can be achieved by changing the capacitance values, but the problem is, that this capacitance is then necessary to change for every pulse duration change, when proper values should be obtained. This is caused just by the fact that the capacitance in this case cannot be represented by the simple capacitor as mentioned above.

The measurement using different pulse duration and simulation in SPICE has been done. The example of comparison of achieved results for high efficiency multi c-Si PV module is shown in **Fig. 34**. For calculation, *TT* = 500 μs was used. From this comparison, it is obvious that the *TT* parameter can be applied. The capacitance effects and its other propagation will be the subject of further examination in the future.

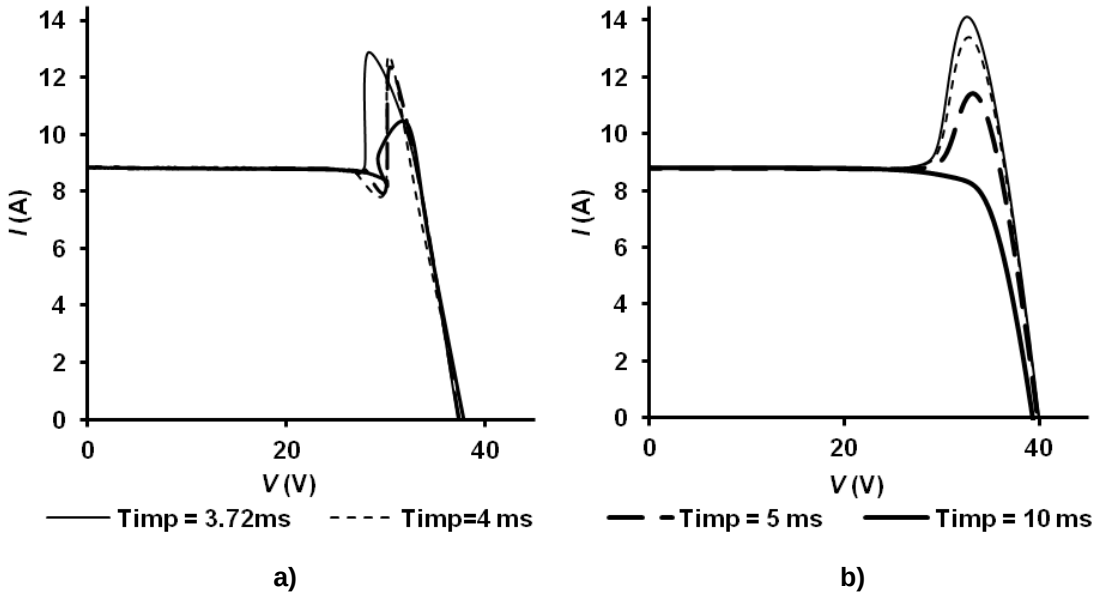

Fig. 34: Comparison of measured (a) and simulated (b) *I-V* curves of high efficiency c-Si module

5.2.2 Dark *I-V* Curve Measurement – Dark Current Measurement

A very interesting part of static characteristics measurement is the dark current measurement. This method is usually used for determination of dominant disorder and its concentration in PV cells, especially silicon ones.

5.2.2.1 Recombination Centres Type Determination

Following recombination processes inside the PV cell are possible:

- radiative recombination,
- recombination through the local recombination centres,
- Auger recombination.

In the silicon cells which have indirect band structure (unlike GaAs or amorphous silicon), the recombination caused by local recombination centres predominates. This theory is also known as Shockley-Read-Hall (SRH) theory [46]. Local centres are created by dopant atoms whose energy lies inside the cell band gap. Such dopant atoms function as local recombination centres, also called traps, which capture generated electrons during their transit back to valence band. During their passage, these electrons cannot be thermally excited back to conduction band – at first, they recombine at the local centre, then they go back to the valence band, so consequently, the resulting recombination significantly increases. Therefore, it's important to know their character, concentration and distribution. One of the methods that makes to obtain dominant disturbance energy level and its concentration possible is dark current measurement.

5.2.2.2 Dark Current Measurement – Recombination Centres Character Determination

The method is based on measuring temperature dependence of dark *I-V* characteristics. In this field, some papers were published, like [47] and also equipment for automatic measurement has been constructed [48]. Measurement was performed in temperature interval from 20 °C to 115 °C at the set of BSF mono and mc-Si cells. It is possible to determine τ, energy level of dominant disturbance E_t and its concentration N_t and shunt resistance R_{SH} by evaluation. The measurement can be performed in both voltage polarities. The cell is powered by current in interval from 0 mA to approx. 100 mA and measured values are read by computer. The evaluation is based on formula (1.2).

At low current densities, the series resistance of large-area solar cells is small and can be neglected. The *I-V* characteristics can be then divided into three regions:

1. in the range 0–40 mV, the influence of shunt resistance dominates and can be calculated; the current through the cell (I_{DF} – Dark Forward Current) can be expressed by:

$$I_{\mathrm{DF}} \approx \frac{V}{R_{\mathrm{SH}}} \tag{5.1}$$

2. in the range 40–300 mV, the generation-recombination compound of the total current predominates, so it can be expressed by:

$$I_{DF} \approx AJ_{02} \exp\left(e\frac{V}{\eta_2 kT}\right) + \frac{V}{R_{SH}} \tag{5.2}$$

3. above 300 mV, the first term in the expression of the total current (diffusion compound) is dominant, so, by the curve fitting method, the diffusion saturation current and the diffusion diode factor can be extracted.

The generation-recombination current density J_{02} can be expressed by:

$$J_{02} = \frac{n_i ed}{\tau_{SC}} \tag{5.3}$$

This means that the density J_{02} is inversely proportional to the lifetime of the charge carriers in the space charge region of thickness *d*, for which, in the case of a single trapping level, the following formula can be obtained:

$$\tau_{SC} = \tau_{p0} \exp\left(-\frac{E_t + E_i}{kT}\right) + \tau_{n0} \exp\left(\frac{E_t + E_i}{kT}\right) \tag{5.4}$$

Here, τ_{p0} and τ_{n0} stand for the lifetime of the minority carriers in an N-type semiconductor or a P-type semiconductor, respectively, E_{t} is the energy level of the G-R centre (or trap), and E_{i} is the intrinsic Fermi level [49].

Extraction of single recombination level parameters from temperature dependence of J_{02} is relatively simple. If there are more recombination centres characterized by τ_{SCj}, the resulting τ_{SC} can be found from

$$\frac{1}{\tau_{SC}} = \sum_j \frac{1}{\tau_{SCj}} \tag{5.5}$$

If one deep level is dominant, the extraction of parameters can be done in the same way as in the occurrence of one single level. However, for two or more deep levels of approximately the same concentration, the standard extracting technique will lead to incorrect values of deep level energy.

By reverse voltage-current characteristic measurement in the range of voltage $V = 40 \div 300$ mV is the total current given by [1]:

$$I = I_{01} + I_{02} + \frac{V}{R_{\mathrm{SH}}} \Rightarrow I \approx I_{02} + \frac{V}{R_{\mathrm{SH}}} \tag{5.6}$$

Parameters are extracted then by the similar procedure like in forward voltage-current characteristic measurement. In the future, especially the other crystalline cell types like PERC structure and also modules affected by PID will be examined.

5.3 Dynamic Parameters Measurement - Impedance Spectroscopy

The AC parameters can be measured using frequency domain technique – impedance spectroscopy. The Impedance Spectroscopy is characterized by the measurement and analysis of some or all impedance related functions of an electronic device. In impedance spectroscopy, the complex impedance $Z(\omega) = R(\omega) + jX(\omega)$ of a device is measured directly within a large range of frequencies. A purely sinusoidal voltage with varying frequency is applied to the terminals of the device under test and the phase shift and amplitude of the voltage and current signals are measured. The ratio between the applied voltage and the resultant current is calculated and this gives the impedance $Z(\omega)$ of the device under test. The plotting of $R(\omega)$ and $X(\omega)$ on a complex plane, in function of the varying frequency, gives the impedance spectrum of the device. In the photovoltaic area, this method has been in use for many years, mainly for AC parameters estimation such as R_{P} determination (e.g. [50], [51]), but in [52] the usage for the donor concentration determination is presented as well. For measurement, the LCR meter is usually used.

5.3.1 Cole-Cole Diagram

The graphical representation of X(ω) vs. R(ω) is called the "Cole-Cole diagram" of the solar cell, and it gives the impedance arcs from which the different AC parameters can be extracted. The construction of Cole-Cole diagram allows simple evaluation of parameters and also the quality of the tested cell, module respectively [23]:

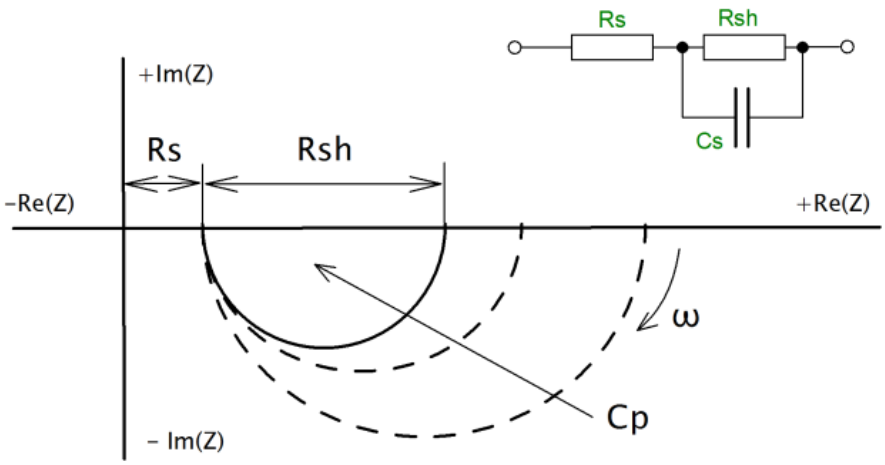

Fig. 35: Cole-Cole diagram of PV cell (module) [53]

The problem of measurement of the Cole-Cole diagrams lies in many factors that can influence the resulting curves. The Cole-Cole circle diameters correspond with the PV cell parameters, but also with other aspects like irradiance level and its spectrum, DC biasing, test signal level and cable length.

The most problematic parameter is the capacitance which is the representation of physical capacitances inside the structure, particularly space charge capacitance of depletion region (transition capacitance C_T) and capacitance due to minority carriers oscillation in response to the AC signal (diffusion capacitance C_D). Both capacitances represent relatively difficult problem because it shows strong dependence on the voltage and injection level.

Transition capacitance is very important namely in the case of reverse biased junction. It represents the ability to store electric charge. In reverse bias, the depletion region behaves like the classical dielectric, because the depletion region can be considered as free of charge carriers and the P and N regions like plates in the basic capacitor. Therefore, if the reverse bias voltage is applied, the depletion region width d increases and capacitance decreases. For abrupt junction, the capacitance can be expressed by [54]:

$$C_J = \frac{A\varepsilon_0\varepsilon_r}{d} = A\sqrt{\frac{e\varepsilon_0\varepsilon_r}{2}\frac{N_\mathrm{A}N_\mathrm{D}}{N_\mathrm{A}+N_\mathrm{D}}}\left(\psi_{bi} - V - \frac{2kT}{e}\right)^{-\frac{1}{2}}, \tag{5.7}$$

where ε_0 denotes permittivity of vacuum, ε_r relative permittivity and ψ_{bi} is the built-in potential, where *V* is positive for forward bias and negative for reverse bias.

In forward direction, the transient capacitance still remains (theoretically it grows to infinity), but with rising forward bias voltage, there is a diffusion of charge carriers, which is connected with so called diffusion capacitance which can exceed the junction capacitance and therefore it is usually considered as dominant component of capacitive behaviour of a forward biased junction.

The diffusion capacitance, sometimes referred also as storage capacitance, represents the capacity caused by the moving charge carriers. In the reverse direction, there is almost no flowing current, thus the capacitance is also negligible, in the forward direction, the situation changes. The depletion region is flooded by the charge carriers to such an extent, that the remaining are coupled around the transition similarly to the previous situation. If more charge carriers are generated, higher amount of charge must be stored – the capacitance rises. Diffusion capacitance is than defined as C_D = dQ/dV, where Q represents injected positive charge (caused by minority carriers) and V the voltage [1]. For lower frequencies it can be expressed by [55]:

$$C_D = \frac{e}{kT}\left(\frac{eL_p p_{n0}}{2} + \frac{eL_n n_{p0}}{2}\right)\exp\left(\frac{eV}{kT}\right), \tag{5.8}$$

where e is electron charge, k Boltzmann constant, T temperature, L_p and L_n diffusion lengths of holes and electrons and p_{n0} and n_{p0} initial minority carriers concentrations. From the equation above it is apparent that injection level is directly proportional to applied voltage and also tightly connected with minority carriers generation, thus, in the case of PV structures, also with irradiance. Because the irradiation of structure is never sufficiently constant, different results can be obtained when evaluating these parameters, so the results then are unrepeatable (although there are some efforts to measure under light e.g. [56]). For these reasons, it can be recommended to perform the AC measurement in dark conditions

The AC power voltage value (measuring signal) has, if usual range is used (tens of millivolts), no significant effect on the measured values, but DC biasing is changing the operational point

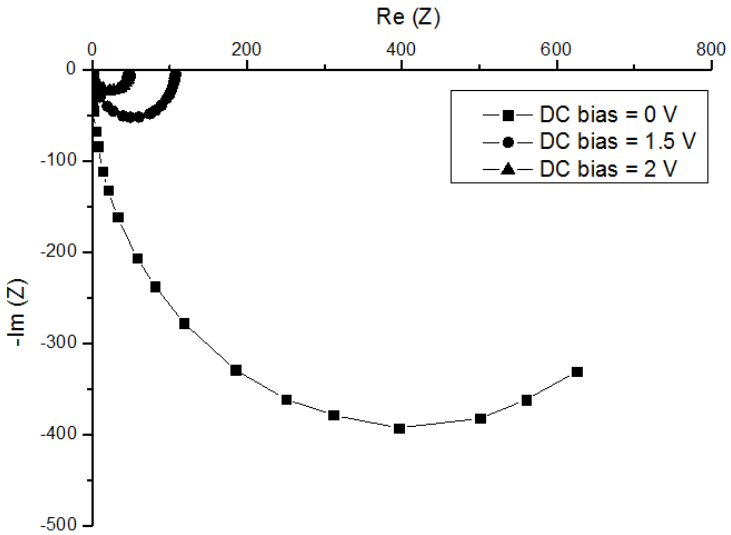

Fig. 36: Cole-Cole diagram of 4 multicrystalline PV module [53]

of the cell and thus influences the diameter and area of measured Cole-Cole diagram. Extracted parameters are than strongly influenced by this value as can be seen on **Fig. 36**. The reason is in properties of the P-N junction inside the cell and changes of both capacitances, especially the junction capacitance. With rising capacitance, the complex part of impedance decreases which propagates in circle dimensions.

DC biasing also influence the value of shunt resistance. When the junction is opened, R_{SH} also decreases – the capacitor representation of the junction behaves like resistor when the frequency is equal to zero, thus it doesn't behave like open circuit and lowers final R_{SH} value.

The question is which value of DC bias could be set to achieve parameters values corresponding to values obtained by standard measurement methods like *I-V* curve measurement under STC (standard test conditions).

5.3.2 Resistances Extraction Methods

To find the proper configuration of Impedance Spectroscopy method it is essential to determine the correct values of resistances. The methods for series resistances were already discussed in the previous text. It is necessary to mention that it is not only the series resistance which shows dependence on irradiance, but the shunt resistance R_{SH} as well. The experiments proved that the dependence on irradiance is similar to the series resistance dependence.

There was a comparison of impedance spectroscopy (IS), flash test (FT) and resistance determination used. For measurement, the multicrystalline Si modules consisting of 4 serially

connected PV cells were used. For IS measurement, the LCR meter HP 4284A has been used and FT have been performed at PASAN Sun Sim 3c.

From the presumptions mentioned above, it is obvious that IS performed under zero voltage DC bias should give the value of R_{SH} corresponding to value measured under dark current measurement method. From the graph at **Fig. 36**, it can be found that the value for zero biasing will be approx. 800 Ω. From the dark current measurement, the value of approx. 750 Ω has been calculated (see **Fig. 37**). The value of dark shunt resistance then can be considered as corresponding to measured ones at zero voltage bias.

The value of series resistance is in this case too low, so every measurement obtained by IS will be burden by relatively high uncertainty, so it has not been performed in this case nor further examined. The comparison of R_{SH} values obtained by FT and IS is apparent from the following table:

Tab. 5: Dependence of R_{SH} at injection level controlled by irradiance G and DC biasing

DC Biasing (V)	***G* (W/m^2)**	**R_{SH} – IS (Ω)**
0	0	800
1.5	450	108
2.0	1000	48

From the comparison of measured values it can be stated that it doesn't matter if the P-N junction is opened by biasing or by irradiation. After biasing of approx. 0.5 V per one cell, the

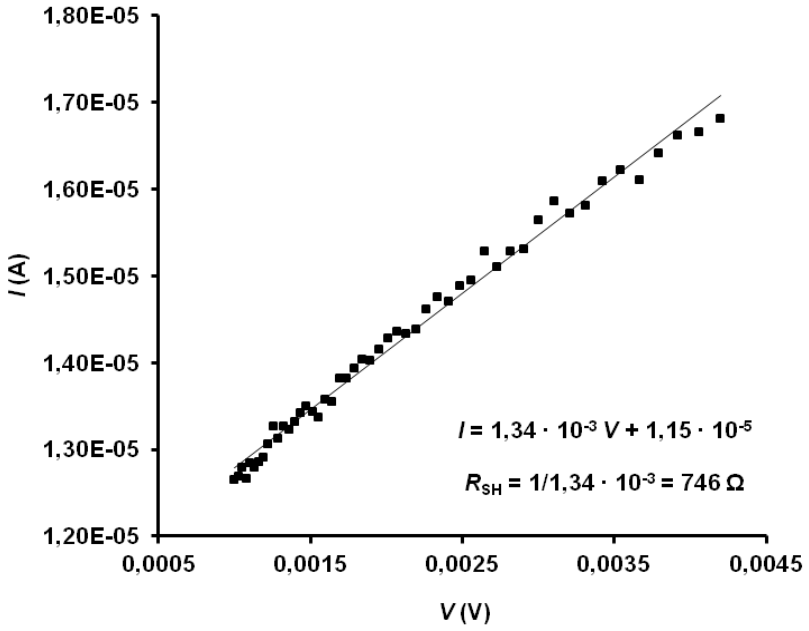

Fig. 37: Shunt resistance determination [53]

results obtained by IS should be corresponding to those obtained by STC measurement. On the other hand, when lower injection is used, lower biasing can relatively well serve as the simulator of this condition and provide the possibilities of studying the defects behaviour under AC conditions like they would be under constant irradiation. These results will be presented at EUPVSEC'17 conference [53].

The common property of the above mentioned measurement methods is the fact that they can be, commonly or with little adjustment, used on-site. Due to this, the further work is focused on on-site diagnostics and in particular on the evaluation of the obtained results.

6 On-site Diagnostic Tools and their Evaluation for Large PV Systems

The diagnostics of the power plant usually consists of a few steps. The first one is to decide, how to diagnose. Methods, which can be used at small systems, are different from the ones used at larger systems. If thousands of modules are installed than the measurement of every module is practically impossible. The diagnostics of small system can be sufficiently performed using standard methods described above, like thermography or static volt-ampere characteristic measurement. But in the case of larger system, there are still gaps which leave the space for new approaches.

The basic diagnostics of large PV systems is based on data analysis. Usual configuration of large systems in the middle Europe consists of string inverters with the middle power (about 5 kW – 10 kW) because of the problems with local shading caused by clouds movements. The problem of data evaluation is out of range of this work and is described in many publications e.g. [57], [58], [59]. When the suspicion on the wrong component is detected, the concrete strings are then evaluated using other methods. The favourite one is, as mentioned before, thermography.

The biggest problem of thermography is the lack of the information about the impact on performance. The possible guide can be in evaluation of Schottky diodes heating as was presented in [60]:

6.1 Thermograms Evaluation

To check the possibility of quantification of thermograms there were many measurements performed at the real system and in a laboratory. PV modules with defects were detected and were subsequently tested by a flash tester (a device for accurate measuring of *I-V* curves of modules – establishing nameplate parameters of PV modules). All acquired results can be found in [61]. Examples of thermograms and corresponding flash tests during standard testing conditions (STC) are apparent in **Fig. 38**, **Fig. 39** and **Fig. 40**.

All examined PV modules had a nominal output of 230 W. Obtained thermograms show that for quantification the most crucial area is above junction boxes where bypass diodes are located. The amount of current going through diode depends on voltage loss which is caused by an impaired cell or segment of a module. With the rise of current going through the diode the power loss and temperature of the diode rise as well.

Measurements were performed during two various irradiances and clear weather. The temperature of modules was higher during a higher irradiance. However, temperature differences of individual areas stayed mostly constant.

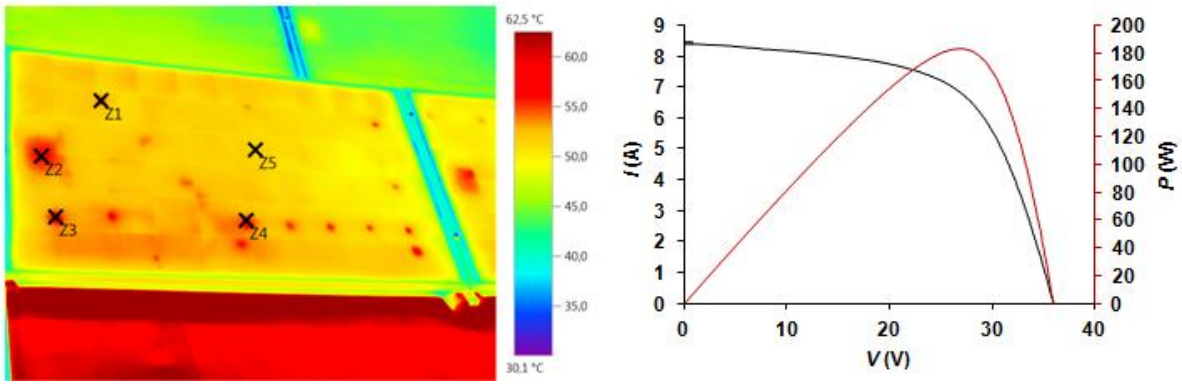

Fig. 38: A thermogram with marked points of measured temperature and flash tests of PV module with defects type hot-spot

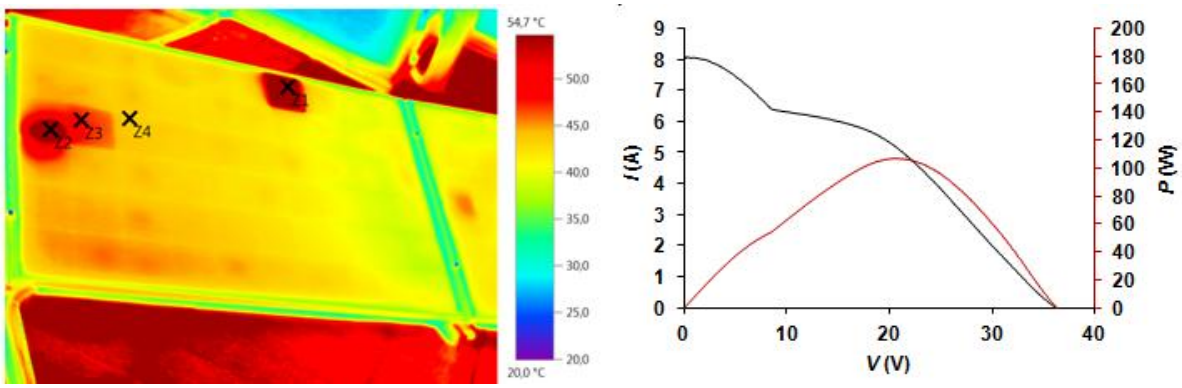

Fig. 39: A thermogram with marked points of measured temperature and flash tests of PV module with an overheated cell

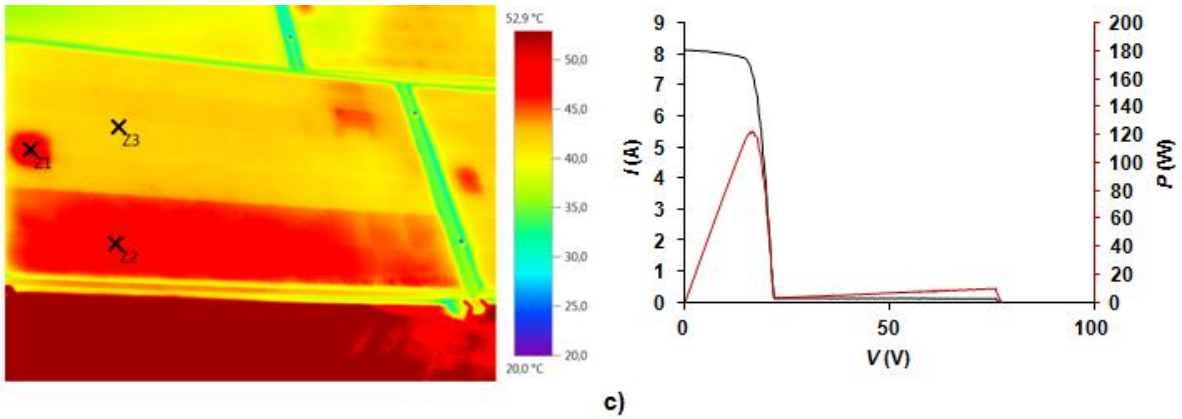

Fig. 40: A thermogram with marked points of measured temperature and flash tests of PV module with a non-functional segment

Comparison of thermograms and flash tests shows that for the evaluation of thermograms, it is not necessary to pay attention to amount and number of cells visible on a thermogram. For the evaluation of a difference of output power to the nominal power it is enough to observe the temperature difference in the area where junction box is located and the rest of the surface of the examined module. For PV modules of the examined configuration (junction box without silicone filling), a following correlation for typical defects was found, after evaluation of temperature anomalies ($\Delta\ T$ marks the difference of temperatures in between the area above junction box and the rest of the module and $\Delta\ P_{MAX}$ proportional output decrease from the nominal value).

Tab. 6: Correlation between the temperature difference in the area of junction box location and the rest of the module and PV module performance under STC, thermograms were measured at *G* from 970 to 1000 W/m^2

$\Delta\ T$	$\Delta\ P_{MAX}$
< 3 K	< 10 %
4 K – 5 K	approx. 20 %
≥ 9 K	> 50 %

The results showed that even a temperature difference of over 30 K between a defective cell and the rest of module do not have to result in an output lowered under the value guaranteed by the manufacturer. On the contrary, there was a correlation found in the difference of temperatures of the area where the junction box is located and the rest of the module and the output of PV module. A difference above 4 K indicates a considerably lower output from the nominal value. This temperature difference is also dependent on the configuration of the junction box and the size of the bypass diodes.

During the work on evaluation of thermograms, there was another very important fact connected with the bypass diode found. Some operators are sometimes very confused by the thermography results, because when the thermograms are obtained in winter (in clear-sky conditions) they look different from the ones taken in sunny summer days. Also the measurement of the affected modules performed directly at the PV power plant using Solar analysers show some stairs at *I-V* curves, but no such damage has been found when measured under STC in the lab. This effect is caused by the Schottky diodes behaviour and their characteristics as was presented in [62].

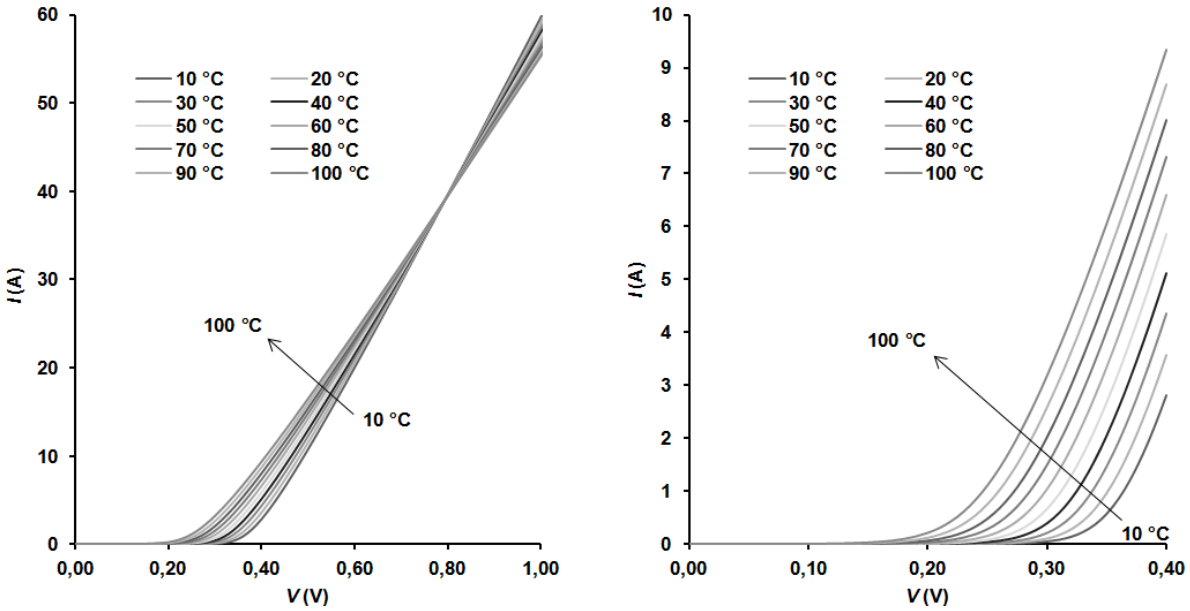

Fig. 41: Schottky diode temperature characteristics (detail on right)

6.1.1 Schottky Diode Temperature Dependence

If the simulation of Schottky diode temperature behaviour is performed, the dependence shown in the **Fig. 41** can be obtained. From this dependence it is obvious that when the same voltage drop appears at the bypass diode, the resulting current flowing through it will be significantly dependent on the temperature. The diode temperature is influenced by two aspects – ambient temperature and temperature difference caused by flowing current.

Influence of the ambient temperature

From the real operation, it is known that the temperature of the module is approx. about 20 °C higher than the ambient temperature. The bypass diode is usually located in junction box which is located directly at the PV module rear side. Because the diodes inside the junction box are in an immediate vicinity of the module surface, their temperature must also be very similar (in thermal equilibrium the same, of course). It means that in idle state, the diode will have the ambient temperature + 20 °C. In clear summer days about 55 °C and in winter about 20 °C. From the graph in the **Fig. 41** it is obvious that the current flowing through the diode as a consequence of a defect (voltage drop at diode terminals is dependent on the damage level) will be approx. twice as high in the summer than in the winter conditions.

Influence of the flowing current

For dependence of flowing current on temperature, it is important to define the structure of the bypass diode. This structure is shown in **Fig. 42**.

The current temperature dependence has been well known for many years. Among the theoretical equations, there is also the semi-empirical relation between the temperature, current and voltage which can be used when operating in the estimated temperature and current range (usual PV systems operational conditions). When the current is high (it means the diode is fully opened), this relation can be expressed by [9]:

$$V = \frac{kT}{e} \ln \frac{I}{I_0} + RI, \tag{6.1}$$

where R is given by the sum of resistances of N layer, N+ layer and contacts as marked in **Fig. 42**:

$$R = R_N + R_{N+} + R_C \tag{6.2}$$

and the saturation current is given by:

$$I_0 = c_1 \cdot T^2 \cdot \exp\left(\frac{c_2}{T}\right), \tag{6.3}$$

where c_1 (A·K^{-2}) and c_2 (K) are constants characteristic for every diode.

Determination of these constants is relatively problematic in real operation conditions, but their values are constant in the whole operation conditions range, so when the small current is applied ($RI << V_B$ (threshold voltage)), the series resistance can be neglected and constants can be extracted directly from the Schottky junction characteristic with utilization of the

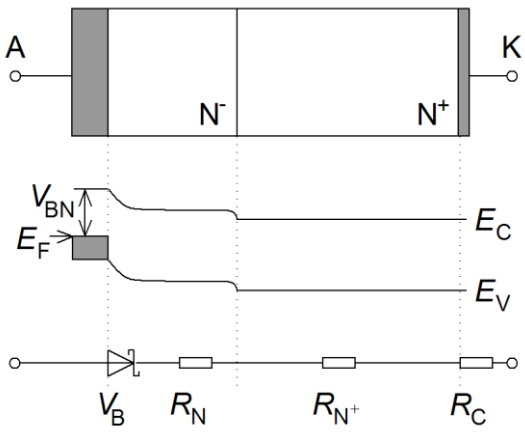

Fig. 42: Basic Schottky diode structure

following equation [9]:

$$I \approx c_1 \cdot T^2 \cdot \exp\left(\frac{c_2}{T}\right) \cdot \left[\exp\left(\frac{eV}{kT}\right) - 1\right]. \quad (6.4)$$

There were experiments with the real three bypass diodes performed and by the nonlinear regression constants c_1 and c_2 have been found. For the measurement, constant current source of 6.42 mA has been used, so the condition of small *RI* was accomplished. Diodes, together with the thermocouple, were located in the isothermal cavity. Thermal regulation was set to the constant value and left until constant values at thermocouple and diodes voltages were achieved. The measurement was than performed. Results of measured voltages under different temperatures are summarized in **Tab. 7**. The differences between the temperature at the surface of the diode and inside it were neglected, because such a difference can in the case of such a small current, cause the difference of about 30 mK only ($V_D \cdot 0.00642 \cdot R_{th} = = 0.2 \cdot 0.00642 \cdot 25 = 32$ mK).

Tab. 7: Measured forward voltage values of diodes for the current of 6.42 mA

T (°C)	V_{D1} (mV)	V_{D2} (mV)	V_{D3} (mV)
22.4	189.94	180.65	192.06
38.6	159.95	150.57	162.07
56.1	127.14	117.71	129.26
83.8	77.27	68.3	79.17
120.1	26.71	21.53	27.84
149.3	8.54	6.60	9.03
155.0	6.79	5.19	7.12
156.3	6.44	4.93	6.76

Parameters obtained by the non-linear regression are summarized in the **Tab. 8**.

Tab. 8: Calculated parameters obtained by non-linear regression

Parameter	D1	D2	D3
c_1 (A·K^{-2})	19.6	22.1	19.8
c_2 (K)	-7934.5	-7861.6	-7961.9

For verification of obtained constants, fitting measured data with utilization of equations (6.1), (6.3), (6.4) and obtained constants was performed as well. As obvious from the **Fig. 43**, the reliability of the obtained constants and given equations is very high.

By utilization of obtained constants, the measurement of the temperatures in the real junction box has been performed. These tests came from the procedure described in ČSN EN ISO/IEC 61215. During these tests, the surface temperature of the module is considered to be 75 °C (the worst case in hot summer weather). Therefore, the junction box with the diodes was located at the heating plate and then the different constant current was applied. The results show that the internal diodes temperature is much higher than the surface temperature of the module and consequently the flowing current will be very different in dependent on the ambient temperature:

When the ambient temperature is low, the current flowing through the diode will be lower because of the higher value of threshold voltage. Also the heating by the flowing current will be then limited. When the ambient temperature is high (hot summer), the threshold voltage value will decrease and it will cause higher flowing currents and another additional bypass diode heating.

This is the reason why during winter, the defects are visible at the thermography and during summer they virtually disappear – people usually perform thermography from the front side of the module and they don't evaluate the changes of temperatures of bypass diodes if they are not shunted. If the temperature changes of the diodes are implemented into the SW for *I-V* curve modelling, another additional effect is achieved. When the *I-V* curves at a partially defective module are measured under the natural conditions – usually during the summer (or late spring), the modules have higher temperature as well as the bypass diode and typical stairs are apparent at the measured *I-V* curve. But when the measurements are performed

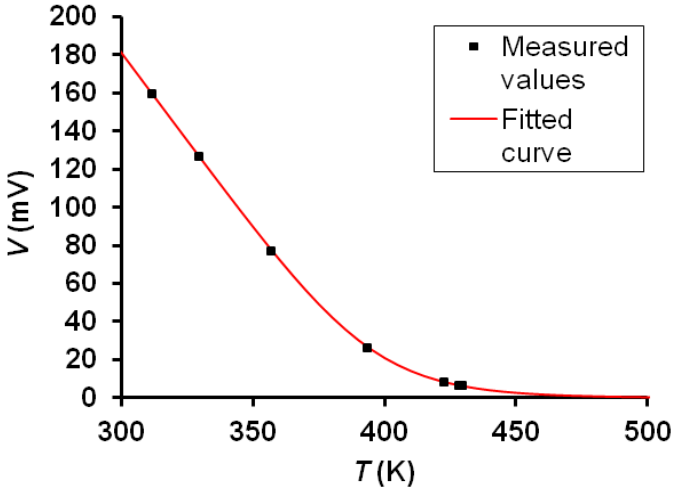

Fig. 43: Fitted data of D1

under STC in the laboratory (or during the winter), there is neither effect of heating of the tested sample nor the bypass diode. The defect influence can be too low to open the bypass diode and the module seems to be without any defect, or less serious. The temperature dependence of the bypass diode and its knowledge is then very important factor which cannot be neglected when the thermograms are evaluated.

6.2 Dark Current Measurement – Tool for Degradation Evaluation

During the work on this thesis, another very interesting possible utilization of dark current measurement has been found. As mentioned in the previous section, at low voltages under dark conditions, the shunt resistance influence predominates. The degradation of thin-film modules is often connected just with the shunt resistance decrease. It is understandable because during degradation, local shunts occur in the structure and the shunt resistance must be consequently decreased. This fact was used for quick diagnostics of micromorphous PV modules and the tester was constructed and patented (currently there is the utility model [63] and the patent [64]).

6.2.1 Principle of method

The principle of this newly developed method, further referred to as Dark Current Test (DCT), is based on the comparison of the degraded modules performance with the presumed shunt resistance value. For evaluation at the system, there is no need to determine the resistance value itself, the voltage at specific constant current will do the same service, because from the equation (5.1) it is obvious that

$$V \approx R_{SH} \cdot I_{DF} \tag{6.5}$$

and consequently, when the current will be constant, the shunt resistance value will be proportional to it. The comparison of two modules – one defective and one without defect is given in the **Fig. 44**.

The dependency of performance on shunt resistance (voltage measured by dark current test at specific current) is not linear, because the predomination of shunt influence doesn't come gradually, so, for evaluation, it is necessary to "calibrate" the tester first. The lowest acceptable performance value of the module is calculated taking into account the tolerance, guarantee, natural aging, measurement uncertainties and other expected influences.

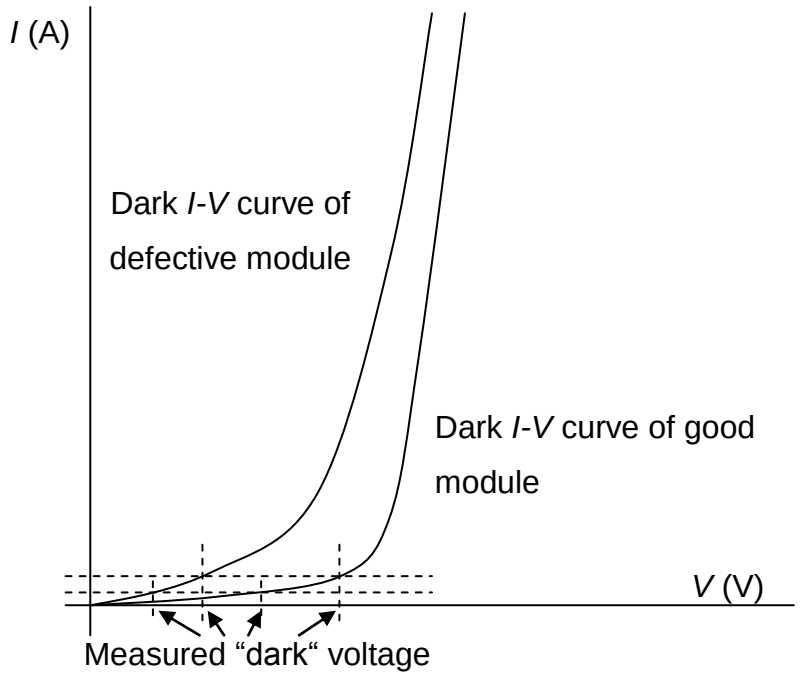

Fig. 44: An example of comparison of *I-V* curves of good and defective PV modules

Performance of set of modules by FT (or by solar analyzer) is measured. Furthermore, the dark current test is performed and the results compared. From the comparison of flash test and dark current test results, the threshold voltage corresponding to lowest acceptable performance value is then determined (of course, if such value is achieved). After that, the diagnostics by dark current only can be easily performed.

6.2.2 Experiments

For verification, set of measurement at the real PV system has been performed. First, according to the procedure described above, there was a set of modules by flash test measured. Second, dark current test using the constant current source supplied by the battery was used and results with FT measurements were compared. The dependence of the measured MPP by FT on the voltage measured by dark current test is shown in the **Fig. 45**. The nominal MPP of the measured modules was 97 W and the lowest acceptable performance value was determined to approx. 80 W. From the graph, this value corresponds approx. with the voltage value (measured by dark current test) of approx. 5 V.

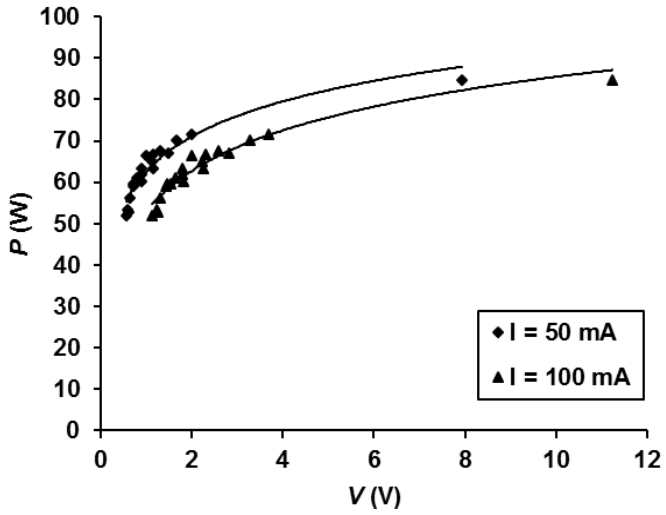

Fig. 45: Dependence of PV module performance measured by FT on voltage measured by dark current test with two different currents

Further the whole PV power plant (approx 20 000 PV modules) was measured. Measured data was processed into the graph (**Fig. 46**) and the possibly wrong series (according to the serial number) has been identified – marked red in the graph. This series has been further examined after half of a year and the sample (59 modules) from this series has been measured again in detail (some of them also by using FT and EL test) and the continuing degradation has been confirmed. The results are summarized in the **Tab. 9**, **Tab. 10** and **Fig. 47**.

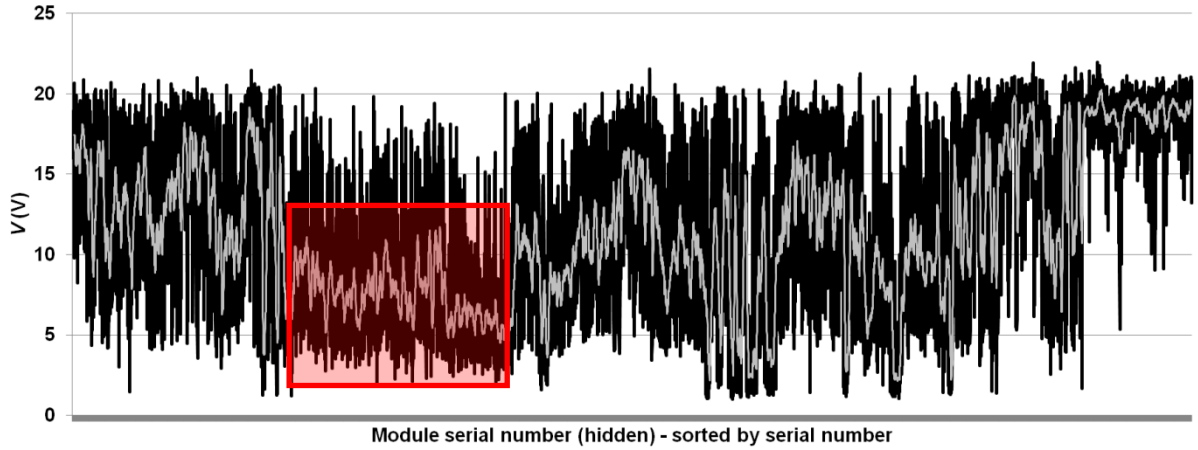

Fig. 46: Distribution of the modules voltage drop values according to the Dark Current Test - I_{DF} =100 mA (black line), grey line shows the moving average, red area suggests the possible degradation within one production series.

Tab. 9: Distribution of the sample of modules according to the Dark Current Test (I_{DF} = 100 mA)

	Year	
V (I_{DF} = 100 mA)	**2016**	**2017**
0-5 (V)	15	40
5.5-10 (V)	33	12
10.5-15 (V)	5	3
15.5-22 (V)	6	4
Sum	59	59

Tab. 10: Comparison of Flash Test results of 7 modules from the tested series – decrease compared to the previous state, expressed as a percentage

Module efficiency	-3.6	-5.4	-5.4	-3.6	-5.5	-3.6	-1.8
Fill factor	-2.4	-2.2	-2.4	-2.5	-2.6	-1.0	-0.2
I_{SC}	-0.6	-1.0	-1.2	-0.8	-1.1	-0.8	-1.2
V_{OC}	-1.0	-1.2	-0.9	-1.2	-1.1	-0.8	-0.7
P_{MAX}	**-4.0**	**-4.5**	**-4.4**	**-4.6**	**-4.7**	**-2.6**	**-2.0**
V_{MP}	-2.2	-2.5	-2.2	-2.9	-2.7	-2.0	-1.8
I_{MP}	-1.8	-2.0	-2.3	-1.7	-2.1	-0.6	-0.2
Series resistance	5.1	5.1	5.8	6.3	5.6	3.8	2.8
Shunt resistance	-4.1	-1.5	-3.8	-1.9	-4.6	4.9	10.9
V at I = 100 mA	**-1.9**	**-10.4**	**-1.7**	**-10.8**	**-1.9**	**-11.2**	**-14.1**
V at I = 50 mA	**-5.4**	**-14.0**	**-8.8**	**-13.0**	**-6.8**	**-17.3**	**-20.6**

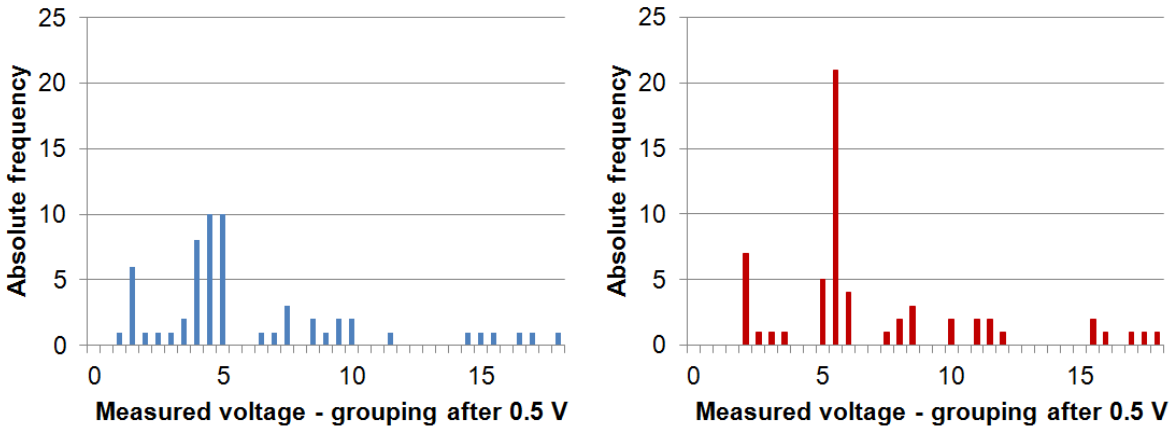

a) **b)**

Fig. 47: Comparison of histograms of distribution of the modules according to the Dark Current Test I_{DF} =100 mA in the year: a) 2016 and b) 2017

The big advantage of this method is that there are no special requirements on ambient conditions. The measurement can be performed during the night, so there are no additional

losses by the need of disconnecting the modules during the sunny days. There will be other technologies examined by this method and results published in journals.

6.3 Defects Detection by Impedance Spectroscopy and Time Domain Reflectometry

The last particularly examined measurement methods were the ones connected with AC parameters evaluation. The particular emphasis has been placed on Impedance Spectroscopy and Time Domain Reflectometry.

Impedance Spectroscopy

Although IS is usually used for dynamic parameters determination, there is also another utilization which was found during the work at this thesis. It is its sensitivity regarding the possibility of detection of defects which are in the beginning, like microcracks or local shunts of the PN junction. The following results were presented at EUPVSEC'16 [65] and NZEE'17 [66] conferences.

9 monocrystalline and 9 multicrystalline silicon PV modules consisting of 4 serially connected PV cells were examined. All modules were new with the same dimensions, configuration, age and storage conditions. First, flash tests and electroluminescence was performed. Than all the modules were measured using impedance spectroscopy. For measurement, the LCR meter HP 4284A was used.

Electroluminescence showed that all of the modules except for one are without visible defects – see **Fig. 48**. One of multicrystalline PV modules showed cracks inside, but the affected parts are still electrically connected to the rest of module (no "dark places"). This presumption was confirmed also by *I-V* curve where affected module didn't show any significant difference from the rest of modules of the measured group. On the other hand, the impedance spectroscopy showed significant difference which is well observable at Cole-Cole diagrams (**Fig. 49**). For easier evaluation, the average of measured values at "good" modules as well as parameters were calculated and compared with the "wrong" one (see **Tab. 11**).

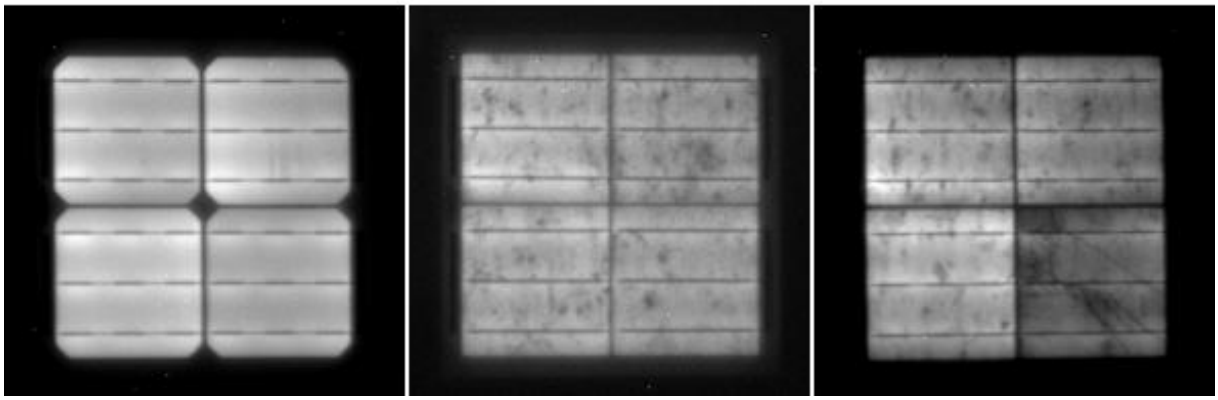

A **B** **C**

Fig. 48: Example of electroluminescence images (A – typical monocrystalline, B – typical multicrystalline, C – defective multicrystalline)

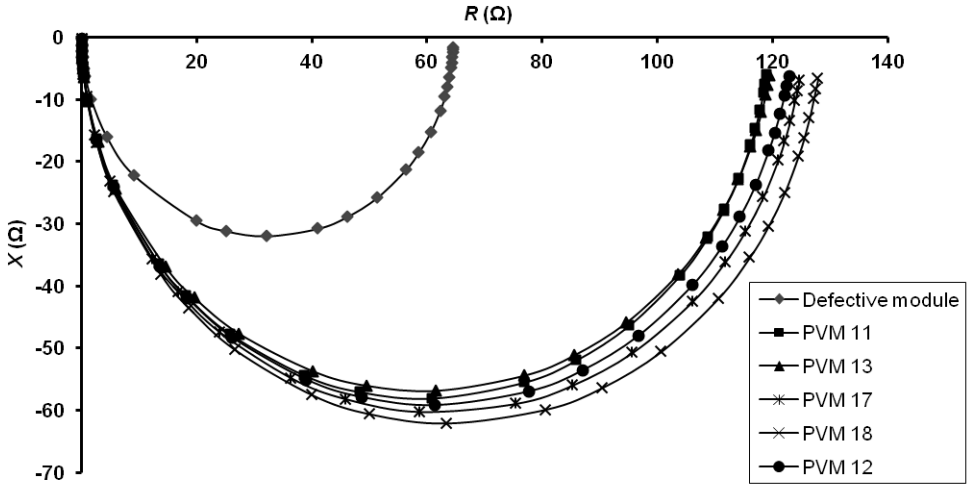

Fig. 49: Cole-Cole diagrams of measured multicrystalline PV modules

Tab. 11: Parameters obtained by *I-V* curve measurement

		Defective PVM	**Average value of samples 11 – 20**
G	**(kW/m^2)**	1.00	1.0
I_{SC}	**(A)**	8.81	8.83
V_{OC}	**(V)**	2.56	2.54
η	**(%)**	11.20	11.29
FF	**(%)**	70.19	70.91
P_{MAX}	**(W)**	15.83	15.87
V_{Pmax}	**(V)**	1.96	1.94
I_{Pmax}	**(A)**	8.07	8.17
R_S	**(Ω)**	0.01	0.01
R_{SH}	**(Ω)**	66.5	72.8

The results proved that if there is some distortion inside the module which does not influence the performance yet, IS can be a very useful tool for revealing it, because this diagram takes into account capacitances, that can be strongly influenced by PV module internal structure, as well.

In the future, other aspects like temperature and different defects propagation will be investigated. Currently, there is a research on the PID effect and its influence on Cole-Cole diagrams investigated.

Time Domain Reflectometry (TDR) & Impulse Response

Another AC method which can be used for PV cells and modules diagnostics is Time Domain Reflectometry. By specific frequency distribution of impedance, it is possible to find the location and to determine the nature of a defect. Moreover, this method can be used to differentiate modules that have the same nameplate values (and same producer) but slightly different fabrication process.

TDR is a method mostly used to localize defects in transmission lines [67]. The method is based on sending a simple signal (such as a Volt Step-Wave) to an examined object (e.g. PV module) and measuring the waveform of the reflected voltage wave that is sent back to the oscilloscope (**Fig. 50**). Evaluating the TDR is then fairly easy [68]:

- Taking into account the time of the wave reception by the oscilloscope in the case of a good module, a difference signals that there is a defective cell within the panel/array.

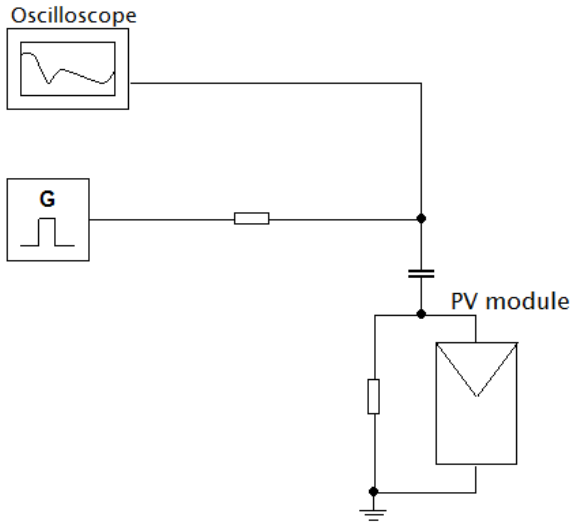

Fig. 50: The block diagram for measurements using TDR

- A larger amplitude of the peaks of the voltage wave according to the peaks obtained on a good PV module of the same type indicates that the defective PV cell is acting like a short circuit inside the panel/array.
- A larger amplitude of the valleys of the voltage wave according to the valleys obtained on a good PV module of the same type indicates that the defective PV cell is acting like an open circuit inside the panel/array.
- The rising of the response voltage wave to a certain level relates to an increase in the string impedance, which may indicate a degradation of the connectors.

Modified TDR method can be used for evaluation of differences between the modules. The modification lays in a fact that only the impulse response instead of a reflective signal is measured. The impedance profile obtained by this method is specific for every technology and also varies from manufacturer to manufacturer, as well as for single generations of the "same" PV module type. This was verified by measurement of old and new generation of CIGS modules. As described in chapter 3.1, there were differences in technology when the soda-lime glass was started to use. The older versions used only soda-lime glass without any other structures changes, because in these days, no positive effect of sodium indiffusion was known (today also the negative influence is known as PID). On the other side, the second generation had the additional Na^+ targets, which both prevented the unintentional sodium diffusion and serve as the efficiency harvesting factor, inside the structure. The nameplate values haven't shown any significant differences, but the impedance profiles had (**Fig. 51**).

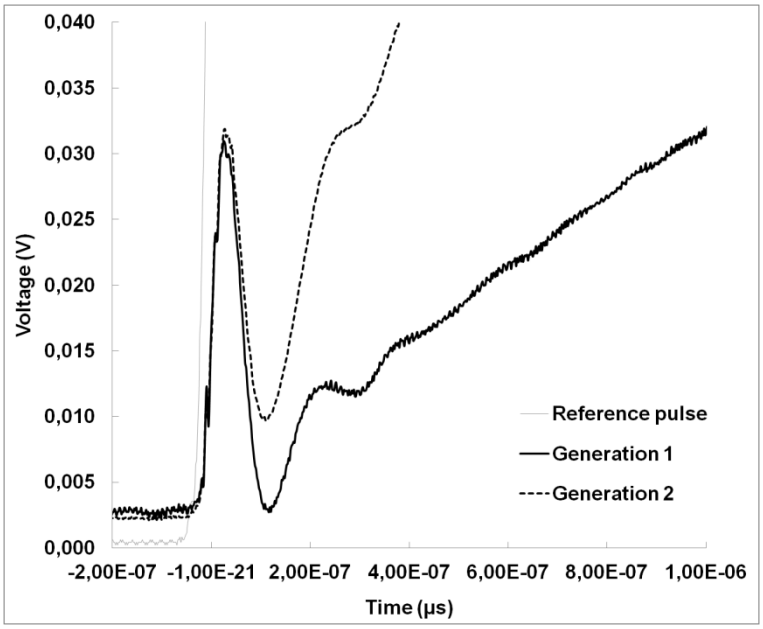

Fig. 51: Measured waves on various generation CIGS PV modules by impulse response technique

7 Conclusion

7.1 Achieved Results

During the work on the dissertation many scientific papers were published. Their list is given at the end of this work. The aim of this work was to find the correlation between the common and new methods and to identify the limitations of common methods.

There was a comparison between the Impedance Spectroscopy, Flash Test, Electroluminescence and Dark Current Measurement presented. A strong correlation between these methods has been found and the guidelines for successful utilization of IS have been described. This is very important namely because IS is performed under dark conditions, so there is no limitation by weather conditions. Another advantage of this method is its possibility of using on thin-film modules.

The subject of series resistance determination and its dependence on irradiance has been described. This dependence is usually neglected and wrong simulation results are than obtained. The knowledge of this dependence can be used for estimation of the specific technology which is suitable to the given climatic conditions.

Another part of this work was dedicated to thermography and its correct evaluation. During work at this thesis, many measurements have been performed. The results were discussed with Czech service companies and also with companies dealing with thermography applications. The problems connected with evaluation have been defined and the possible solution found. The main acquisition of this work in this field is especially the evaluation methodology by bypass diodes temperature detection and evaluation and also explanation of variability of the obtained thermograms due to Schottky diode temperature dependence, which is unfortunately usually neglected. All of these aspects were presented at scientific conferences as well as local conferences for direct users (e.g. Termografie v praxi, TMV SS Open House) where it was very favourably received.

Last but not least, the new quick diagnostic method based on dark current measurement, called Dark Current Test, was developed, verified in praxis and the tester was constructed and successfully patented.

7.2 Future Development

In the further research, AC methods and their other utilization will be examined in more detail. These methods have proven as very promising for early diagnostics, because they are more sensitive regarding defects when compared with common methods. This will be examined especially in the connection with PID, LS and TA effect.

The emphasis will also be placed on other aspects of thermography, like direct evaluation of PV power plants performance in dependence on obtained thermograms.

Last but not least, the newly developed Dark Current Test method will be performed at other technologies with emphasis on PID effect.

8 References

[1] LUQUE, A., HEGEDUS, S. *Handbook of photovoltaic science and engineering* [online]. 2. Hoboken, NJ: Wiley, c2011. ISBN 978-0-470-97466-7. Available at: http://eu.wiley.com/WileyCDA/WileyTitle/productCd-0470976128.html

[2] MOHR, P. J., TAYLOR, B. N., NEWELL, A., CODATA D.B. Recommended values of the fundamental physical constants. *Reviews Of Modern Physics*. April - June 2008, 80, s. 633 - 730.

[3] WAGNER, A. PEAK-POWER AND INTERNAL SERIES RESISTANCE MEASUREMENT UNDER NATURAL AMBIENT CONDITIONS. In: *Proceedings of EuroSun 2000 Conference* [online]. Copenhague, 2000. Available at: www.adler-instrumentos.es

[4] ČSN EN 60891. *Fotovoltaické součástky - Postupy pro korekce teploty a ozařování na změřených voltampérových charakteristikách.* Praha: Český normalizační institut, 2010.

[5] CHIBBARO, C.; ZIMBONE, M.; LITRICO, G.; BAERI, P.; LO TROVATO, M. L.; ALEO, F. A general and precise method to evaluate the series resistance of photovoltaic cells from I-V characteristics. *Journal of Applied Physics*. Aug2011, year 110, issue 4, p044505. 9p. DOI: 10.1063/1.3622617.

[6] CHAN, D.S.H., J.R. PHILLIPS, PHANG, J.C.H. A comparative study of extraction methods for solar cell model parameters. *Solid-State Electronics* [online]. 1986, **29**(3), 329-337. DOI: 10.1016/0038-1101(86)90212-1. ISSN 00381101. Available at: http://linkinghub.elsevier.com/retrieve/pii/0038110186902121

[7] VAN DYK, MEYER. Analysis of the effect of parasitic resistances on the performance of photovoltaic modules. *Renewable Energy*: *An International Journal* [online]. Kidlington: Elsevier, 2004, roč. 29, č. 3, s. 333-344. ISSN 0960-1481. Available at: www.sciencedirect.com

[8] KAMPWERTH, H., T. TRUPKE, J. W. WEBER a Y. AUGARTEN. Advanced luminescence based effective series resistance imaging of silicon solar cells. *Applied Physics Letters* [online]. 2008, roč. 93, č. 20, s. 202102. ISSN 00036951. DOI: 10.1063/1.2982588. Available at: http://link.aip.org/link/APPLAB/v93/i20/p202102/s1

[9] BENDA, V., GOWAR, J., and GRANT, D. Power Semiconductor Devices. 1. ed. Chichester: John Wiley. 1999, ISBN 0-471-97644-X.

[10] ČERNÁ, L., BENDA, V., MACHÁČEK, Z.: A Note on Irradiance Dependence of Photovoltaic Cell and Module Parameters. In *Proceedings MIEL 2012*. Piscataway: IEEE, 2012, p. 273-276. ISBN 978-1-4673-0235-7.

[11] CHAUDHARI, V.A. and SOLANKI, C.S. From 1 Sun to 10 Suns c-Si Cells by Optimizing Metal grid, Metal Resistance and Junction Depth. *International Journal of Photoenergy*, Vol 2009, Article ID 827402

[12] ŠÁLY, V., et al. Characterisation of crystalline silicon solar cells of concentration applications. In *Proceedings of 21st European Photovoltaic Solar Energy Conference*, paper 1DV.1.2, September 2006.

[13] KAPLANIS, S. and KAPLANI, E. Transient and steady state simulation studies and experiments for the performance of c-Si and pc-Si PV cells in high illumination levels. In *Proceedings of the 5th International Workshop on Teaching in Photovoltaics*, pp. 18-23, Prague, 2010.

[14] BENDA, V. Using Carrier Lifetime Dependences on Temperature and Current Density in Diagnostics of Silicon Structures. In *Proceedings of EPE-MADEP Conference*, pp. 65-68, 1991

[15] CUEVAS, A. and R. A. SINTON. Detailed modelling of silicon solar cells. In *Proceedings of 23rd European Photovoltaic Solar Energy Conference*, paper 1CV1.30. 2008

[16] BENDA, V., MACHÁČEK, Z. A Note on Parameters of Photovoltaic Cells in Dependence on Irradiance and Temperature. In *Proceeding MedPower 2010* [CD-ROM]. Nicosia: IET Cyprus LN, 2010

[17] FINSTERLE, T., ČERNÁ, L., BENDA, V.: Účinnost fotovoltaických modulů v podmínkách ČR. In *36. Nekonvenční zdroje elektrické energie*. 2015, s. 34-37. ISBN 978-80-02-02593-1.

[18] REINDL, T., OUYANG, J., KHAING, A.M., DING, K., KHOO, Y. S., WALSH, T. M., ABERLE, A. G. Investigation of the Performance of Commercial Photovoltaic Modules under Tropical Conditions. *Japanese Journal of Applied Physics* [online]. 2012, č. 51, 10NF11. DOI: 10.1143/JJAP.51.10NF11. Available at: http://stacks.iop.org/1347-4065/51/10NF11

[19] VALENTINI, M., RADUCU, A., SERA, D., TEODORESCU, R. PV inverter test setup for European efficiency, static and dynamic MPPT efficiency evaluation. In: *2008 11th International Conference on Optimization of Electrical and Electronic Equipment* [online]. IEEE, 2008, s. 433-438. ISBN 978-1-4244-1544-1. DOI:

10.1109/OPTIM.2008.4602445. Available at: http://ieeexplore.ieee.org/lpdocs/epic03/wrapper.htm?arnumber=4602445

[20] STANĚK, K. *Fotovoltaika pro budovy*. 1. vyd. Praha: Grada pro Katedru konstrukcí pozemních staveb Fakulty stavební Českého vysokého učení technického v Praze, 2012, 223 s. ISBN 978-80-247-4278-6.

[21] SERA, D.; TEODORESCU, R.; , "Robust series resistance estimation for diagnostics of photovoltaic modules," *Industrial Electronics, 2009. IECON '09. 35th Annual Conference of IEEE* , vol., no., pp.800-805, 3-5 Nov. 2009 doi: 10.1109/IECON.2009.5415022 Available at: http://ieeexplore.ieee.org/stamp/stamp.jsp?tp=&arnumber=5415022&isnumber=5414636

[22] POLVERINI, D., TZAMALIS, G., MÜLLEJANS, H. A validation study of photovoltaic module series resistance determination under various operating conditions according to IEC 60891. *Progress in Photovoltaics: Research and Applications* [online]. 2011, n/a-n/a. ISSN 10627995. DOI: 10.1002/pip.1200. Available at: http://doi.wiley.com/10.1002/pip.1200

[23] CHEVNIDHYA, D., K. KIRTIKARA a C. JIVACATE Dynamic Impedance Characterization of Solar Cells and PV Modules Based on Frequency and Time Domain Analyses. *Trends In Solar Energy Research*. Hough, T.P. New York: Nova Science Publishers, 2006, s. 21-45. ISBN 1-59454-866-8; LCCN: 2005034740.

[24] CZOCHRALSKI, J. (1918) "Ein neues Verfahren zur Messung der Kristallisationsgeschwindigkeit der Metalle", *Zeitschrift für Physikalische Chemie*, **92** : 219–221.

[25] International Technology Roadmap for Photovoltaic: Results 2016. In: *International Technology Roadmap for Photovoltaic (ITRPV) - Home* [online]. Germany: VDMA, 2017. Available at: http://www.itrpv.net/.cm4all/iproc.php/ITRPV%20Eighth%20Edition%202017.pdf?cdp=a

[26] GOODRICH, A., HACKE, P., WANG, Q., SOPORI, B., MARGOLIS, R., JAMES, T. L., WOODHOUSE, M. A wafer-based monocrystalline silicon photovoltaics road map: Utilizing known technology improvement opportunities for further reductions in manufacturing costs. *Solar Energy Materials and Solar Cells* [online]. 2013, **114**, 110-135. DOI: 10.1016/j.solmat.2013.01.030. ISSN 09270248. Available at: http://linkinghub.elsevier.com/retrieve/pii/S0927024813000457

[27] GREEN, M. A. The path to 25% silicon solar cell efficiency: History of silicon cell evolution. *Progress in Photovoltaics: Research and Applications* [online]. 2009, **17**(3),

183-189. DOI: 10.1002/pip.892. ISSN 10627995. Available at: http://doi.wiley.com/10.1002/pip.892

[28] GREEN, Martin A., Yoshihiro HISHIKAWA, Wilhelm WARTA, Ewan D. DUNLOP, Dean H. LEVI, Jochen HOHL-EBINGER a Anita W.H. HO-BAILLIE. Solar cell efficiency tables (version 50). *Progress in Photovoltaics: Research and Applications* [online]. 2017, **25**(7), 668-676. DOI: 10.1002/pip.2909. ISSN 10627995. Available at: http://doi.wiley.com/10.1002/pip.2909

[29] REICHL, C., F. FELDMANN, R. MÜLLER, A. MOLDOVAN, M. HERMLE a S.W. GLUNZ. Interdigitated Back Contact Silicon Solar Cells with Tunnel Oxide Passivated Contacts Formed by Ion Implantation. In: *EU PVSEC Proceedings* [online]. München: WIP, 2016, s. 487-491. DOI: 10.4229/EUPVSEC20142014-2CO.1.1. ISBN 3-936338-34-5. Available at: https://www.eupvsec-proceedings.com/proceedings/checkout.html?paper=30438

[30] THEUERER, H. C. *Method of processing semiconductive materials*. US 3060123 A Patent.

[31] CHEN, C. Julian. *Physics of solar energy*. 1. Hoboken, N.J.: John Wiley, c2011. ISBN 04-706-4780-9.

[32] *PVEducation* [online]. Arizona: Solar Power Labs at ASU, 2013. Available at: http://www.pveducation.org/

[33] LI, Y. Passivated Emitter Rear Locally Diffused Solar Cells. *Bulletin of Advanced Technology Research* [online]. Ahenzen Institutes of Advanced Technology, Chinese Academy of Science, 2011, **5**(8), 41-43. Available at: http://www.siat.cas.cn/xscbw/xsqk/201109/W020110913360382095140.pdf

[34] Manufacture of CIGS thin-film solar cells. In: *ZSW: Thin-film solar cells and modules* [online]. Zentrum für Sonnenenergie- und Wasserstoff-Forschung Baden-Württemberg: Zentrum für Sonnenenergie- und Wasserstoff-Forschung Baden-Württemberg, 2017. Available at: https://www.zsw-bw.de/en/research/photovoltaics/topics/thin-film-solar-cells-and-modules.html#c460

[35] WESOFF, E. Oerlikon and the Fate of Amorphous Silicon Solar Technology | Greentech Media. In: *Green Technology | Cleantech and Renewable Energy News and Analysis | Greentech Media* [online]. USA. 2010. Available at: https://www.greentechmedia.com/articles/read/Oerlikon-Amorphous-Silicon-and-The-Fate-of-a-Si-Solar-Technology

[36] NOUFI, R., ZWEIBEL, K.. High-Efficiency CdTe and CIGS Thin-Film Solar Cells. *2006 IEEE 4th World Conference on Photovoltaic Energy Conference* [online]. IEEE, 2006. DOI: 10.1109/WCPEC.2006.279455. ISBN 1-4244-0016-3. Available at: http://ieeexplore.ieee.org/document/4059628/

[37] INTERNATIONAL ENERGY AGENCY PHOTOVOLTAIC POWER SYSTEMS PROGRAMME, . *Performance and Reliability of Photovoltaic Systems: Subtask 3.2: Review of Failures of Photovoltaic Modules*. 2014. ISBN 978-3-906042-16-9. Available at: http://www.iea-pvps.org/index.php?id=95&eID=dam_frontend_push&docID=2064

[38] PV-Modul-Bewertungskriterien. In: *MBJ services to know what's up* [online]. Hamburg: MBJ Services, 2014. Available at: https://www.mbj-services.com/fileadmin/cont_services/downloads/MBJ_PV-Modul_Bewertungskriterien_3.1.pdf

[39] VANĚK, J.: Trendy diagnostických metod FV článků pro dosažení maximální délky života panelů. Brno: Česká agentura pro obnovitelné zdroje energie, 2010. *Sborník příspěvků z 5. České fotovoltaické konference*. ISBN: 978-80-254-8906-2. s. 60 – 65.

[40] ČSN EN 60904-2 ed. 3 (364604). *Fotovoltaické součástky - Část 2: Požadavky na referenční fotovoltaické součástky*. 3. Praha: Úřad pro technickou normalizaci, metrologii a státní zkušebnictví, 2015.

[41] MACHÁČEK, Z., ČERNÁ, L., BENDA, V.: Electrical parameters of c-Si and CIS photovoltaic cells in dependence on temperature and irradiance. In *34th International Spring Seminar on Electronics Technology*. Košice: Technical University of Košice, 2011, s. 492-496. ISBN 978-1-4577-2111-3.

[42] STAEBLER, D. L. a C. R. WRONSKI. Reversible conductivity changes in discharge-produced amorphous Si. *Applied Physics Letters*. 1977, **31**(4), 292-. DOI: 10.1063/1.89674. ISSN 00036951. Available at: http://link.aip.org/link/APPLAB/v31/i4/p292/s1

[43] NOVALIN, S., RENNHOFER, M., SUMMHAMMER, J., Electrical metastabilities in chalcogenide photovoltaic devices, *Thin Solid Films*, 535 (2013) 261–264, 2012

[44] TAYLOR, N. (Ed.): *Guidelines for PV Power Measurement in Industry*, Italy: European Comission, JRC, Institute for Energy. 2010-04. ISBN: 978-92-79-15780-6.

[45] VIRTUANI, A., RIGAMONTI, G., BELJEAN, P., FRIESEN, G., PRAVETTONI, M., CHIANESE, D. A fast and accurate method for the performance testing of high-efficiency C-Si photovoltaic modules using A 10 Ms single-pulse solar simulator. In: *2012 38th IEEE Photovoltaic Specialists Conference* [online]. IEEE, 2012, s. 000496-

000500. DOI: 10.1109/PVSC.2012.6317664. ISBN 978-1-4673-0066-7. Available at: http://ieeexplore.ieee.org/lpdocs/epic03/wrapper.htm?arnumber=6317664

[46] SHOCKLEY, W., W. READ, HALL, RN.. Statistics of the Recombinations of Holes and Electrons. *Physical Review*: *Series II* [online]. 1952, roč. 87, č. 5, s. 835-842. DOI: 10.1103/PhysRev.87.835. Available at: http://link.aps.org/doi/10.1103/PhysRev.87.835

[47] ČERNÁ, L., MACHÁČEK, Z., BENDA, V.: Determination of recombination centers in c-Si solar cells from dark I-V characteristics. In *34th International Spring Seminar on Electronics Technology*. Košice: Technical University of Košice, 2011, s. 172-175. ISBN 978-1-4577-2111-3.

[48] ČERNÁ, L., KUŘÍK, O. BENDA, V.: Zařízení pro měření neosvětlených fotovoltaických článků. [Functional Sample]. 2010.

[49] TRAN HUNG, Q. *Diagnostics of large-area crystalline silicon cells*. Diplomová práce. Praha: ČVUT, FEL, katedra elektrotechnologie, 2003.

[50] THONGPRON, J.; KIRTIKARA, K. Voltage and frequency dependent impedances of monocrystalline, polycrystalline and amorphous silicon solar cells. In: *Photovoltaic Energy Conversion*, Conference Record of the 2006 IEEE 4th World Conference on. IEEE, 2006. p. 2116-2119.

[51] JOHNSON, J. et al. Creating dynamic equivalent PV circuit models with impedance spectroscopy for arc fault modelling. In: *Photovoltaic Specialists Conference (PVSC), 2011 37th IEEE*. IEEE, 2011. p. 002328-002333.

[52] AL ABDULLAH, K., AL ALLOUSH, F., TERMANINI, M.J., SALAME, C.. Low Frequency and Low Temperature Behavior of Si, solar cell by AC Impedance Measurements. *Energy Procedia* [online]. 2012, roč. 19, č. 22, s. 183-191. ISSN 1876-6102. Available at: www.sciencedirect.com

[53] ČERNÁ, L., FINSTERLE, T., HRZINA, P. and V. BENDA. Note on Cole-Cole Diagrams of Photovoltaic Modules Evaluation. To be published In *Proceedings of EUPVSEC'17.* 2017

[54] SZE, S. M., KWOK KWOK, NG. *Physics of semiconductor devices* [online]. 3rd ed. Hoboken, N.J.: Wiley-Interscience, c2007. ISBN 04-711-4323-5.

[55] FRANK, H.; ŠNEJDAR, V. Principy a vlastnosti polovodičových součástek. SNTL-Nakladatelství technické literatury. Prague 1976.

[56] PROSKURYAKOV, Y. Y., DUROSE, K., M. K. AL TURKESTANI, I. MORA-SERÓ, G. GARCIA-BELMONTE, F. FABREGAT-SANTIAGO, J. BISQUERT, V. BARRIOZ, D. LAMB, S. J. C. IRVINE a E. W. JONES. Impedance spectroscopy of

thin-film CdTe/CdS solar cells under varied illumination. *Journal of Applied Physics* [online]. USA: American Institute of Physics, 2009, roč. 106, č. 4. ISSN 0021-8979. DOI: 10.1063/1.3204484.

[57] DHIMISH, M., HOLMES, V., MEHRDADI, B., DALES, M. Diagnostic method for photovoltaic systems based on six layer detection algorithm. *Electric Power Systems Research* [online]. 2017, **151**, 26-39. DOI: 10.1016/j.epsr.2017.05.024. ISSN 03787796. Available at: http://linkinghub.elsevier.com/retrieve/pii/S0378779617302201

[58] HONG, F., SI, CH. A study of evaluation system based on large scale photovoltaic power generation. *2016 IEEE 11th Conference on Industrial Electronics and Applications (ICIEA)* [online]. IEEE, 2016, 2507-2510. DOI: 10.1109/ICIEA.2016.7604014. ISBN 978-1-4673-8644-9. Available at: http://ieeexplore.ieee.org/document/7604014/

[59] PEPPANEN, J., RENO, M. J., BRODERICK, R. J., GRIJALVA, S. Distribution System Model Calibration With Big Data From AMI and PV Inverters. *IEEE Transactions on Smart Grid* [online]. 2016, **7**(5), 2497-2506. DOI: 10.1109/TSG.2016.2531994. ISSN 1949-3053. Available at: http://ieeexplore.ieee.org/document/7426397/

[60] CERNA, L., FINSTERLE, T., HRZINA, P. and BENDA, V. A Simple Method of Evaluating Thermograms of Photovoltaic Modules. In *Proceedings of 2015 EU PVSEC*. Hamburg. 2015. DOI: 10.4229/EUPVSEC20152015-5AV.6.32. Available at: https://www.eupvsec-proceedings.com

[61] ŠTĚPÁNEK, M. *Korelace mezi termogramem a flashtestem fotovoltaického modulu*. Praha, 2013. Diploma thesis. CTU in Prague, FEE. Guarantor Ladislava Černá.

[62] CERNA, L., FINSTERLE, T., HRZINA, P., CERQUEIRA, J. C. and BENDA, V. A Note on Evaluation of PV Module Thermograms. Submitted to *Solar Energy (under review).*

[63] ČERNÁ, L., HRZINA, P., a HOCHMAL, P. *Zařízení pro rychlou analýzu fotovoltaických modulů.* České vysoké učení technické v Praze, Fakulta elektrotechnická, Praha 6, CZ; Ing. Patrik Hochmal, zadní Třebáň, CZ 30095 Utility model. 29.11.2016.

[64] ČERNÁ, L., HRZINA, P., HOCHMAL, P. *Způsob rychlé analýzy fotovoltaických modulů a zařízení k jeho provádění.* Czech Republic. Patent. CZ 306858. 2017-06-28.

[65] ČERNÁ, L., FINSTERLE, T., HRZINA, P. and V. BENDA. Impedance Spectroscopy and Its Possible Use for Defects Detection. In *Proceedings of EUPVSEC'16.* 2016

[66] FINSTERLE, ČERNÁ, L., T., HRZINA, P. and V. BENDA. Impedance Spectroscopy and Its Possible Use for Defects Detection. In *Proceedings of 38th NZEE'17.* 2017

[67] AGILENT TECHNOLOGIES, Inc. *Time Domain Reflectometry Theory: Application Note 1304-2* [online]. USA, 2006, p. 16. ISBN 5966-4855E. Available at: http://cp.literature.agilent.com/litweb/pdf/5966-4855E.pdf

[68] LOYO PRADO, M., ČERNÁ, L.: *Application of alternate methods of measurement of PV modules*. [Research Report]. 2012. p. 46

9 List of Publications

List of Publications - with Relationship to Doctoral Thesis

	Authorial Share (%)	Citations
Publications in Impacted Journals		
CERNA, L., FINSTERLE, T., HRZINA, P., CERQUEIRA, J. C. and BENDA, V. A Note on Evaluation of PV Module Thermograms. Submitted to *Solar Energy (under review)*	**40**	
HOLOVSKÝ, J., DE WOLF, S, WERNER, J., REMEŠ, Z., MULLER, M., NEYKOVA, N., LEDINSKÝ, M., ČERNÁ, L., HRZINA, P., LÖPER, P., NIESEN, B., BALLIF, C. Photocurrent Spectroscopy of Perovskite Layers and Solar Cells: A Sensitive Probe of Material Degradation. *Journal of Physical Chemistry Letters.* 2017, **8**(4), s. 838-843. ISSN 1948-7185. Available at: http://pubs.acs.org/doi/abs/10.1021/acs.jpclett.6b02854	**5**	**1**
Publications in Reviewed Journals		
FINSTERLE, T. (50 %), ČERNÁ, L. (20 %), HRZINA, P. (20 %), BENDA, V. (10 %) PID efekt na fotovoltaických elektrárnách. *Energetika.* 2015, **65**(12), s. 659-661. ISSN 0375-8842.	**20**	
ČERNÁ, L. (30 %), HRZINA, P. (20 %), ČERNEK, P. (20 %), BENDA, V. (20 %), ŠTĚPÁNEK, M. (10 %) Termografie ve fotovoltaice. *Energetika.* 2014, 64(8-9), s. 440-442. ISSN 0375-8842.	**30**	
ČERNÁ, L. (30 %), ČERNEK, P. (25 %), HRZINA, P. (30 %), BENDA, V. (15 %). Diagnostics of PV Modules Using Time Domain Reflectometry [online]. *Transaction on Electrical Engineering.* 2013, **2**(4), s. 106-108. ISSN 1805-3386.	**30**	
ČERNÁ, L. (40%), HRZINA, P. (35 %), a BENDA, V. (25%) Diagnostika fotovoltaických modulů. *Alternativní energie.* 2012, **15**(4), s. 1-4. ISSN 1212-1673.	**40**	
Patents, Utility Models, Functional Samples		
ČERNÁ, L., HRZINA, P., HOCHMAL, P. *Způsob rychlé analýzy fotovoltaických modulů a zařízení k jeho provádění.* Czech Republic. Patent. CZ 306858. 2017-06-28. *(Will be available in September, 2017)*	**45**	
ČERNÁ, L., HRZINA, P., a HOCHMAL, P. *Zařízení pro rychlou analýzu fotovoltaických modulů.* České vysoké učení technické v Praze, Fakulta elektrotechnická, Praha 6, CZ; Ing. Patrik Hochmal, zadní Třebáň, Utility model CZ. 30095. 29.11.2016.	**45**	
ČERNÁ, L., KUŘÍK, O., a BENDA, V. Zařízení pro měření neosvětlených fotovoltaických článků. [Funkcional sample]. 2010	**40**	

Publications Excerpted by ISI		
ČERNÁ, L., et al. Using Measurement of AC Parameters for CIGS PV Modules Degradation Studying. In: *2014 29th INTERNATIONAL CONFERENCE ON MICROELECTRONICS - PROCEEDINGS.* 2014 29th INTERNATIONAL CONFERENCE ON MICROELECTRONICS. Bělehrad, 12.05.2014 - 14.05.2014. Piscataway: IEEE - Electron Devices Society. 2014, s. 307-310. ISSN 2159-1660. ISBN 978-1-4799-5296-0.	**40**	
ČERNÁ, L., BENDA, V., a MACHÁČEK, Z. A Note on Irradiance Dependence of Photovoltaic Cell and Module Parameters. In: *Proceedings MIEL 2012.* MIEL 2012 : 28th International Conference on Microelectronics. Niš, 13.05.2012 - 16.05.2012. Piscataway: IEEE. 2012, s. 273-276. ISSN 2159-1660. ISBN 978-1-4673-0238-8.	**40**	**1**
ČERNÁ, L., MACHÁČEK, Z., a BENDA, V. Determination of recombination centers in c-Si solar cells from dark I-V characteristics. In: *34th International Spring Seminar on Electronics Technology.* 34th International Spring Seminar on Electronics Technology. Tatranská Lomnica, 11.05.2011 – 15.05.2011. Košice: Technical University of Košice. 2011, s. 172-175. ISBN 978-1-4577-2111-3.	**50**	
MACHÁČEK, Z., ČERNÁ, L., a BENDA, V. Electrical parameters of c-Si and CIS 5otovoltaické cells in dependence on temperature and irradiance. In: *34th International Spring Seminar on Electronics Technology.* 34th International Spring Seminar on Electronics Technology. Tatranská Lomnica, 11.05.2011 – 15.05.2011. Košice: Technical University of Košice. 2011, s. 492-496. ISBN 978-1-4577-2111-3.	**30**	

Grants (without contract research)	**Years**
ČERNÁ, L.: Centre of Advanced Photovoltaic. 2017 - 2022, CZ.02.1.01/0.0/0.0/15_003/0000464 – principal investigator (173 mil. CZK)	**2017-2022**
ČERNÁ, L.: Diagnostics of photovoltaic modules using alternate methods of measurement. 2013 - 2013, SGS13/070/OHK3/1T/13 – principal investigator (130 000 CZK)	**2013**
ČERNÁ, L.: Photovoltaic Systems Diagnostics. 2012 - 2012, SGS12/062/OHK3/1T/13 – principal investigator (84 000 CZK)	**2012**
BENDA, V.: Diagnostics of photovoltaic systems. 2010 - 2011, SGS10/162/OHK3/2T/13 - research team member (714 000 CZK)	**2010-2011**

Other Publications	**Authorial Share (%)**	**Citations**
To be published in September 2017: ČERNÁ, L., FINSTERLE, T., HRZINA, P. and V. BENDA. Note on Cole-Cole Diagrams of Photovoltaic Modules Evaluation. In *Proceedings of EUPVSEC'17.* 2017	**40**	
FINSTERLE, ČERNÁ, L., T., HRZINA, P. and V. BENDA. Impedance Spectroscopy and Its Possible Use for Defects Detection. In *Proceedings of 38th NZEE'17.* 2017	**40**	
FINSTERLE, T., et al. Degradace tenkovrstvých modulů. In: *37. Nekonvenční zdroje elektrické energie.* 37. Nekonvenční zdroje elektrické energie. Vyškov, 18.05.2016 – 20.05.2016. Praha: Česká elektrotechnická společnost. 2016, s. 33-36. ISBN 978-80-02-02653-2.	**30**	

Other Publications	**Authorial Share (%)**	**Citations**
FINSTERLE, T., et al. Study of Shunt Distributions in Thin Film Multijunction Solar Cells [online]. In: *EU PVSEC Proceedings.* European Photovoltaic Solar Energy Conference and Exhibition. Mnichov, 20.06.2016 – 24.06.2016. Munich: WIP – Renewable Energies. 2016, s. 1250-1252. ISBN 3-936338-41-8. Available at: http://www.eupvsec-proceedings.com/	**5**	
ČERNÁ, L., et al. IMPEDANCE SPECTROSCOPY AND ITS POSSIBLE USE FOR DEFFECTS DETECTION [online]. In: *EU PVSEC Proceedings*. Mnichov, 20.06.2016 – 24.06.2016. Munich: WIP – Renewable Energies. 2016, s. 1842-1845. ISBN 3-936338-41-8. Available at: http://www.eupvsec-proceedings.com	**50**	
FINSTERLE, T., ČERNÁ, L., a BENDA, V. Účinnost fotovoltaických modulů v podmínkách ČR. In: *36. Nekonvenční zdroje elektrické energie.* 36. Nekonvenční zdroje elektrické energie. Vyškov, 13.05.2015 – 15.05.2015. Praha: Česká elektrotechnická společnost. 2015, s. 34-37. ISBN 978-80-02-02593-1.	**35**	
ČERNÁ, L., et al. A Simple Method of Evaluating Thermograms of Photovoltaic Modules [online]. In: *EU PVSEC 2015 Proceeding.* 31st European Photovoltaic Solar Energy Conference and Exhibition. Hamburg, 14.09.2015 – 18.09.2015. Munich: WIP – Renewable Energies. 2015, s. 2035-2036. ISBN 3-936338-39-6. Available at: 6oto://www.eupvsec-proceedings.com	**25**	
HRZINA, P., et al. Method of Reducing Losses of PV Power Plants Based on CIGS Technology with Transformerless Inverters [online]. In: *EU PVSEC 2015 Proceeding.* 31st European Photovoltaic Solar Energy Conference and Exhibition. Hamburg, 14.09.2015 – 18.09.2015. Munich: WIP – Renewable Energies. 2015, s. 2384-2386. ISBN 3-936338-39-6. Available at: 6oto://www.eupvsec-proceedings.com	**10**	
ČERNÁ, L., et al. Termografie ve fotovoltaice (unpublished 6otovo). 04.06.2014.	**30**	
VOKÁČ, M. a ČERNÁ, L. *Mechanické zkoušky fotovoltaických modulů FVE Zbudov a posouzení jejich vlastností v laboratoři diagnostiky fotovoltaických systémů.* Na Bělidle 198/21, 15000 Praha 5: STRABAG a.s.. 2014, 1400J153.	**50**	
LOYO PRADO, M. a ČERNÁ, L. *Application of 6otovolta methods of measurement of PV modules.* Praha: ČVUT v Praze, Fakulta elektrotechnická, Katedra elektrotechnologie – Laboratoř diagnostiky fotovoltaických systémů. 2013	**20**	
ČERNÁ, L., et al. DIAGNOSTIKA FOTOVOLTAICKÝCH MODULŮ S VYUŽITÍM STŘÍDAVÝCH METOD MĚŘENÍ [online]. In: *Sborník příspěvků z 8.ČFVK.* 8. Česká 6otovoltaické konference. Brno, 14.05.2013 – 15.05.2013. 2013	**30**	
HRZINA, P., et al. *Test teplotní odolnosti TF PV modulů.* Neuvedeno. 2013	**25**	
HRZINA, P., et al. *Metodický pokyn k postupu identifikace stupně poškození PV modulů požárem.* Neuvedeno. 2013	**25**	

Other Publications	Authorial Share (%)	Citations
ČERNÁ, L. a MUSÁLEK, L. Modelling of Photovoltaic Modules. In: *POSTER 2012 – 16th International Student Conference on Electrical Engineering.* POSTER 2012 – 16th International Student Conference on Electrical Engineering. Prague, 17.05.2012. Praha: Czech Technical University in Prague. 2012, s. 1-4. ISBN 978-80-01-05043-9.	**50**	
ČERNÁ, L., HRZINA, P., a BENDA, V. Diagnostika fotovoltaických modulů. In: *7. Česká 7otovoltaické konference – Sborník příspěvků.* 7. Česká 7otovoltaické konference. Brno, 03.05.2012. Rožnov pod Radhoštěm: Czech RE Agency, o.p.s.. 2012, s. 1-5. ISBN 978-80-260-2232-9.	**40**	
ČERNÁ, L. The Comparison of Dirty and Clear Solar Module Properties. In: *POSTER 2011 – 15th International Student Conference on Electrical Engineering.* POSTER 2011 – 15th International Student Conference on Electrical Engineering. Prague, 12.05.2011. Praha: České vysoké učení technické v Praze, Fakulta elektrotechnická. 2011, s. 1-4. ISBN 978-80-01-04806-1.	**100**	
BENDA, V., et al. Diagnostics of Photovoltaic Systems. In: *Workshop 2011,CTU Student Grant Competition in 2010 (SGS 2010).* Workshop 2011. Praha, 01.02.2011 – 04.02.2011. Praha: ČVTVS. 2011, s. 1-4.	**20**	
ČERNÁ, L. a MACHÁČEK, Z. Měření voltampérových charakteristik neosvětlených fotovoltaických křemíkových krystalických článků. In: *Sborník příspěvků z 5. České fotovoltaické konference.* 5. Česká 7otovoltaické konference a výstava. Brno, 10.11.2010 – 13.11.2010. Rožnov pod Radhoštěm: Czech RE Agency o.p.s.. 2010, s. 33.	**60**	

List of Publications – Other Publications

	Authorial Share (%)	Citations
Publications in Impacted Journals		
X		
Publications in Reviewed Journals		
X		
Patents		
X		
Publications Excerpted by ISI		
X		
Grants (without contract research)		**Years**
Studie na téma - Ekonomická bilance výroby a likvidace fotovoltaických modulů instalovaných v ČR – Inovavoucher 2015 – principal investigator at CTU. (160 000 CZK)		**2015**
Other Publications	**Authorial Share (%)**	**Citations**
ČERNÁ, L. a FINSTERLE, T. Economic Balance of Disposal of Photovoltaic Modules Installed in the Czech Republic [online]. In: HUSNÍK, L., ed. *Proceedings of the 20th International Scientific Student Conferenece POSTER 2016.* 20th International Student Conference on Electrical Engineering. Praha, 24.05.2016. Praha: Czech Technical University in Prague. 2016, ISBN 978-80-01-05950-0.	**50**	
HRZINA, P., REICHL, T., a ČERNÁ, L. *Analýza příčin selhání baterií.* Utajený. 2015, B2015-072-Z.	**15**	
ČERNÁ, L., et al. *EKONOMICKÁ BILANCE VÝROBY A LIKVIDACE FOTOVOLTAICKÝCH MODULŮ INSTALOVANÝCH V ČR.* Praha: REsolar s.r.o.. 2015	**30**	**1**
KUDLÁČEK, I., BUŠEK, D., a ČERNÁ, L. *Kapitola 25. Protikorozní ochrana úložných zařízení a konstrukcí.* Praha: SŽDC s.o.. 2015	**5**	
ČERNÁ, L., HRZINA, P., a BENDA, V. Students' projects at the Department of Electrotechnology CTU FEE Prague. In: BENDA, V. a MOLHANEC, M., eds. *Proceedings of the 7th International Workshop on Teaching in Photovoltaics IWTPV'14.* 7th International Workshop on Teaching in Photovoltaics. Praha, 27.03.2014 - 28.03.2014. Praha: ČVUT v Praze. 2014, s. 36-38. ISBN 978-80-01-05477-2.	**50**	
HRZINA, P., ČERNÁ, L., a BENDA, V. From Basic Knowledge to Diagnostics. In: BENDA, V. a MOLHANEC, M., eds. *Proceedings of the 7th International Workshop on Teaching in Photovoltaics IWTPV'14.* 7th International Workshop on Teaching in Photovoltaics. Praha, 27.03.2014 - 28.03.2014. Praha: ČVUT v Praze. 2014, s. 57-59. ISBN 978-80-01-05477-2.	**30**	

Other Publications	Authorial Share (%)	Citations
ČERNÁ, L., et al. Ekonomické a technologické trendy ve fotovoltaice. In: *Sborník odborná konference Aktuální otázky a vybrané problémy řízení elektrizační soustavy*. PODĚBRADY 2013 - Aktuální otázky a vybrané problémy řízení elektrizační soustavy - 18. ročník. Poděbrady, 19.11.2013 - 20.11.2013. Praha: EGÚ Praha Engineering a.s.. 2013, ISBN 978-80-87774-10-6.	**40**	
ČERNÁ, L., HRZINA, P., a BENDA, V. Laboratory Exercises in Teaching Solar Systems at the Department of Electrotechnology CTU FEE Prague. In: BENDA, V. a MOLHANEC, M., eds. *6th International Workshop on Teaching in Photovoltaics.* 6th International Workshop on Teaching in Photovoltaics. Prague, 22.03.2012 - 23.03.2012. Praha: Nakladatelství ČVUT. 2012, s. 49-52. ISBN 978-80-01-05022-4.	**40**	
ČERNÁ, L. a HRZINA, P. Possibilities of Using Photovoltaics in Automobiles. In: *XIX. International Symposium On Electric Machinery In Prague.* XIX. International Symposium On Electric Machinery In Prague. Praha, 07.09.2011 - 09.09.2011. Praha: ČVUT FEL, Katedra elektrických pohonů a trakce. 2011, s. 27-32. ISBN 978-80-01-04890-0.	**50**	
ČERNÁ, L., MACHÁČEK, Z., a BENDA, V. Fotovoltaické pracoviště na ČVUT-FEL. In: *Sborník příspěvků z 5. České fotovoltaické konference.* 5. Česká fotovoltaická konference a výstava. Brno, 10.11.2010 - 13.11.2010. Rožnov pod Radhoštěm: Czech RE Agency o.p.s.. 2010, s. 55.	**65**	